UNIVERSITA' VITA-SALUTE SAN RAFFAELE

CORSO DI DOTTORATO DI RICERCA INTERNAZIONALE IN MEDICINA MOLECOLARE

CURRICULUM IN IMMUNOLOGIA E ONCOLOGIA DI BASE E APPLICATE

Dissecting the functions of promyelocytic leukemia gene in renal cancer

DoS: Dr. Rosa Bernardi

Second Supervisor: Prof. Ian Frew

Tesi di DOTTORATO di RICERCA di Matilde Simoni

matr. 013954

Ciclo di dottorato XXXIV

SSD: B/13

Anno Accademico 2020/2021

CONSULTAZIONE TESI DI DOTTORATO DI RICERCA

Il/la sottoscritto/*I*	Matilde Simoni
Matricola / *registration number*	013954
nat_ a/ *born at*	Fiesole
il/*on*	22/12/1991

autore della tesi di Dottorato di ricerca dal titolo / *author of the PhD Thesis titled*

Dissecting the functions of promyelocytic leukemia in renal cancer

X AUTORIZZA la Consultazione della tesi / AUTHORIZES *the public release of the thesis*

☐ NON AUTORIZZA la Consultazione della tesi per …… mesi /DOES NOT AUTHORIZE *the public release of the thesis for …… months*

a partire dalla data di conseguimento del titolo e precisamente */ from the PhD thesis date, specifically*

Dal / *from*   ……/……/……   Al / *to*   ……/……/……

Poiché /*because*:

☐ l'intera ricerca o parti di essa sono potenzialmente soggette a brevettabilità/ *The whole project or part of it might be subject to patentability;*

☐ ci sono parti di tesi che sono già state sottoposte a un editore o sono in attesa di pubblicazione/ *Parts of the thesis have been or are being submitted to a publisher or are in press;*

☐ la tesi è finanziata da enti esterni che vantano dei diritti su di esse e sulla loro pubblicazione/ *the thesis project is financed by external bodies that have rights over it and on its publication.*

E' fatto divieto di riprodurre, in tutto o in parte, quanto in essa contenuto / *Copyright the contents of the thesis in whole or in part is forbidden*

Data /Date 31/01/2022

Firma/Signature……

DECLARATION

This thesis has been composed by myself and has not been used in any previous application for a degree. Throughout the text I use both 'I' and 'We' interchangeably.

All the results presented here were obtained by myself, except for:

1) *Evaluation of PML expression in ccRCC and normal tissue and cell lines.*

    Sample preparation, immunohistochemistry, tumor staging ad western blotting analyses (Results, chapter 1, figure 7), were performed by Dr. S. Signoretti, Brigham and Women's Hospital in Boston, USA, and Dr. Rosa Bernardi, Preclinical models of cancer Unit, San Raffaele Scientific Institute, Milan, Italy.

2) *Transmission electron microscopy.*

    Electron-microscopy specimens (Results, chapter 3.1.7, figures 23, 25, 26 and 27), were processed by Dr. A. Raimondi, Alembic, Experimental Imaging Centre, San Raffaele Scientific Institute, Milan, Italy.

3) *Bioinformatic analysis of RNA-sequencing data.*

    Bioinformatic analysis (Results, chapter 3.1.9, figures 30, 31 and 32), was performed by Dr. E. Zapparoli, Centre for Translational Genomics and Bioinformatics, San Raffaele Scientific Institute, Milan, Italy.

4) *Immunohistochemistry and images acquisition*

    Sample preparation, immunohistochemistry and slide scanning (Results, chapter 3.1.10, figures 35, 36, 37, 38, 39 and 40), were performed by Dr. A. Fiocchi, Alembic, Animal Histopathology facility, San Raffaele Scientific Institute, Milan, Italy.

All sources of information are acknowledged by means of reference.

ABSTRACT

The role of the promyelocytic leukemia gene (*PML*) has long been investigated in cancer, where it was found to play tumor-suppressor and oncogenic functions. We previously found that PML is over-expressed in triple negative breast cancer (TNBC), promoting metastatic dissemination by enhancing HIF1α transcriptional program. HIF1α and its paralogue HIF2α, are overexpressed in clear cell renal cell carcinoma (ccRCC) and play key roles in cancer progression. We found that PML is overexpressed in ccRCC and is a marker of unfavorable clinical outcome, leading us to hypothesize that the oncogenic PML-HIFα axis is conserved in these tumor settings. Unexpectedly, here demonstrate that PML is not involved in cell migration and invasion in ccRCC, but rather it is essential for cell proliferation and tumor progression *in vitro* and *in vivo*, showing a non oncogene addiction to PML. Moreover, PML inhibition leads to extensive morphological rearrangements akin to aberrant differentiation, and strongly suggestive of cell senescence. Accordingly, profiling of the PML-regulated transcriptome revealed that PML suppresses genes involved in cholesterols biosynthesis and glycolytic pathways while positively regulating gene networks implicated in cell proliferation, partially through regulation of HIF1α and HIF2α gene networks, but most prominently in a self-directed manner.

In this work, we characterized a previously unreported role of the *PML* gene in ccRCC as a requirement for growth and metabolic decisions. Moreover, we dissected the feasibility of PML pharmacological targeting to repurpose arsenic trioxide as a cytostatic drug in ccRCC therapy.

TABLE OF CONTENTS

ACRONYMS AND ABBREVIATIONS

Akt – Ak strain transforming

ADAMTS1 – ADAM Metallopeptidase With Thrombospondin Type 1 Motif 1

ALT – Alternative Lengthening of Telomeres

ANGPT2 – Angiopoietin 1

ANGPTL4 – Angiopoietin-like 4

AP-1 – Acrivator Protein 1

APL – Acute Promyelocytic Leukemia

Arf – ADP-ribosylation Factor

ATO- Arsenic Trioxide

ATP – Adenosine Tryphosphate

ATR – Ataxia Telangiectasia

ATRA – All Trans Retinoic Acid

B – B-box

BAP1 – BRCA1 Associated Protein 1

bHLH – Basic helix-loop-helix

BLM – Bloom Syndrome

BNIP3 – BCL2/Adenovirus E1B 19 kDa protein-interacting protein 3

BrdU - Bromo-deoxy Uridine

BUB3 – Budding Inhibited By Benzimidazoles 3 Homolog

c-Myc – cellular Myc

CA9 – Carbonic Anhydrase 9

CC – Coiled Coil domain

CEBP – CCAAT/Enhancer Binding Protein

CDC – Cell Division Cycle

CDKN2A – Cyclin-dependent Kinase Inhibitor 2A

CDK – Cycline-dependent Kinase

ChRCC – Chromophobe Renal Cell Carcinoma

CML – Chronic Myeloid Leukemia

CoIP – Co-immunoprecipitation

CPT1A – Carnitine Palmitoyltransferase 1A

CREB - cAMP-response element binding protein

CSCs – Cancer Stem Cells

CTLA-4 – Cytotoxic T-lymphocyte-associated protein 4

DAXX – Death-Associated protein 6

DBS – Double Strand Break

DDIT4 – DNA-damage-inducible transcript 4

DDR – DNA Damage Response

DMBA – 7,12-dimethylbenz(α)anthracene

E2F – E2 Transcription Factor

ELK1 - ETS Like-1 Protein

eIFF4E – eukaryotic Initiator of Translation Factor 4 E

ELOV6 – ELOVL Fatty acid elongase 6

ENO1 – Enolase 1

EMT – Epithelial-to-mesenchymal Transition

EPAS – Endothelial PAS domain-containing protein 1

ERK – Extracellular signal- regulated Kinase

FABP – Fatty Acid Binding Protein

FACS – Fluorescence Assisted Cell Sorting

FDA – Food And Drug Association

FH – Fumarate Hydratase

FIH – Factor inhibiting HIF

FOX - Forkhead transcription factor

GAPDH – Gkyceraldehyde—Phosphate Dehydrogenase

GLUT1 – Glucose Transporter 1

GPI – Glucose-6-Phosphate Isomerase

GPC4 – Glypican 4

HAF – Hypoxia Associated Factor

HCMV – Human Cytomegalovirus

HIF – Hypoxia-Inducible Factors

HK2 – Hexokynase 2

HMGB1 – 3-Hydroxy-3-Methylglutaryl-CoA Reductase

HMGCS - 3-Hydroxy-3-Methylglutaryl-CoA Synthase 1

HRE – Hypoxia-responsive Element

HS2ST – Heparan Sulfate 2-O-Sulfotransferase 1

JAK – Janus Kinase

ICF – Instability-facial Anomalies Syndrome

IDI1 – Isopentenyl-Diphosphate Delta Isomerase 1

IE1 – Immediate Early 1

IF - immunofluorescence

IHC – Immunohistochemistry

IRS2 – Insulin Receptor Substrate 2

L1 – Ligand 1

LAMP – Lysosomal Associated Membrane Protein

LAMTOR – Late Endosomal/Lysosomal Adaptor, MAPK and mTOR Activator 1

LCAD – Long Chain acyl-CoA Dehydrogenase

LCMV – Lymphocytic choriomeningitis

LDHA – Lactate Dehydrogenase A

LOX – Lysyl Oxydase

LOXL – Lysyl Oxydase-like 1

LSD1 – Lysine-specific histone Demethylase 1

KDM5 – Lysine Demethylase 5

MAM – Mitochondrial associated membranes

MAPK – Mitogen-activated Protein Kinase

MAPPs – Mitotic Accumulations of PML protein

MCAD – Medium Chain acyl-CoA Dehydrogenase

MEFs – Murine Embryonic Fibroblasts

MIX1 – MAX Interacting Protein 1

MMP – Metalloproteinase

MSH2 – MutS Homolog 2

mTORC1 – Mammalian Target of Rapamycin Complex 1

NDRG1 – n-Myc Downstream Regulated 1

NLS – Nuclear Localization Signal

NSCLC – Non Small Cell Lung Cancer

O_2 – Molecular Oxygen

Oct4 – Octamer Binding Transcription Factor 4

ODD – Oxygen-dependent Degradation Domain

ORO – Oil red O

P4HA1 – Prolyl 4-Hydorxylase Subunit A

PAI1 – Plasminogen Activator Inhibitor 1

PAS – Per-ARNT-Sim

PAXIP1 – PAX Interacting Protein 1

PBRM1 – Polybromo 1

PCNA – Proliferating Nuclear Antigen

PD1 – Programmed Cell Death Protein 1

PDH – Pyruvate Dehydrogenase

PDK – Pyruvate Dehydrogenase Kinase

PGK1 – Phosphoglycerate Kinase 1

PGM2 – Phosphoglucomutase 1

PDL-1 – Programmed Death-ligand 1

PDX – Patient-derived Xenografts

PFKP – Phosphofructokinase

PGF – Prostaglandin F

PLA – Proximity Ligation Assay

PHD – Prolyl Hydroxylase

PHGDH – Phosphoglycerate Dehydrogenase

PI - Propidium Iodide

PI3K – Phosphatidylinositol 3-kinase

PML – Promyelocytic Leukemia Protein

PLOD – Procallagen-Lysine,2-Oxoglutarate 5-Dioxygenase

PML-NBs – PML Nuclear Bodies

pO_2 – Partial Oxygen Pressure

POLE – Polymerase E

PRIM2 – DNA Primase Subunit 2

PTEN – Phosphatase and tensin homolog

qRT-PCR - quantitative real time PCR

pRCC – Papillary Renal Cell Carcinoma

R – Ring Finger

RAD51 – Rad51 DNA repair protein RAD51

RARα − Retinoic Acid Receptor α

Ras – Rat Sarcoma

RCC – Renal Cell Carcinoma

RFC – Replication Factor Subunit

RING – Really Interesting New Gene

RNF4 – Ring Finger Protein

RPA1 – Replication Protein 1

SA β-Gal - Senescence associated β-Galactosidase

SASP – Senescence Associated Secretory Phenotype

SCF – Skp1-cullin-F-box-protein Complexomplex

SCP1 – Small C-terminal domain phosphatase

SET – Su(var)3-9-Enhancer-of-zeste and Trithorax

SDF1 – Stromal cell-derived Factor 1

SHMT2 – Serine Hydroxymethyltransferase 2

shRNA – short hairpin RNA

SIM – SUMO interacting motif

SNAI2 – Snail Family Transcriptional Repressor 2

SOX2 – Sex Determining Region 2

SP1 - Stimulatory Protein 1.

SREBP – Srterol Regulatory Element Binging Protein

STAT – Signal Transducer and Activated Transcription

STED2 – SET Domain-containing 2

SUMO – Small ubiquitin modifier

TAD – Trans Activation Domain

TBX2 – T-Box transcription factor 2

TCGA-KIRC - The Cancer Genome Atlas and the Clinical Proteomic Tumor Analysis Consortium of the National Cancer Institute

TCGA-KIRP - The Cancer Genome Atlas Cervical Kidney Renal Papillary cell carcinoma

TEM - Transmission Electron Microscopy

TERT – Telomerase Reverse Transcriptase

TFE3 – Transcription Factor E3

TKI – Tyrosine Kinase Inhibitor

TNBC – Triple Negative Breast Cancer

TOP3A – DNA Topoisomerase 3 Alpha

TPA – 12-O-tetradecanoylphorbol-13-acetate

TPM – Transcript per million

TRACK – Transgenic Model of Cancer of the Kidney

TRIM19 – TRIpartite Motif

UBC9 – Ubiquitin conjugating enzyme 9

USF1 - Upstream Stimulating Factor 1

VEGF – Vascular Endothelial Growth Factor

VEGFR – vascular Endothelial Growth Factor Receptor

VHL – Von Hippel Lindau

WB – Western Blotting

LIST OF FIGURES AND TABLES

1. INTRODUCTION

1.1 Promyelocytic leukemia (PML) protein

1.1.1   Discovery of PML and its therapeutic targeting by arsenic trioxide

Promyelocytic leukemia (*PML*) gene was discovered in patients affected by acute promyelocytic leukemia (APL) in 1990. Here, *PML* was cloned at the breakpoint of the typical chromosomal translocation t(15;17), which juxtaposes *PML* sequence to the nuclear retinoic acid receptor α (*RARα*)gene (de Thé *et al*, 1991; Goddard *et al*, 1991; (Pandolfi *et al*, 1992) (Figure 1).
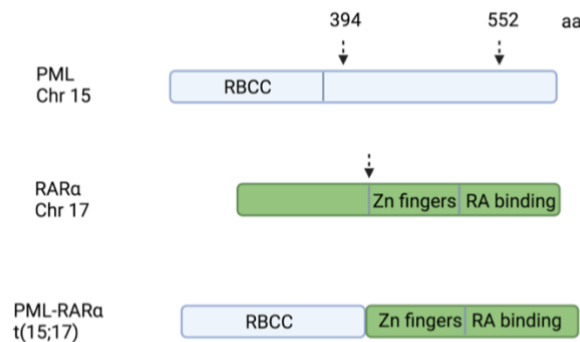
Figure 4. The PML-RARα fusion protein. *PML-RARα fusion protein results from a chromosomal translocation between PML (on chromosome 15) and RARα (on chromosome 17) genes. The two main breakpoints within PML are shown by the arrows, corresponding to amino acids (aa) 394 and 552. The fusion protein preserves the RBCC (RING, B-boxes, Coiled-Coil) domain of PML and the Zinc fingers and RA binding domains of RARα. Created with Biorender.com*

This chromosomal rearrangement generates the PML-RARα fusion protein, which exhibits strong oncogenic properties. When ectopically expressed, PML-RARα induces *in vitro* transformation of murine hematopoietic progenitors and initiates leukemia development in mice (Altabef *et al*, 1996; Brown *et al*, 1997). Structurally, PML-RARα contains the N-terminal region of PML and the C-terminal domains of the RARα transcription factor (Figure 1). Typically, t(15;17) involves only one chromosome 15 and one chromosome 17, with the other copies remaining intact and expressing wild type

16

proteins. However, PML-RARα acts in a dominant-negative manner (Brown *et al*, 1997) and inhibits the physiological functions of wild type PML and RARα, namely the formation of nuclear condensates known as PML nuclear bodies (PML-NBs), and activation of RARα transcriptional program needed for promyelocytic differentiation. Mechanistically, the chimeric protein inhibits RARα transcriptional activity by recruiting transcriptional co-repressor complexes onto RARα target genes, thus blocking myeloid differentiation. At the same time, PML-NBs are disaggregated by interactions with PML-RARα, and as a consequence promyelocytes are blocked in an undifferentiated and hyperproliferative state (Mazza & Pelicci, 2013).

Nowadays, APL patients are successfully cured by combined treatment with *all*-trans retinoic acid (ATRA) and arsenic trioxide (ATO) (Lo-Coco *et al*, 2013; Lo-Coco *et al*, 2016). Notably, these two compounds act synergistically to induce PML-RARα degradation, thus inducing differentiation and apoptosis of APL blasts via re-expression of RARα target genes and reconstitution of physiologic PML-NBs (de Thé *et al*, 2012). ATRA acts selectively onto the RARα moiety and induces its conformational switch from a transcriptional co-repressor to a transcriptional co-activator thus promoting expression of canonical RARα target genes (Melnick & Licht, 1999). On the other hand, ATO selectively targets the PML moiety and directs PML-RARα to proteasomal-mediated degradation. The mechanism of PML-RARα degradation by ATO has been described as a multi-step process (Figure 2): i) ATO oxidases thiol groups of cysteine residues in the RING (Really Interesting New Gene) finger of the PML moiety, generating arsenic-sulfur bonds; ii) the formation of arsenic-sulfur bonds lead to PML-RARα conformational changes that facilitate its oligomerization by exposing SUMOylation sites within PML, and the consequent formation of PML-RARα aggregates; iii) the SUMO-conjugating enzyme UBC9 is recruited into PML-RARα aggregates; iv) extensive SUMOylation promotes PML-RARα ubiquitination mediated by RNF4 and subsequent proteasomal-mediated degradation of the oncogenic fusion protein (Lallemand-Breitenbach *et al*, 2008; May *et al*, 2010). Thus, once the dominant-negative effect of PML-RARα is relieved, PML monomers undergo self-assemble and restore physiological PML-NBs, inducing apoptosis and eradicating APL cells (Takahashi *et al*, 2004).

Importantly, since ATO targets the N-terminal region of the PML protein, beside PML-RARα it also induces degradation of the wild-type protein. As discussed later in more

detail, as it is increasingly emerging that *PML* is involved in the pathogenesis of a number of solid tumors beside to APL, and the ability of ATO to target PML makes this protein an attractive and druggable target in pathological contexts characterized by PML deregulation.
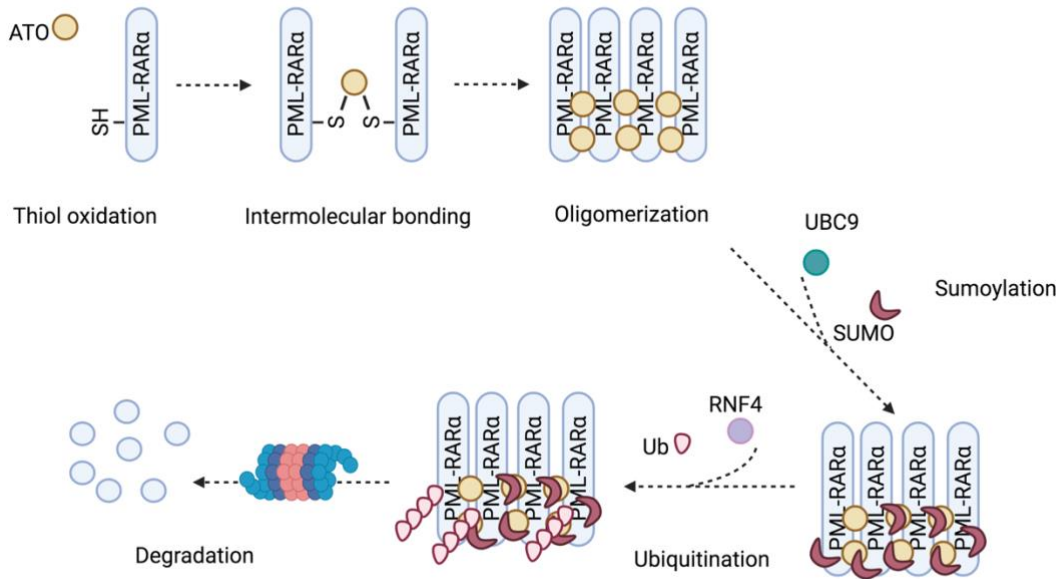
Figure 5. Arsenic trioxide induces PML-RARα proteasomal-mediated degradation by acting onto the PML moiety. Arsenic trioxide (ATO) oxidizes thiol functional groups (SH) present at cysteine residues. Intermolecular arsenic disulfuric bonds formation lead to the oligomerization of PML-RARα molecules. Subsequently, UBC9 SUMOylates PML-RARα aggregates, RNF4 is recruited to allow ubiquitination of PML-RARα and consequent proteasomal-mediated degradation. Created with Biorender.com

1.1.2   The genetic structure of *PML*

The *PML* gene (also known as *TRIM19*) encodes a member of the TRIM (TRIpartirte motif) family of proteins, whose genomic locus maps in 15q22. The *PML* gene spans 35kb and is partitioned in 9 exons (Figure 3). *PML* primary transcript undergoes extensive alternative splicing reactions, resulting in 11 *PML* transcript variants, 7 of which have been fully characterized and shown to encode for protein isoforms PMLI-VII, according to Jensen's nomenclature (Jensen *et al*, 2001) (Figure 3).
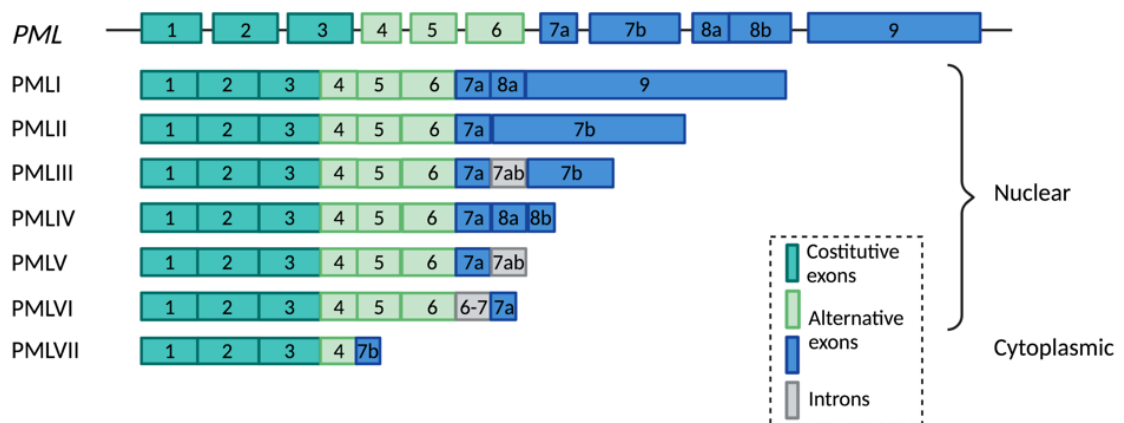
Figure 3. The genetic structure of the PML gene and its isoforms. *The PML gene is composed by 9 exons and alternative splicing leads to the formation of 7 PML isoforms, named PMLI-VII. Exons 1-6 are contained by most isoforms, except for PMLVII that contains exon 4 and not exons 5 and 6. Exons 7a, 7b, 8a and 8b are alternatively spliced in different combinations giving rise to PML C-terminal variability. Exon 9 is exclusively present in PMLI. PMLI-VI isoforms are localized in the nucleus, while PMLVII is cytoplasmic. Created with Biorender.com*

At the protein level (Figure 4), PML harbors a highly conserved N-terminal RBCC domain (RING finger, B-boxes, coiled-coil) also known as TRIM, and variable and less characterized C-terminal domains that specify each isoform (Jensen *et al*, 2001; Nisole *et al*, 2013) (Figure 3 and 4). The RBCC motif is encoded by exons 1-3 and comprises three cysteine-rich zinc binding domains; a RING finger (R) and two B-boxes (B), and an □-helical coiled-coil (CC) motif (Figure 4). The RBCC domain is crucial for PML self-aggregation and the biogenesis of PML-NBs via self-interaction sites within the RING finger and one B box. Other structural features that are conserved among the majority of PML isoforms are: i) a nuclear localization signal (NLS) encoded by exon 6 (that is spliced out in PMLVII thus causing its cytoplasmic localization) (McNally *et al*, 2008); ii) a SUMO-interacting domain (SIM) in exon 7a that is absent in PMLVI and VII (Figure 3).
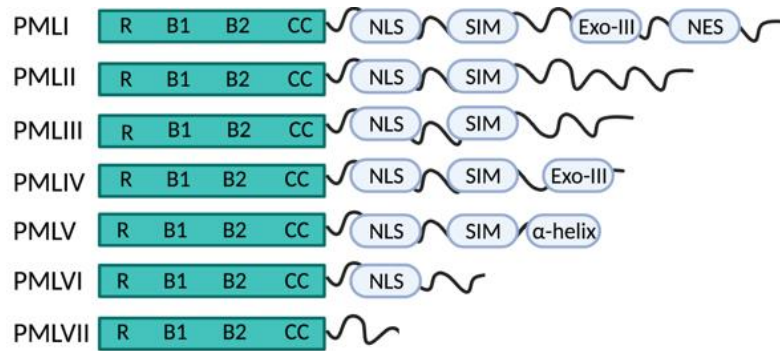
Figure 4. Protein structure of the PML isoforms. *All PML isoforms share the N-terminal RBCC domain. At the C-terminal, PML I-VI contain a NLS. PML I-V contains a SIM which is not present in PML VI. In PML VII both the NLS and the SIM are lacking. Few isoform specific C-terminal domains or motifs have been identified. PML I harbors a NES and an exonuclease III (Exo-III) domain, partly present in PML IV, while PML V contaisn a C-terminal alpha-helix motif. Created with Biorender.com*

In addition to the RBCC domain, SIM motifs mediate PML homo-multimerization with SUMOylated PML moieties or with other SUMOylated PML interactors (Jensen *et al*, 2001; Condemine *et al*, 2006) and contribute to the formation of mature PML-NBs. Finally, alternative splicing of exons from 4 to 9 allows specification of PML C-terminal regions, which does not contain well-defined structural motifs (Figure 4). Notably, unique PML C-terminal regions promote isoform specific interactions with a spectrum of protein partners (Nisole *et al*, 2013). In conclusion, because of the high degree of complexity and extraordinary variability of PML C-terminal composition, it is being suggested that each isoform might exert unique functions dictated by specific interactions with different proteins (Jensen *et al,* 2001; Nisole *et al*, 2013).

1.1.3 The biogenesis of PML-NBs

An essential aspect of PML proteins is their extraordinary ability to self-assembly in membrane-less organelles called PML-NBs. These structures usually appear as nuclear speckles with a toroidal donut-shaped architecture, in which PML and its interactors localize to the outer shell and surround an inner core of proteinaceous nature. PML homo- and heteromerization are principally mediated by the RBCC and SIM domains. Originally, the mechanism underlying PML-NBs biogenesis, was described as a well-ordered cascade of events (Figure 5) : i) free PML monomers interact via non-covalent interactions mediated by their RBCC domains and nucleate in a given point within the

nucleus; ii) PML undergoes extensive lysine SUMOylation mediated by UBC9, with SUMO1 localizing to the outer shell along with PML, while SUMO2/3 poly-chains localize into the inner core; iii) other SUMOylated client proteins are recruited to the PML-NBs through SUMO/SIM interactions (Figure 5) (Hoischen *et al*, 2018). Alternatively, it has been proposed that the first step of PML-NBs assembly, consists of oxidation-mediated PML multimerization and subsequent recruitment of partner proteins through polarized SIM/SUMO interactions (Sahin *et al*, 2014).
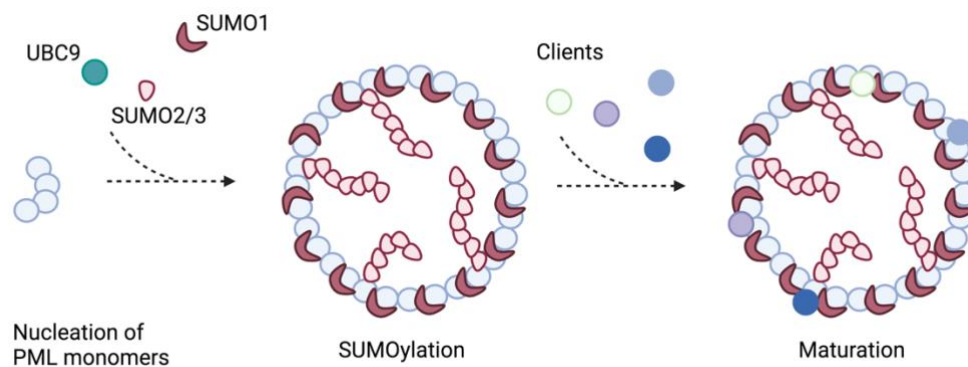
Figure 5. The model of PML-NBs biogenesis. PML oligomers are formed as a consequence of the non-covalent interaction of PML monomers through their RBCC, initiating the nucleation step. UBC9 SUMOylates nucleating PML, and SUMO1 and PML start to form the outer shell surrounding the inner core with protruding SUMO2/3 chains. Finally, SUMOylated PML client proteins are recruited into PML-NBs that reach maturation. Created with Biorender.com

Interestingly different types of PML aggregates can be observed within the nucleus, from condensed aggregates to empty spheres with toroidal topology (Carracedo *et al*, 2011; Li *et al*, 2017; Fonin *et al*, 2021). It has been suggested that the presence within the same nucleus of morphologically heterogeneous PML-NBs might represent different states of their maturation, from condensed PML aggregates to toroidal, mature PML-NBs, where PML and PML interactors dispose at the outer shell (Lallemand-Breitenbach & de The, 2010; Fonin *et al*, 2021). However, recently it has been proposed that PML-NBs can also assemble in a more disordered manner via liquid-liquid phase separation (Banani *et al*, 2016; Hoischen *et al*, 2018; Corpet *et al*, 2020). Accordingly, PML C-terminal tails (containing a huge number of charged amino acids and tandem repeats that are intrinsically prone to phase separation (Das *et al*, 2020; Fonin *et al*, 2021).

1.1.4 PML-NBs are highly dynamic and heterogeneous structures

PML is ubiquitously expressed in mammalian tissues and mainly resides in the nucleus. Notably, PML moieties exchange from the nucleoplasm to the PML-NBs (Lallemand-Breitenbach & de The, 2010), but the function of nuclear soluble PML has not been characterized so far.

Typically, 1-30 discrete 0.2-1 □m wide PML-containing speckles are visible in mammalian nuclei. These bodies lie juxtaposed to chromatin in the inter-chromosomal space and are physically associated with the nuclear matrix (Lallemand-Breitenbach *et al*, 2001; Bernardi & Pandolfi, 2007; Lallemand-Breitenbach & de Thè, 2010). Although the vast majority of PML interactors are transcription factors and regulators of chromatin dynamics (Corpet *et al*, 2020), nucleic acids are mostly absent from the PML-NBs but can be found at their periphery. Indeed, PML-NBs are spatially associated with chromatin and juxtaposed to sites of active transcription, as well as to nascent RNA (Corpet *et al*, 2020).

The expression of PML and the number of PML-NBs differ on the basis of the tissue compartment (Bernardi & Pandolfi, 2007) and of the cell differentiation stage (Aoto *et al*, 2006; Labbaye *et al*, 1999). As examples, in the mouse neocortex, *Pml* expression is restricted to neural progenitor cells, where it regulates cell fate and lineage commitment (Regad *et al*, 2009). Moreover, the number, size and dynamics of PML-NBs differ during the cell cycle (Kießlich *et al*, 2002; Dellaire *et al*, 2006a; Dellaire *et al*, 2006b, Lång *et al*, 2019), and on the basis of specific stimuli or stressors to which cells are exposed (Lallemand and & Thé, 2010). During cell cycle progression, the high dynamicity of PML-NBs is particularly evident in S phase, when PML-NBs undergo partitioning via a fission mechanism caused by chromatin de-condensation due to DNA replication that is associated to PML deSUMOylation and PML-NBs disaggregation into micro-speckles (Chang *et al*, 2018). As a consequence, PML-NBs increase in number, so that they are twice as many in G2 than in G1 (Dellaire *et al*, 2006b). Another evident change in PML-NB distribution occurs in mitosis, when PML-NBs condense into Mitotic Accumulations of PML protein (MAPPs), which disperse into the mitotic cytoplasm after nuclear envelope disruption. A subset of MAPPs remains associated with mitotic chromatin and allows reconstitution of PML-NBs in the nucleus of daughter cells (Dellaire *et al*, 2006a).

PML-NBs also undergo rearrangements and increase in their number and size following exposure to interferonγ (Regad & Chelbi-Alix, 2001).

Intriguingly, some nuclear bodies stand as alternative structures that differ from the canonical PML-NBs in terms of shape and/or specialization, such as PML aggregates in cells undergoing alternative lengthening of telomeres (ALT), which contain telomeric DNA and are functionally involved in telomere maintenance (Hsu *et al*, 2012; Loe *et al*, 2020; Zhang *et al*, 2021b) or giant toroidal PML-NBs in immunodeficiency-centromeric region instability-facial anomalies syndrome (ICF), which contain satellite DNA and promote its heterochromatinization after DNA replication (Luciani *et al*, 2005).

Thus, PML is found in heterogeneous aggregates that may regulate specific processes. The reason for such heterogeneity is not well known. It is possible that different PML isoforms may drive the assembly of dedicated and specialized nuclear bodies by interacting with specific client proteins (Lallemand-Breitenbach & de Thé, 2010) via their unique C-terminal regions (Nisole *et al*, 2013). To cite a few relevant examples, it has been shown that PMLIV is the main component of ALT-associated PML nuclear bodies (APBs) (Yu *et al*, 2010; Hsu *et al*, 2012; Loe *et al*, 2020; Zhang *et al*, 2021b), and PMLII forms particular PML bodies in a cell-type specific manner, like thread-like NBs in senescent cells (Wang *et al*, 2020), or lipid-associated PML-NBs in hepatocytes (Ohsaki *et al*, 2016). However, a complete characterization and understanding of the full heterogeneity of PML structures and the molecular mechanisms at their basis is still lacking. Nonetheless, because of their dynamicity in terms of subcellular localization and composition, PML-NBs have been shown to regulate a plethora of cellular functions.

1.1.5 The functions of PML and PML-NBs: an overview

Given the high dynamicity and heterogeneity of PML-NBs, it is difficult to provide a unique definition of PML functions. To gain insights into PML molecular and cellular functions, more than 170 PML interactors have been identified (Van Damme *et al*, 2010). These include few PML-NB-resident proteins (i. e. DAXX and Sp100) and a plethora of transient interactors (e.g. p53 and CIITA) (Ferbeyre *et al*, 2000; Ulbricht *et al*, 2012). On the basis of these interactors and of studies on the behavior of PML-NBs in stress conditions a number of functions have been attributed to PML, which are briefly summarized in the following paragraphs.

1.1.5.1 Viral infections. Several lines of evidences have demonstrated that PML is an interferon-induced viral restriction factor that interacts with proteins, DNA or RNA of viral origin (Regad & Chelbi-Alix, 2001; McNally *et al*, 2008) to counteract viral infection (Neerukonda, 2021; Everett, 2001). In line with its anti-viral function, many viral proteins like IE1 of human cytomegalovirus (HCMV) or Z protein of lymphocytic choriomeningitis (LCMV) promote disassembly of PML-NBs (Mounira L Chelbi-Alix & de Thé, 1999; Everett *et al*, 1998) and PML redistribution into the cytoplasm (McNally *et al*, 2008).

1.1.5.2 PML-NBs as post-translational modifications sites. The PML-NBs dynamically recruit a large number of protein interactors that include protein-modifying enzymes and their client proteins. The most characterized post-translational modifications occurring within the PML-NBs are those of the tumor-suppressor protein p53. Many p53 modulators (CBP, HDM2, HIPK2, HAUSP, and PIAS) get recruited into the PML-NBs, where p53 undergoes acetylation, SUMOylation, and phosphorylation, thus getting fully activated to exploit its transcriptional activity (Matt & Hofmann, 2018). Moreover, PML can also regulate p53 stabilization via alternative mechanisms, such as sequestering its negative regulator Mdm-2 in the nucleolus (Bernardi *et al*, 2004).

1.1.5.3 Regulation of cellular senescence. PML was first found to promote senescence in human fibroblasts expressing oncogenic *ras* (RasV12) (Ferbeyre *et al*, 2000). Here, PML was up-regulated in response to RasV12 over-expression, and induced senescence by recruiting p53 to the PML-NBs and promoting its transcriptional activation (Ferbeyre *et al* 2000; Pearson *et al*, 2000; de Stanchina *et al*, 2004). Interestingly, the ability of PML to induce senescence appears specific of PMLIV (Bischof, 2002; Vernier *et al*, 2011; Martin *et al*, 2012; Ivanschitz *et al*, 2015). Over-expression experiments in PML-expressing cells showed that PMLIV specifically interacts with Arf via its unique C-terminal motif, resulting in enhanced p53 SUMOylation and p53 stabilization (Ivanchitz *et al*, 2015). Surprisingly, however, if PMLIV is overexpressed in *Pml null* murine embryonic fibroblasts (MEFs), it fails to induce senescence, suggesting that cooperation between all the PML isoforms might be necessary (Bishof *et al*, 2002).

1.1.5.4 DNA damage response (DDR). The role of PML in DDR is controversial since it is not clear whether PML is directly involved in DNA repair (Yeung *et al*, 2011), or if PML-NBs act as storage sites of DNA repair enzymes (Dellaire & Bazett-Jones, 2004; Dellaire *et al*, 2006). For instance, it was shown that when double strand break (DBS) occur, PML-NBs increase in number via a fission mechanism and coalesce at DBS regions, suggesting that they act as primary sensors of DNA damage (Dellaire *et al*, 2006). Moreover, it was demonstrated that ATR and BLM are released from PML-NBs upon genotoxic stress (Dellaire & Bazet-Jones, 2004) and that PML is involved in DNA repair via homologous recombination (Vancurova *et al*, 2019). However, the recruitment of factors involved in DNA repair including RAD51 and □H2A.X to sites of DNA damage remained unaffected upon PML knockdown, suggesting that the PML-NBs are not directly involved in the early steps of DNA repair (Yeung *et al*, 2012). In contrast, γ–irradiated cells fail to induce DNA repair via homologous recombination upon PML silencing (Yeung *et al*, 2012; Boichuck *et al*, 2011). In summary, it appears that PML may be directly involved in specific types of repair, such as homologous recombination-mediated repair, and its role may be particularly important in later steps of the pathway (Yeung *et al*., 2012; Vancurova *et al*, 2019).

1.1.5.5 PML-mediated transcriptional regulation. As mentioned above, the PML-NBs modulate the activity of a number of transcriptional regulators (e. g. p53 and DAXX) via sequestration or post-translational activation mechanisms, suggesting that the role of PML in regulating transcription is mainly indirect. However, it is recently emerging that PML regulates transcription at multiple levels. For example, PML-NBs were found to be proximal to sites of active transcription (Wang *et al*, 2004; Kießlich *et al*, 2002), and PML associates with chromatin in sites that are bound by and regulated by specific transcription factors (Kießlich *et al*, 2002; Martin *et al*, 2012; Yang *et al*, 2013; Ponente *et al*, 2017). Such is the case of a subset of hypoxia-induced transcription factor 1 α (HIF1α) target genes whose expression is enhanced by PML in breast cancer cells (Ponente *et al*, 2017). In this context, PML may function as a transcriptional co-activator, for example by promoting the cooperative binding of transcriptional activators to gene promoters such as that of *Oct4* in murine embryonic stem cells (Aoto *et al*, 2006). Conversely however, it has been reported that PML also functions as a transcriptional co-

repressor, by associating to the *TBX2* gene promoter and enforcing deposition of the repressive H3K27me3 histone modification (Martin et al., 2012). Interestingly, chromatin-associated proteins like histones and histones chaperones are found into PML-NBs, expanding PML transcriptional regulation to the modulation of chromatin dynamics (Corpet *et al*, 2020). In this respect, PML-NBs have been shown to regulate gene expression by inducing chromatin looping, organizing higher-order chromatin architecture and cooperating to the deposition of repressive histone marks at specific genomic *loci* (Delbarre *et al*, 2017; Kurihara *et al*, 2020).

1.1.5.6 Regulation of pro-apoptotic pathways. PML has been described as an important regulator of apoptosis via its ability to regulate p53, as previously mentioned. However, other p53-independent pathways that involve PML in apoptotic cell death have been reported. One such example is that of DAXX, a transcriptional repressor originally described as the mediator of the cytoplasmic transduction of Fas (Yang *et al*, 1997) and TGF-β pro-apoptotic signals (Perlman *et al*, 2001). PML antagonizes DAXX-mediated repression of anti-apoptotic genes by sequestering DAXX into the PML-NBs or via direct repression in the nucleoplasm, thus sensitizing cells to apoptosis (Bernardi & Pandolfi, 2003).

1.1.5.7 Regulation of neo-angiogenesis. The involvement of PML in neo-angiogenesis has been observed in both ischemic tissues and in tumors. Here, the hypoxic environment induces the up-regulation of HIF1α that promotes the formation of new blood vessels through the induction of VEGF expression. PML was shown to negatively regulate HIF1α thus inhibiting neo-angiogenesis in contexts such as prostate cancer or ischemic limbs (Bernardi *et al*, 2006).

1.1.5.8 Stemness. An involvement of PML in the regulation of stem cell maintenance has been demonstrated by a large number of studies. To cite relevant examples, it has been shown that in murine embryonic stem cells (mESC), PML promotes the expression of *Oct4* by maintaining an open chromatin conformation in its promoter region (Aoto *et al*, 2006). In the central nervous system, PML is expressed in neural progenitor cells, where it acts synergistically with Oct4 and Nanog to repress the transcription of genes driving

neural differentiation, it inhibits cell proliferation and promotes maintenance of the neural progenitor pool and correct corticogenesis (Regad *et al*, 2009). A similar phenotype was observed in the mammary gland, where PML is highly expressed in progenitor cells in which it determines lineage commitment (Li *et al*, 2009). Finally, PML was found to promote the maintenance of hematopoietic stem cells (HSCs) via a metabolic function that was similarly described in breast cancer (Ito *et al*, 2012; Carracedo *et al*, 2012a). Specifically, it was shown that PML inhibits asymmetric cell division of HSCs by promoting fatty acid oxidation (FAO) (Ito *et al*, 2012).

1.1.5.9 Cell metabolism. The finding that PML confers self-renewal capacity by regulating cell lipid metabolism (Ito *et al*, 2012) initiated a new line of research into the metabolic functions of PML. In mouse adipose tissue, PML finely regulates adipogenesis in a diet and strain-specific manner. Specifically, in C57BL/6J mice, PML expression gradually decreases during adipogenesis and PML KO mice display fat accumulation when fed with high fat diet (Kim *et al*, 2011). In contrast, knocking-out PML in $129^{s1/SvImJ}$ background, protects from western-diet induced obesity (Cheng *et al*, 2013). Interestingly, in the latter study, it was shown that PML regulates lipid metabolism at the transcriptional level, by inducing the expression of genes involved in lipid anabolic process and, at the same time, promoting FAO. This contradictory transcriptional program orchestrated by PML gives rise to a futile cycle that prevents an increase in body weight, thereby dissipating energy deriving from energy-wasting lipid catabolic process, indicated by an increase in body temperature (Cheng *et al*, 2013). Importantly, PML regulates lipid metabolism also in the context of cancer biology, and relevant examples are reported in the following sections.

1. 2. *PML* gene in cancer biology: one protein, opposite roles

Given the high level of complexity and heterogeneity of the oncogenic process, the inflexible definition of tumor-suppressor or oncogene may be inapplicable and unrealistic in some instances, as it happens frequently that the same gene can exert both tumor-suppressive and oncogenic functions in different contexts (Soussi & Wiman, 2015). This appears to be the case also for *PML* (Datta *et al*, 2020).

The cellular functions mediated by PML and described in part in the previous section (senescence, apoptosis, the regulation of oncogenic transcription factors, neo-angiogenesis, self-renewal and cell metabolism), are of fundamental implication in cancer biology. Therefore, it is intuitive that PML might be de-regulated in specific tumor settings. Indeed, starting from its discovery in APL and the observation that PML is down-regulated in a variety of other solid tumors, *PML* was defined a tumor-suppressor gene. However, in the last decade, an ever-growing mass of data has revealed that in certain tumor types *PML* is over-expressed and actively promotes tumor progression. Such complexity might be explained by the fact that PML is a stress-responsive gene governing a number of cellular processes that might be tissue specific. In the next section, the pro-oncogenic and tumor-suppressive functions of PML will be discussed separately.

1.2.1 *PML* as a tumor-suppressor gene

Since its discovery in APL, substantial evidences demonstrated that PML plays tumor-suppressive roles in cancer. Firstly, targeting of the PML-RARα protein in APL induces reformation of PML-NBs that commit undifferentiated blasts toward apoptosis (Shao *et al*, 1998; Lallemand-Breitenbach *et al*, 2008; Zang *et al*, 2010). Positive regulation of p53 by PML is a strong driving force towards inhibiting tumor progression, mainly via induction of senescence or apoptosis. In line with this, murine *Pml* null cells show resistance to senescence and apoptosis and display genomic instability (Mazza & Pellicci, 2013).

PML tumor-suppressive functions were further validated by *in vivo* studies in *Pml* knock-out mice, which do not develop tumors spontaneously but are sensitized to develop cancers upon carcinogen exposure or when intercrossed with tumor-prone mice (Mazza & Pellicci, 2013). For example, in animal models of non-small cell lung cancer (NSCLC) and skin papilloma, *Pml$^{-/-}$* mice display higher incidence of NSCLC when breed with mice harboring the *K-RasG12D* mutation (Fisher *et al*, 1999) or when are challenged with skin carcinogens 7,12-dimethylbenz(α)anthracene (DMBA) and 12-O-tetradecanoylphorbol-13-acetate (TPA) (Wang *et al*, 1998). These data suggest that loss of *PML* is not sufficient for cell transformation, but promotes cancer progression in specific contexts (Mazza & Pellicci, 2013).

Interestingly, histochemical analysis of PML expression in a panel of human cancers and in adjacent normal tissues, showed that PML was frequently down-regulated in tumor tissue compared to the normal counterpart (Gurrieri *et al*, 2004). In particular, PML expression was reduced in central nervous system tumors (CNS) (49%), non-Hodgkin's lymphoma (68%), colon (17%) and prostate (27%) adenocarcinoma and in lung cancer (21%) (Guerrieri *et al*, 2004). Moreover, PML protein loss correlated with high tumor grade in prostate, in CNS tumors and in breast cancers (Guerrieri *et al*, 2004). In line with these findings, it was demonstrated that in glioblastoma, PML expression promotes apoptosis and inhibits cell proliferation and migration (Kuwayama *et al*, 2009; Wu *et al*, 2014). Nonetheless, the *PML* locus is infrequently mutated or subjected to loss of heterozygosity in solid tumors, and that virtually all the specimens that were analyzed displayed positivity to PML mRNA, thus suggesting that PML protein loss occurs via post-translational mechanisms, and not through genetic alterations (Gurrieri *et al*, 2004). Consistently, in prostate cancer PML undergoes proteasomal-mediated degradation through a hypoxia-dependent mechanism (Yuan *et al*, 2011), and PML expression correlates with better patient prognosis (Birch *et al*, 2014). Similarly, PML degradation induces a pro-metastatic and immune-suppressive tumor microenvironment in lung cancer, and correlates with worse patients outcome (Wang *et al*, 2017).

1.2.2 *PML* as an oncogene

In the last decade, accumulating evidence is revealing unexpected oncogenic functions of *PML*. It was first demonstrated that *PML* is over-expressed in hematopoietic stem cells and in chronic myeloid leukemia (CML), where it slows cell cycle progression, and its inhibition promotes leukemic cells exhaustion (Ito *et al*, 2008). Notably, this study emphasizes the complexity of *PML* biology: on one hand PML suppresses leukemic cells proliferation thus suggesting a tumor-suppressive role, at the same time however it promotes tumor maintenance by safeguarding the reservoir of tumor initiating cells, ultimately acting in a tumor-promoting manner (Ito *et al*, 2008).

In the last few years, several studies demonstrated that *PML* is over-expressed in specific types of tumors and that it promotes pro-oncogenic pathways in specific contexts. In triple negative breast cancer (TNBC) and in ovarian cancer, PML finely tunes tumor energetic metabolism (Carracedo *et al*, 2012; Gentric *et al*, 2019). In particular, PML promotes

fatty acid oxidation and ATP synthesis resulting in the inhibition of anoikis in TNBC (Carracedo *et al*, 2012). Interestingly, in the same tumor context, PML promotes cancer stem cell maintenance (Martín-Martín *et al*, 2016) and in contrast to its senescence-promoting functions in other cellular contexts, in TNBC inhibition of PML elicits senescence (Arreal *et al*, 2020). In ovarian cancer, PML protects cancer cells that experience oxidative stress by promoting mitochondrial respiration (Gentric *et al*, 2019). Beside metabolic and cancer stem cell regulation, PML has also been implicated in the promotion of tumor metastasis by different studies. In glioblastoma, PML promotes cell migration and cancer stem cell maintenance and its targeting with ATO inhibits tumor growth (Zhou *et al*, 2015; Amodeo *et al*, 2017). PML exerts pro-metastatic functions also in TNBC, where PML over-expression correlates with a HIF1α-dependent metastatic gene signature that is co-regulated by PML (Ponente *et al*, 2017). Accordingly, pharmacological inhibition of PML with ATO delays tumor growth and inhibits metastatic dissemination (Ponente et al, 2017).

The finding that PML can be pharmacologically inhibited in several types of cancers characterized by PML over-expression (e. g., TNBC and glioblastoma), has important therapeutic implications, as its targeting may represent a valuable future approach for future strategies of cancer treatment.

1.3 Hypoxia inducible factors (HIFs)

1.3.1 Hypoxia

An intimate relationship exists between atmospheric composition and the evolution of living organisms. About 1.5 million years ago, cyanobacteria developed the ability to fuel energetic metabolism through photosynthesis, generating molecular oxygen (O_2) as a toxic by product. As evolution proceeded, pluricellular organisms have adapted to the increasing O_2 atmospheric concentration and became dependent on it to produce ATP and satisfy their energetic demand (Taylor & McElwain, 2010). Due to their gradually increased addiction to O_2, metazoans evolved a highly sophisticated system to survive a state of reduced oxygen availability, defined as hypoxia, that manifests when oxygen supply do not satisfy cellular demand. Transcriptionally, the hypoxia-induced stress response is finely orchestrated by a group of transcription factors, known as hypoxia

inducible transcription factors (HIFs), encoded by a group of paralogue genes that are restricted to metazoans (Loenarz *et al*, 2011; Graham & Presnell, 2017). HIFs are oxygen-labile proteins that are specifically activated at low oxygen conditions. However, it is not possible to univocally establish oxygen cut-off values for HIFs activation and define the partial oxygen pressure (pO_2) that distinguishes normoxic from hypoxic tissue microenvironments. This is because human tissues are exposed to different pO_2 ranging from 13.5 % in pulmonary alveoli during inspiration, to 1-7% in other tissues like the bone marrow (McKeown, 2014; Spencer *et al*, 2014). Therefore, the 20-21% pO_2 commonly adopted in *in vitro* settings actually represents a non-physiological hyperoxic situation, and what many refer to as hypoxia rather reflects physioxia (McKeown, 2014). Cellular adaptation to hypoxia is crucial both in physiology and cancer, so that such capability is widely considered as a hallmark of cancer (Hanahan & Weinberg, 2011). Consistently, cancer cells rely on HIFs to drive the expression of genes involved in metabolic reprogramming, neo-angiogenesis, and survival (Keith & Simon, 2007). In the following section, I will summarize the molecular structure, the regulation and the transcriptional program driven by HIFs, with particular attention to how cancer cells take advantage of HIFs to survive hypoxic stress.

1.3.2 The molecular structure of HIF proteins

HIF transcription factors are basic helix-loop-helix (bHLH) DNA binding proteins belonging to the PER-ARNT-SIM (PAS) family of proteins (Wang & Semenza, 1993). HIFs consist of heterodimeric complexes composed by two subunits: an α subunit (HIFα), and a β subunit (HIF1β also known as ARNT) that coevolved during metazoan diversification (Graham *et al*, 2017). Notably, HIFα subunits are oxygen-labile, whereas HIF1β is not subjected to oxygen-dependent regulation (Gu *et al*, 1998; Wang & Semenza, 1993; Tian *et al*, 1997; Wang *et al*, 1995). In humans, three paralogs encode HIFα subunits called HIF1α, HIF2α or EPAS1 and HIF3α and two paralogs exist for HIF1β subunits (ARNT and ARNT2) (Graham *et al*, 2017) (Figure 6).

In hypoxic conditions, HIFα subunits heterodimerize with the 1β subunit to form a transcriptionally active complex (HIF1, HIF2 or HIF3) that binds the *cis*-regulatory consensus sequence 5'-(A/G)CGTG-3' known as hypoxia-responsive element (HRE) in

the enhancer and promoters of hypoxia-inducible genes (Mole *et al*, 2009; Smythies *et al*, 2019).

Since the bHLH domains of HIF1α and HIF2α share 85% identity, they are able to bind indistinguishable DNA sequences (Tian *et al*, 1997). The DNA binding domain of HIF3α is less conserved (52-58% identity), suggesting a more divergent activity of this subunit (Dengler *et al*, 2014).
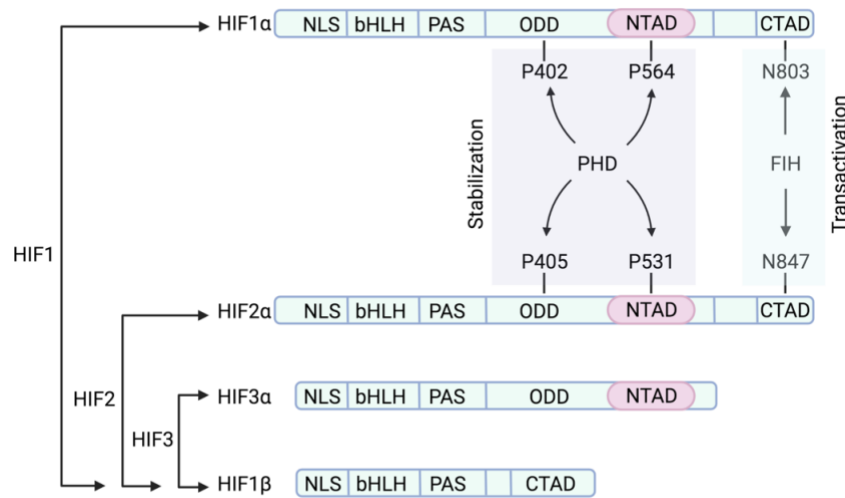
Figure 6. Protein structure and oxygen-dependent modifications regulation of HIF transcription factors. The N-terminal region is shared among HIF subunits and it is characterized by the presence of a nuclear localization signal (NLS), and bHLH and PAS domains that mediate DNA binding and heterodimerization, respectively. The C-terminal half of HIF1α and HIF2α consists of an ODD domain, and two TADs (NTAD and CTAD. The ODD and TAD domains orchestrate oxygen-dependent regulation and transcriptional activation respectively. In the ODD domain, P402 and P564 of HIF1α and P405 and P531 of HIF2α are hydroxylated by members of the prolyl hydroxylase (PHD) family of enzymes that modulate their post-translational stabilization. In the CTAD, N803 within HIF1α, and N847 of HIF2α, are hydroxylated by the Factor Inhibiting HIFs (FIH), which regulates their transactivation. HIF3α and HIF1β have only a single NTAD domain, and in HIF1β the ODD is lacking.

From a molecular point of view, HIF1α HIF2α and HIF1β subunits are the most extensively characterized. The N-terminal region is conserved among HIFs subunits (Figure 6) and contains the NLS, flanked by the bHLH DNA binding domain, and two PAS domains (PAS-A and PAS-B) mediating heterodimerization with HIF1β (Wang & Semenza, 1993; Wang *et al*, 1995). The C-terminal regions of HIFα subunits contain an oxygen-dependent degradation domain (ODD) that is crucial for the post-translational

stabilization of the α subunits in hypoxia, as described later. Conversely, HIF1β is devoid of the ODD and is not subjected to oxygen-dependent regulation. Moreover, HIFα contain two trans-activation domains (TAD) known as N- and C-terminal TADs (NTAD and CTAD respectively). The NTAD overlaps with the ODD (Jiang *et al*, 1996; Huang *et al*, 1998), whereas the CTAD falls outside. In contrast, HIF1β contains the CTAD only, whereas HIF3α contains the NTAD exclusively (Maynard *et al*, 2003). As it will be discussed more extensively later, TADs are essential for the regulation of HIFα transcriptional activity and target gene selectivity, suggesting that HIF1α and HIF2α are not functionally redundant and that they orchestrate unique transcriptional programs in response to hypoxia (Lendahl *et al*, 2009).

1.3.3 The oxygen-dependent regulation of HIFα subunits

In normoxic conditions, cells continuously transcribe, translate and degrade HIF proteins, in order to guarantee a constant supply of HIFs to promptly face hypoxic stress. The HIFα degradation pathway is regulated by a system of cellular oxygen sensors, that mediate both HIFα post-translational modification and transactivation.

HIFα degradation is initiated by a family of prolyl-4-hydroxylase (PHD1-4, most prominently PHD2/EGLN1), which are dioxygenase α-ketoglutarate dependent enzymes (Appelhoff *et al*, 2004; Berra, 2003). When oxygen is available, PHD2 hydroxylate Pro-402 and Pro-564 or Pro-405 and Pro-531 in the ODD domain of HIF1α and HIF2α respectively (Figure 6). Hydroxylated proline residues serve as binding sites for the von Hippel Lindau protein (pVHL) E3 ubiquitin ligase complex that directs HIFα proteasomal-mediated degradation (Huang *et al*, 1998; Jaakkola *et al*, 2001). Under hypoxia, PHDs do not hydroxylate HIFα subunits due to the lack of substrate and HIFα heterodimerizes with HIF1β to run the hypoxic transcriptional response.

Notably, HIFα subunits are subjected to another regulatory hydroxylation event occurring on asparagine residues (Asn803 on HIF1α and Asn851 on HIF2α) within the CTAD. This reaction is catalyzed by the factor inhibiting HIF (FIH) (Lando, 2002; Mahon, 2001) (Figure 6) that restrains the trans-activation of HIFα subunits by inhibiting recruitment of the transcriptional co-activator (CBP/p300) (Dames *et al*, 2002). Importantly, FIH has a higher affinity than PHDs for O_2 and is active at lower pO_2 than

PHDs, indicating that that the activity of HIFα may still be inhibited after their stabilization until O_2 levels drop under a lower threshold (Bracken *et al*, 2006).

1.3.3 Regulation of HIFα subunits by pseudohypoxic pathways

HIFα were firstly identified as mediators of the hypoxic response but accumulating evidence demonstrates that HIFα can be activated via multiple hypoxia-independent pathways acting at different steps of their degradation process (Hayashi *et al*, 2019). This condition is defined as pseudohypoxia, as it mimics the hypoxia-mediated transcriptional response (Iommarini *et al*, 2017; Hayashi *et al*, 2019), and is particularly evident in cancer downstream activated oncogenes, loss of tumor-suppressors or growth factor hyperstimulation (Hanahan & Weinberg, 2011).

The most relevant examples of hyperactivated pathways that activate HIFα in cancer are PI3K/Akt/mTOR, ERK/MAPK and JAK/STAT (Iommarini *et al*, 2017). The STAT3 transcription factor can directly boost HIF1α expression (Xu *et al*, 2005; Niu *et al*, 2008); PI3K/Akt/mTOR stimulation leads to increased HIF1α mRNA translation by phosphorylation of the eukaryotic translation initiation factor eIF4E (Zhong *et al*, 2000; Laughner *et al*, 2001), shifting the balance between protein synthesis and degradation and leading to HIF1α accumulation; ERK/MAPK signaling leads to phosphorylation of the p300/CBP co-activator complex thereby trans-activating HIF1α (Sang *et al*, 2003).

In addition, PHDs can be indirectly inhibited by mitochondrial disfunctions that occur in some tumors. For example, accumulation of oncometabolites like lactate, 2-hydroxyketoglutarate, succinate or fumarate compete with a-ketoglutarate for PHDs binding thus causing aberrant stabilization of HIFα (Sciacovelli & Frezza, 2016).

Other mechanisms that counteract pVHL activity are: HIF1α acetylation on K32 by SET7/9 and LSD1, which inhibits its recognition by PHDs (Kim et al., 2016); pVHL ubiquitination by WSB1 (Kim *et al*, 2015); binding of c-Myc to HIF1α to counteract pVHL recognition (Doe *et al*, 2012).

Finally, aberrant post-translational stabilization of HIFα upon inactivating mutations of the *VHL* gene is a genetic hallmark of clear cell renal cell carcinoma (ccRCC), and the functional consequence of pVHL loss-of-function on HIF1α and HIF2α activity will be discussed in the next session.

1.3.4 Cellular functions of HIFα subunits in cancer

Intra-tumoral hypoxia is a common feature of cancer, leading to the stabilization and activation of HIF transcription factors, which variously contribute to cancer progression. HIF1α has been studied more extensively, and it is well known that this transcription factor contributes to neo-angiogenesis, metabolic reprogramming, cell migration, epithelial-mesenchymal transition, and metastasis formation. Here, the contribution of HIFα subunits to cancer progression are briefly described.

1.3.4.1. Angiogenesis. Hypoxic or anoxic areas are frequently observed not only at early stages of tumor growth, when small lesions lack vascularization, but also in larger masses. In these regions, HIFs are stabilized and stimulate the expression of several angiogenic genes encoding soluble proteins that are released in the tumor microenvironment to act on endothelial cells, pericytes and vascular smooth muscle cells that express their receptors (Rey & Semenza, 2010). These include VEGF, SDF1, ANGPT2, PGF, SCF. Due to the massive secretion of pro-angiogenic factors, newly formed cancer blood vessels are highly disorganized and structurally abnormal (Carmeliet & Jain, 2011).

1.3.4.2 Cellular metabolism. Metabolic adaptation to hypoxia consists in a switch from cellular respiration to aerobic glycolysis (Al Tameemi *et al*, 2019). HIF1α is the main inducer of hypoxic metabolic reprogramming, by promoting the expression of several glycolytic enzymes and glucose transporters including GLUT1, LDHA, and PDK and PDH (Rey & Semenza, 2010). Moreover, thanks to the activation of *GYS1* expression, HIF1α redirects overabundant glucose toward glycogenesis (Xie *et al*, 2021). Notably, hypoxic cells display inefficient mitochondrial electrons transport chain, thus resulting in electrons leakage and generation of ROS (Waypa *et al*, 2016) that can stabilizes HIF1α HIF1α in turn acts as modulator of mitochondrial redox homeostasis, by decreasing oxidant production and increasing antioxidant scavenging. (Semenza, 2013; Nagao *et al*, 2019). In addition, HIF1α-dependent transcription of *BNIP3* and *MXI1* leads to mitophagy and suppression of mitochondrial biogenesis (Semenza, 2013). Mitochondrial activity is further attenuated by HIF1αthrough reprogramming of lipid metabolism. This consists in the up-regulation of fatty acid uptake and inhibition of fatty acid catabolism, by up-regulation of fatty acid binding proteins (FABP3 and FABP7) as well as inhibition

of enzymes involved in mitochondrial fatty acid α-oxidation, including MCAD and LCAD (Bensaad *et al*, 2014; Huang *et al*, 2014). Finally, HIF1α also regulates serine synthesis and one carbon metabolism by up-regulating *PHGDH* and *SHMT2* expression, concomitantly increasing NADPH generation ((Ye *et al*, 2014; Samanta *et al*, 2016)). In cancer and other proliferative tissues, decreased mitochondrial respiration leads to compensatory anaplerosis that fuels anabolic pathways, leading to macromolecule biosynthesis to produce biomass and sustain cell expansion (Cassim *et al*, 2020)

1.3.4.3 Metastatization. The metastatization process is the result of a series of events that ultimately lead to the colonization of tissues distant from primary tumor, that include: epithelial-to-mesenchymal transition (EMT), local invasion, intravasation, circulation in blood or lymphatic vessels, extravasation and metastatic niche formation (Schito & Semenza, 2016). Interestingly, several studies demonstrate that HIF1α is intimately involved in the regulation of all these processes. HIF1α promotes down-regulation of E-cadherin expression and up-regulation of the mesenchymal marker N-cadherin, accompanied by the loss of epithelial morphology, cell-cell, cell-matrix adhesion and polarity, and the achievement of motile and mesenchymal morphology (Loh *et al*, 2019). HIF1α downregulates E-cadherin by inducing expression of *SNAIL2*, *ZEB1*, *ZEB2*, *TWIST* and *TCF3* genes, transcription factors that activate the expression of mesenchymal markers to promote cell motility (Gilkes & Semenza, 2013). The invasion process consists in the active degradation of the extracellular matrix by the release of metalloproteinase, including *MMP2*, *MMP9*, *MMP14* and *PLAUR* that are HIF1α target genes (Gilkes & Semenza, 2013). Invasive cancer cells also remodel the extracellular matrix by secreting collagen modifying enzymes like PLOD1, PLOD2, LOX, LOXL2, LOXL4, P4HA1 and P4HA2, that are regulated by HIF1α (Schito & Semenza, 2016). This results in the stiffening of extracellular matrix that promotes local invasion (Gkretsi & Stylianopoulos, 2018). Intravasation is promoted by HIF1α–induced VEGF-A release that, beside stimulating angiogenesis, increases blood vessel permeability that is further enhanced by SDF1 production (Jin *et al*, 2012). Once cancer cells reach circulation, HIF1α confers resistance to anoikis by suppressing α5 integrin signaling (Rohwer *et al*, 2008). Extravasation of circulating cancer cells is mediated by the up-regulation and membrane exposure of adhesion molecules. HIF1α stimulates *L1* expression that

interacts with integrins, neuropilin-1 and CD24 expressed by endothelial cells (Zhang *et al*, 2012). Moreover, trans-endothelial passage is induced by HIF1αmediated *ANGPTL4* expression that inhibits endothelial cell-cell contacts (Zhang *et al*, 2012). The choice of secondary sites for colonization can be facilitated by tumor cells via establishment of a pre-metastatic niche. This is mediated by production of tumor-associated factors (TAFs) from tumor cells that recruit stromal cells from the bone marrow to sites of future metastasis, where they create niche remodeling collagen fibers (Psaila & Lyden, 2009). Among TAFs, LOX, LOXL2 and LOXL4 are regulated by HIF1α (Schito & Semenza, 2016).

1.3.4.4 Cancer stem cells maintenance. Cancer stem cells (CSCs), also known as tumor-initiating cells or tumor-propagating cells, are defined as cells within a tumor that similar to normal adult stem cells have self-renewal capacity and give rise to heterogeneous lineages of cancer cells that compose the tumor bulk (Keith & Simon, 2007). In breast cancer, HIF1α promotes the transcription of TAZ, a downstream effector of the Hippo pathway, that crucially regulates CSC activity (Samanta *et al*, 2014). Moreover, HIF1□ and HIF2α play important tumor-initiation capacity in glioma stem cells, as their targeting in mice transplanted with patient-derived CD133⁺ cells inhibited tumor development (Dhatwalia *et al*, 2018). Similar results were obtained in colorectal cancer cells, where knockdown of HIF1α decreased the expression of the stem cell marker Oct4 (Covello, 2006; Vadde *et al*, 2017). On the same line, HIF2 α promotes the activation of Oct4/SOX2 axis by transcriptionally regulating Oct4, enhancing c-Myc activity and stimulating CSCs propagation in glioma (Bhagat *et al*, 2016).

1.3.4.5 Immune evasion. HIF1α dependent metabolic reprogramming also contributes to inhibit anti-tumor adaptive immunity. In particular, glucose withdrawal by cancer cells, causes glucose deprivation for tumor infiltrating T cells that display decreased effector functions (Chang *et al*, 2015; Ho *et al*, 2015). Moreover, it has been reported that programmed death ligand PD-L1 is induced by HIF1α (Barsoum *et al*, 2014) and is required to inhibit T cell activation. Beside this, T cell effector functions are blocked by extracellular adenosine (Hoskin *et al*, 2008) generated by CD39 and CD37 that are both transcriptionally induced by HIF1α (Hatfield *et al*, 2014).

1.3.5 The unique roles of HIF1α and HIF2α in the hypoxic response

The fact that HIF1α and HIF2α share high structural similarity and recognize the same DNA sequence might suggest that these two transcription factors play overlapping functions in the regulation of the hypoxic transcriptional response, so that often many refer to these proteins as *isoforms*. However, they are encoded by two distinct *paralogue* genes, thus suggesting that they must have evolved to orchestrate unique, rather than redundant transcriptional responses. In line with this view, a number of studies revealed that HIFα subunits respond to hypoxic stress in a different fashion, they bind HREs located at different genomic sites and regulate the expression of unique target genes, thus suggesting that their response to hypoxia, as well as their role in cancer biology, is highly specific and only partially overlapping (Mole *et al*, 2009). Interestingly, a recent study investigating the pan-genomic distribution of HIFα across different cell types and under different exposures to hypoxia revealed that neither the degree nor the time of hypoxia exposure alters the occupancy of a given HRE and that HIF1α and HIF2α bind different DNA regions. Specifically, HIF1α binds preferentially promoter-proximal regions, while HIF2α mainly localizes onto promoter-distant and enhancers elements (Smythies *et al*, 2019). Moreover, it was demonstrated that HIFα binding to a given HRE is highly cell-type specific. Indeed, only 25% and 15% of HIF1α and HIF2α binding sites where shared among different cell lines, with the tendency of promoter-proximal regions to be the more conserved in comparison to the promoter-distal intergenic regions (Smythies *et al*, 2019). These data are consistent with the fact that at least 600 HREs have been found in the human genome, of which only 1% are bound by HIFα at any given time (Mole *et al*, 2009). Therefore, HRE binding depends on the cell type, thus expanding the cell-type specific landscape of hypoxic transcriptional response.

HIF1αand HIF2α are able to recognize identical HREs, thus raising the question about the mechanisms responsible for transcriptional specificity by HIF1α and HIF2α. A crucial molecular element that dictates target gene selectivity of HIFα factors is the NTAD. Indeed, although both transactivation domains of HIFα proteins are required to maximally induce target gene expression, it was demonstrated that the CTAD mediates the expression of common target genes (e. g. *PGK* and *GLUT1*), whereas the NTAD directs expression of HIF1α and HIF2α specific targets (Hu *et al*, 2003). Consistently,

through the generation of HIF1α/HIF2α hybrids, it was shown that *bona fide* HIF1α and HIF2α target genes were induced only by hybrids containing the NTAD belonging to HIF1α or HIF2α (Hu *et al*, 2003). Mechanistically, the NTAD mediates the HIFα interaction with specific transcription factors and co-activators like AP1, STAT3, CEBP and CREB for HIF1α and SP1, USF1 and ELK1 for HIF2α (Dengler *et al*, 2014). HIFα subunits also respond differently to hypoxia. HIF1α accumulates early upon severe hypoxia exposure ($pO_2<1\%$ and within 24 hours), while HIF2α accumulates at later time points ($pO_2<5\%$ and after 24 hours) (Koh & Powis, 2009; Magliulo & Bernardi, 2018). In line with this, HIF1α specific transcriptional programs mediates acute adaptation to hypoxia by promoting the expression of genes mediating glycolytic metabolism, pH regulation and apoptosis (Semenza 2013; Choudhry et al, 2018), whereas HIF2α activates genes involved in cell cycle progression, stem cell maintenance, EMT and invasion, and thus showing only partially overlapping functions with HIF1α (Baba *et al*, 2003; Covello, 2006).

Finally, HIFα subunits display different expression patterns, with HIF1α expressed ubiquitously, whereas HIF2α was originally reported to be restricted to endothelial cells (Tian *et al*, 1997). However, subsequent studies revealed that HIF2α is expressed by parenchymal cells in the brain, myocardium, kidney, pancreas and intestine (O'Rourke *et al*, 1999).

Taken together, the observations discussed in this section suggest that target gene selectivity of HIF1α and HIF2α is dictated not only by their molecular structure and interaction with transcriptional co-activators, but also by the cellular context in which they are expressed. As discussed in the next paragraph, the different functions of HIFα subunits are crucial in the context of renal cancer, where HIF1α and HIF2α specific transcriptional programs not only cooperate in tumor-promoting processes, but also appears to antagonize each other during tumor evolution.

1.4 Renal cell carcinoma

Renal cell carcinoma (RCC) represents the 15th most common type of cancer, accounting for 2.2% of all tumors diagnosed and 1.8% of all cancer-related deaths worldwide, and is a heterogeneous group of malignancies arising from different lineages within the nephron (Sung *et al*, 2021). The histopathological analysis of RCC allows its classification in four main subtypes: papillary (pRCC) Type I and Type II, chromophobe (ChRCC), oncocytoma, and clear cell renal cell carcinoma (ccRCC). 75% of RCC is represented by the ccRCC subtype, 10-15% comprises pRCC Type I and Type II, and only about 5% of renal cancer patients are ChRCC (Moch 2014).

Below, the molecular and morphological features of ChRCC, pRCC, and oncocytoma are briefly explained, while the genetic basis and molecular features of ccRCC will be described in greater detail in the following dedicated section.

1.4.1 Histologic classification of RCC

1.4.1.1 Chromophobe RCC (ChRCC). ChRCC are tumors at low malignant potential deriving form distal tubular epithelial cells. They show slow but persistent growth (Davis et al., 2012) and low risk of metastasis (5-6%) (Moch & Ohashi, 2021). Comprehensive genomic characterization of ChRCC identified *TP53* (32%) and *PTEN* (20%) as the most frequently mutated tumor-suppressor genes (Davis *et al*, 2014), and chromosomes 17 and 10 as most commonly deleted (Haake *et al*, 2016). Moreover, structural rearrangement of the *TERT* gene promoter are present in a subtype of ChRCC, leading to TERT overexpression (Davis *et al*, 2014). Morphologically, ChRCC cells are classically defined as "plant-like" displaying pale cytoplasm and thick cytoplasmic membranes. The tumor tissue presents sheets of cells separated by *septae* which may present hyalinized perivascular stroma (Moch & Ohashi, 2021).

1.4.1.2 Papillary RCC (pRCC). The cell of origin of pRCC is still controversial, but it is suggested to be distal tubular epithelial cells. pRCC is divided in Type I and Type II, with pRCC Type I being associated with *MET* missense mutations and Type II being characterized by *CDKN2A* silencing, *TFE3* gene translocations, mutations within *STED2* and germline alterations of the *FH* gene (Comprehensive Molecular Characterization of

Papillary Renal-Cell Carcinoma, 2016). pRCC show a typical papillary structure made by connective tissue organized in spindle-like structures covered by cuboidal small cells displaying basophilic cytoplasm (Type I) or by cuboidal large cells with eosinophilic cytoplasm (Type II) (Leroy *et al*, 2002).

1.4.1.3 Oncocytoma. Kidney oncocytoma is a benign kidney neoplasm arising from epithelial collecting tubular cells (Moch & Ohashi, 2021). Two oncocytoma subtypes have been defined, with diploid Type I characterized by *CCND1* gene rearrangements and aneuploid Type II showing frequent chromosome 1, X or Y, and/or 14 and 21 deletions (Joshi *et al*, 2015). These mutations converge into the alteration of mitochondrial functions, due to disruption of mitochondrial complex I (McIntyre & Hirsch, 2018). Indeed, oncocytoma is characterized by the accumulation of defective mitochondria and Type II may evolve in malignant ChRCC (McIntyre & Hirsch, 2018). Morphologically, oncocytoma appears as lobulated circumscribed lesions associated with edematous stroma. Oncocytoma cells are large with eosinophilic cytoplasm packed with mitochondria (McIntyre and Hirsh 2017).

In 2016 the World Health Organization published a new classification of RCC in which other rare tumor subtypes have been added: hereditary leiomyomatosis, renal cell carcinoma syndrome-associated RCC, succinate dehydrogenase-deficient RCC, tubulocystic RCC, acquired cystic disease-associated RCC and clear cell papillary RCC (Moch et al., 2016).

1.4.2 Clear cell Renal Cell Carcinoma (ccRCC)

ccRCC is the most common type of RCC, accounting for more than 75% of RCC cases in the adult population. ccRCC can be either sporadic or hereditary, in the latter case being associated with Von Hippel Lindau disease (Frew & Moch, 2015). It has been estimated that 50% of patients develop metastasis following 3-30 years from primary tumor removal, and that ~30% of individuals display metastatic disease at time of diagnosis (Turajlic *et al*, 2018).

The most striking morphological feature of ccRCC is the clear cytoplasm of cancer cells due to lipid and glycogen accumulation (Gebhard *et al*, 1987). As a matter of fact, ccRCC

tissue displays cells characterized by "clear" cytoplasm due to the dissolution and removal of cytoplasmic lipid droplets during routine tissue preparation for histopathological analysis. Lipidomic studies of human ccRCC specimens revealed that this morphological appearance reflects the extensive cytoplasmic accumulation of lipids like cholesterol and triglycerides (Saito *et al*, 2016; Qi *et al*, 2021; Xie *et al*, 2021). Besides lipids, also glycogen is responsible of the clear appearance of ccRCC cells, suggesting that glucose metabolism is deregulated in ccRCC. Since both lipid and glucose homeostasis are profoundly affected in ccRCC, this kind of cancer is currently considered a metabolic disease. Consistently, transcriptomic, proteomic and metabolomic studies of ccRCC revealed that the metabolic reprograming consists of: i) up-regulation of aerobic glycolysis and pentose phosphate pathway, *de novo* fatty acid synthesis, and glutamine and glutathione metabolism; ii) down-regulation of the tricarboxylic acid cycle, fatty acid β-oxidation and oxidative phosphorylation (Creighton *et al*, 2013; Hakimi *et al*, 2016; Wettersten *et al*, 2015; Neely *et al*, 2016). As previously mentioned, such metabolic reprogramming is mainly due to the up-regulation of a HIF1α mediated transcriptional program (Qi *et al*, 2021; van der Mijn *et al*, 2020). Indeed, the most common genetic feature of ccRCC is loss-of-function of the tumor-suppressor gene *VHL,* that occurs in 90% of sporadic ccRCC and leads to hyper-activation of HIFα transcription factors (Nickerson *et al*, 2008). Consistently with a direct involvement of HIF1α in regulating lipid metabolism, in a mouse model of low-grade human ccRCC it was recently demonstrated that HIF1α enhances the accumulation of lipids at early stages of disease, through a transcriptional program that promotes uptake of extracellular lipids (van der Mijn *et al*, 2020). Moreover, it was shown that HIF1α suppresses fatty acid catabolism in ccRCC cells via transcriptional repression of CPT1A, which regulates mitochondrial intake of cytoplasmic fatty acids, and that the rescue of CPT1A expression suppresses *in vivo* tumor formation (Du *et al*, 2017).

The biological and functional significance of glycogen and lipids accumulation in ccRCC cells is currently unknown, and has long been considered a side effect of HIF1α activation. However, lipid storage in cytoplasmic droplets was found to sustain ccRCC tumor growth by preventing ER-stress via a mechanism mediated by HIF2α (Qiu *et al*, 2015). Additionally, it was recently demonstrated that ccRCC cells are cholesterol auxotroph (they are unable to synthesize cholesterol), and that cholesterol withdrawal

severely compromises their proliferation (Qi *et al*, 2021). Conversely, glycogen accumulation seems to be dispensable for *in vitro* cell survival, and genetic manipulation of the glycogen metabolic pathway does not affect *in vivo* tumor maintenance, suggesting that this metabolite might accumulate as a secondary byproduct of increased glycolytic flux, due to *VHL* loss and aberrant activation of HIF1α (Xie *et al*, 2021).

1.4.3 The genetic basis of ccRCC

Copy number alteration analysis of human ccRCC samples performed by The Cancer Genome Atlas Consortium (Creighton *et al*, 2013) revealed that ccRCC is characterized by gross deletions and amplifications of large portions of chromosomal loci. In particular, chromosomes 3p, 13q, 17p and 14q undergo deletions, while 5q is amplified. More than 95% of ccRCC are genetically characterized by the chromosome 3p loss. Interestingly, this region contains three of the most commonly mutated tumor-suppressor genes in ccRCC: *VHL*, and the chromatin modifiers *PBRM1* and *BAP1* (Creighton *et al*, 2013). In addition, chromosome 3p contains other tumor-suppressor genes that are deleted with less frequency (*SETD2* and *KDM5*) (Creighton *et al*, 2013). Beside chromosomal deletion, *VHL* loss can occur via promoter methylation (Herman *et al*, 1994) or missense mutations (Razafinjatovo et al., 2016). Although the vast majority of sporadic ccRCC shows loss of *VHL*, biallelic inactivation of *VHL* is not a driver oncogenic event *per se*: pre-neoplastic lesions of VHL patients display pVHL negativity indicating that *VHL* loss is a necessary but not sufficient event for ccRCC oncogenesis. In addition, a small subset of sporadic ccRCC tumors (10%) do not display *VHL* inactivation (Beroukhim *et al*, 2009). In the last decade, several lines of evidence allowed the elaboration of a multistep model of ccRCC development (Brugarolas, 2014). In such model, *VHL* loss-of-function is defined as a classical two-hit process in which first one *VHL* allele undergoes mutations representing the first hit, then *VHL* is lost due to the deletion of 3p, which represents the second hit (Brugarolas, 2014). At this point, two mutually exclusive events may occur, leading to alternative outcomes of the pathology and different prognosis (Peña-Llopis *et al*, 2013; Brugarolas, 2014; Gu *et al*, 2017): i) *PBRM1* and *SETD2* mutations cooperate to tumorigenesis leading to low grade ccRCC development; ii) *BAP1* undergoes deletion and contributes to the development of high grade ccRCC (Brugarolas, 2014). Consistently, it was shown that concomitant deletion of *PBRM1* and *BAP1* is rare in

ccRCC indicating that such event might be functionally redundant, whereas *PBRM1* and *SETD2* mutations display high degree of co-occurrence (Peña-Llopis *et al*, 2013).

This model is further supported by studies on ccRCC animal models. 100% of *Vhl$^{\Delta/\Delta}$/Bap1$^{fl/\Delta}$* mice develop cancer at 11 months, whereas 87.5% of *Vhl$^{\Delta/\Delta}$/Pbrm1$^{\Delta/\Delta}$* models developed low grade ccRCC with higher median latency (8-13 months) (Gu et al., 2017).

Other common mutations in ccRCC (~28% of cases) involve the PI3K/Akt/mTORC1 pathway, like *PTEN*, *MTOR*, *PI3KCA*, *TSC2* (Creighton *et al*, 2013). In addition, less frequently mutated genes are *TP53* and *TCEB1* (Creighton *et al*, 2013), a component of the ubiquitin ligase complex responsible for HIFα degradation besides pVHL (Hakimi *et al*, 2016; Sato *et al*, 2013). Notably, *VHL* deletion and *TCEB1* missense mutations are mutually exclusive in ccRCC (Sato *et al*, 2013; Brugarolas, 2014). Therefore, the disruption of the E3 ubiquitin ligase complex recognizing hydroxylated HIFα subunits is subjected to high selective pressure in ccRCC development, suggesting that ccRCC cells strongly rely on HIFα activity.

Interestingly, the locus in which the HIF1α coding region resides (14q23.2) is often deleted or subjected to structural rearrangements in ccRCC suggesting that: i) HIF1α may play unusual tumor-suppressive functions in ccRCC (Shen *et al*, 2011); ii) HIF1α truncated variants with oncogenic functions may be generated (Swiatek *et al*, 2020). However, contradictory studies also reported that the HIF1α locus is not so frequently mutated in human ccRCC (Shenoy, 2020), and it is needed for ccRCC tumorigenesis in mouse models (Hoefflin *et al*, 2020). In conclusion, the specific tumor-suppressive or oncogenic properties of HIFs in the context of ccRCC is still under debate.

1.4.4 The roles of HIF1α and HIF2α in ccRCC

HIFs functions have been best characterized in the context of ccRCC, being this the prototypic model to study hypoxic signaling due to loss of *VHL*. As previously stated, *VHL* loss is the most common genetic event in ccRCC but it does not appear to be sufficient to promote tumorigenesis. Conditional *Vhl null* mice in proximal tubular epithelial cells develop preneoplastic lesions that do not further evolve in ccRCC (Rankin *et al*, 2006; Hou & Ji, 2018). Also, VHL patients with multifocal ccRCC display neoplastic lesions at a low rate in comparison to the number of sites displaying pVHL

loss (Mandriota *et al*, 2002), thus suggesting that other mutations are required to develop ccRCC (Harlander *et al*, 2017). One possible explanation is that HIFα activation represents a pro-tumorigenic event that facilitates tumor formation driven by other genetic alterations that arise later during ccRCC pathogenesis.

However, as previously mentioned, whether HIF1α displays oncogenic or tumor suppressive function in ccRCC is a debated issue. In ccRCC human cell lines, it was demonstrated that while HIF2α performs oncogenic functions by promoting the expression of pro-survival factors like VEGFA, cyclin D1 and TGFα HIF1α transcriptionally activates the pro-apoptotic gene *BNIP3* (Althaus 2006). This suggested that HIF1α may perform tumor suppressive functions while HIF2α is a ccRCC oncogene. In line with this hypothesis, genetic studies show that 14q deletions encompassing the HIF1α locus occur in ccRCC and positively correlate with worst patient prognosis (Mitsumori *et al*, 2002; Kaku *et al*, 2004; Alimov *et al*, 2004). Moreover, HIF1α expression is lost in many *VHL null* human ccRCC cell lines, in which HIF2α over-expression is conserved (Shen *et al*, 2011). These observations led to deeper investigations of HIF1α functions in ccRCC. HIF1α targeting by shRNA in *VHL null* cells expressing both HIF1α and HIF2α led to increased cell proliferation *in vitro* and *in vivo* (Shen et al., 2011), while HIF2α knockdown reduced tumor growth (Shen *et al*, 2011; Raval *et al*, 2005). Consistently, ectopic expression of wild type HIF1α in cells that have lost the endogenous gene led to growth suppression (Gordan *et al*, 2008; Biswas *et al*, 2010), whether the introduction of constitutively active HIF1α mutants did not increase tumorigenicity of *VHL* proficient cells (Maranchie *et al*, 2002).

However, whether HIF1α exerts tumor-suppressive or oncogenic functions in ccRCC is still a controversial issue, because of discrepancies between *in vitro* and *in vivo* studies. Several studies suggest that human ccRCC cell lines do not fully recapitulate the tumorigenic functions of HIF1α and HIF2α, which can be inferred only through mouse models of human ccRCC. Generation of the TRACK (TRansgenic model of Cancer of the Kidney) mouse model, consisting in *Vhl* proficient mice harboring constitutively active HIFα factors, showed that HIF1α promotes the early steps of tumorigenesis (Fu *et al*, 2011; Qi *et al*, 2021), while HIF2α stabilization in the same genetic background led only to abnormal glycogen deposition (Fu *et al*, 2013). Consistently, in subsequent studies

it was demonstrated that in the VpR transgenic mouse model (*Vhl*, *Trp53* and *Rb1* triple mutant mice) (Harlander *et al*, 2017), which mimics transcriptomic and proteomic signatures of human ccRCC, tumor formation is strongly dependent on HIF1α (Hoefflin et al., 2020), thus suggesting that *in vitro* cancer assays and xenograft mouse models do not fully recapitulate HIF1α properties, while experimental systems that model tumor initiation and progression uncover HIF1α pro-tumorigenic functions (Hoefflin *et al*, 2020). In line with this, recent evidence suggests that HIF1α is not a target of 14q deletion (Shenoy, 2020), and that the HIF1α locus might be rearranged to give rise to alternative HIF1α transcripts that are still functional in *VHL null* human ccRCC cell lines, in which they promote glycolytic metabolism (Swiatek *et al*, 2020). However, somehow in contrast with results obtained in transgenic mice, a syngeneic mouse model of ccRCC represented by the murine RenCa cell line, when *Vhl* was knocked out to increased metastatic potential, showed that HIF1α was necessary to promote metastasis by inducing EMT, while tumor growth was found to be HIF2α-dependent (Schokrpur *et al*, 2016). Therefore, the fine tuning of HIFα functions may favor distinct pro-tumorigenic processes as ccRCC evolves (Frew & Moch, 2015), although a conclusive understanding of its functions in ccRCC is still lacking.

In contrast, the function of HIF2α as an oncogene appears more widely accepted. Firstly, unlike HIF1α, pVHL-defective ccRCC consistently show increased HIF2α expression (Shen *et al*, 2011; Maxwell PH *et al*, 1999; Gordan *et al*, 2008), and HIF2α expression in pre-neoplastic lesions of VHL patients correlates with histologic evidences of imminent malignancy (Mandriota *et al*, 2002). Moreover, genome-wide association studies, revealed that HIF2α polymorphisms are associated with increased risk to develop ccRCC (Purdue *et al*, 2011). Notably, the small molecule PT2399 that selectively targets HIF2α and inhibits its heterodimerization with HIF1α, thereby abrogating HIF2α transcriptional activity, showed strong efficacy in tumor regression of patient-derived xenografts (PDX) (Chen *et al*, 2016a). Of note, inhibitor-resistant PDX models, showed higher HIF1α expression in comparison to HIF2α further suggesting that HIF1α might be oncogenic (Chen *et al*, 2016a; Shenoy & Pagliaro, 2018).

In trying to summarize this mass of data, it may be suggested that HIF1α and HIF2α play opposite roles on established ccRCC proliferation *in vitro*, while both transcription

factors are needed for *in vivo* tumorigenesis. A large body of literature shows that the opposite roles of HIF1α and HIF2α in ccRCC cell lines might be a downstream effect of their regulation of c-Myc activity (Li *et al*, 2020). Indeed, HIF1α antagonizes the pro-proliferative activity of c-Myc through a number of mechanisms: i) direct binding to c-Myc and competition with its co-activators MAX and SP1 (Koshiji *et al*, 2004) ; ii) increased expression of the c-Myc inhibitor MXI1 (Gordan *et al*, 2007); and iii) induction of c-Myc degradation by the proteasome (Zhang *et al*, 2007). In contrast, HIF2α enhances c-Myc activity, resulting in the transcriptional up-regulation of cyclins D1 and D2 that promote cell cycle progression (Gordan *et al*, 2007). This raises the possibility that a fine balancing of HIF1α and HIF2α expression directs cellular proliferation in ccRCC. In support of this, in early neoplastic lesions of VHL patients, HIF1α tends to be over-expressed in comparison to HIF2α whereas in more advanced tumor tissues HIF2α is up-regulated at the expense of HIF1α (Mitsumori *et al*, 2002; Kaku *et al*, 2004; Alimov *et al*, 2004). To explain the switch from HIF1α to HIF2α activity during ccRCC progression it has been proposed that hypoxia-associated factor (HAF) might play a role. HAF is a non-canonical ubiquitin ligase (Koh & Powis, 2009) that targets HIF1α for proteasomal-mediated degradation (Koh *et al*, 2011), while concomitantly promoting HIF2α transcriptional activity via cooperative binding to DNA sequences upstream the HREs of HIF2α target genes (Koh *et al*, 2015). By inducing HIF1α down-regulation while promoting HIF2α transcriptional activity, HAF switches the HIF balance towards HIF2α. Consistently, HAF over-expression leads to reduced expression of HIF1α target genes *CA9* and *DDIT4*, and to up-regulation of HIF2α dependent genes *PAI1, Oct3*/4, *NANOG* and *SOX2* (Koh *et al*, 2011), thus increasing tumor growth and metastasis dissemination in PDX models (Koh *et al*, 2015).

In summary, to reconcile the apparent opposite roles of HIFα genes in ccRCC pathogenesis, it may be speculated that HIF1α over-expression confers proliferative advantage in the early steps of tumorigenesis by promoting metabolic adaptation, but at some point during ccRCC evolution, tumor cells might need to acquire independency from HIF1α persistent activation and escape from its pro-apoptotic effects and they become addicted to HIF2α, which that sustains cell proliferation and cancer progression.

1. 4.5 Approved therapies for ccRCC

The standard of care of non-metastatic ccRCC tumors consists of partial or complete nephrectomy, which is associated with 70-90% 5-years disease-free survival rate (Sorbellini *et al*, 2005). However, due to the fact that symptoms appear at later stages of ccRCC progression, patients are frequently diagnosed with metastatic disease, in which the 5-year survival rate is reduced up to 13% (SEER, National Cancer Institute 2021). Before the introduction of molecular targeted therapies, metastatic disease was treated with systemic therapy based on immune modulators, including interferon γ and interleukin-2 with only slightly improvement on patient's outcome (Capitanio & Montorsi, 2018). Nonetheless, the evolving understanding in the molecular determinants involved in ccRCC pathogenesis allowed the identification of many druggable pathways, including VEGFA and mTOR, and other therapeutic strategies aiming to activate tumor infiltrating lymphocytes against cancer (Serzan and Atkins 2021). ccRCC tumors are enriched in tumor infiltrating CD8+ and CD4+ T cells (Chevrier *et al*, 2017), whose reactivity is directly inhibited by cancer cells by expression of CD80/86 and PDL-1 that inhibit T cells activation following binding to CTLA-4 and PD1 respectively (Zhang *et al*, 2021a). Recently, the American Food and Drug Association (FDA) approved immune checkpoints inhibitors for the treatment of metastatic ccRCC, including the PD-1 inhibitors nivolumab and pembrolizumab (Xu *et al*, 2017). The latter can be used alone or in combination with tyrosine kinase inhibitors (TKI) for metastatic ccRCC (Moreira et al., 2020). ccRCC is characterized by high intra-tumoral VEGF production because of HIFα hyperactivation, resulting in the formation of highly vascularized tumors (Shen & Kaelin, 2013). To target VEGF signaling in ccRCC TKI (sunitinib, pazopanib and cabozantinib) are used to antagonize VEGFR activity (VEGFR-TKI) (Serzan & Atkins, 2021). Importantly at the beginning of 2021, VEGFR inhibitors were FDA approved as first-line treatment for metastatic ccRCC (source: FDA web site. http://www.fda.gov/cder/approval/index.htm). In addition to VEGFR antagonists, other already FDA approved drugs for patients with advanced disease include mTORC pathway inhibitors, such as everolimus (in combination with the VEGFR antagonist, levantinib) (Verhaak, 2016), and temsirolimus (Kwitkowski *et al*, 2010).

Despite the combined treatment with pembrolizumab and VEGFR-TKI, a substantial group of patients do not respond, reflecting primary resistance to immune checkpoint

inhibitors. Thus, the identification of predictive biomarkers of response are urgently required (Moreira *et al*, 2020).

Interestingly, as reported in the previous section, HIF2α is a key oncogene in ccRCC pathogenesis, and its targeting may represent an appealing therapeutic opportunity for ccRCC patients (Cuvillier, 2017). Historically, inhibition of transcription factors has long be considered unfeasible due to their three-dimensional structure (Bushweller, 2019). However, a few years ago it was observed that HIF2α contains a large hydrophobic pocket within its PAS-B domain, which represents a potential binding site for small allosteric molecules (Rogers *et al*, 2013; Scheuermann *et al*, 2013). Since then, a great number of studies were conducted in a short time and led to the generation of the first HIF2α specific inhibitor that impedes its heterodimerization with HIF1β (Rogers *et al*, 2013; Scheuermann *et al*, 2013). A structure-based drug discovery approach by Peloton Therapeutics identified two HIF2α antagonists: PT2399 and PT2385, which were extensively evaluated *in vitro* and *in vivo* for their on-target effects (Chen *et al*, 2016a; Cho *et al*, 2016). Recently, given the great progress of HIF2αinhibitors in the treatment of ccRCC Peloton Therapeutics was purchased by Merk Group and, on the basis of results from a clinical trial (NCT03401788), the HIF2α inhibitor (Belzutifan) was FDA approved for the treatment of patients with VHL-associated RCC disease who require therapy for ccRCC (source: FDA web site. http://www.fda.gov/cder/approval/index.htm)

2. AIM OF THE WORK

The cellular functions mediated by the PML protein are of fundamental importance in cancer. Although PML has been originally described as a tumor suppressor in APL, its role in solid tumors is still controversial as PML has been described to play dichotomic (oncogenic or tumor-suppressive) roles in oncogenesis, indicating that its functions might be tissue- and cell-type specific. In the last decade a large amount of literature unveiled that PML is endowed with pro-tumorigenic functions in TNBC where it regulates pro-survival mechanisms and metastatic spreading (Carracedo *et al*, 2012; Martín-Martín *et al*, 2016; Ponente *et al*, 2017; Arreal *et al*, 2020). Metastasis regulation by PML was found, by our group, to occur via transcriptional co-activation of a subset of HIF1α-target genes (Ponente *et al*, 2017). HIF1α and its paralogue HIF2α, are aberrantly stabilized in ccRCC (Biswas *et al*, 2010), where they variously drive ccRCC pathogenesis. Also, unpublished preliminary evaluation of PML expression in renal cancer showed that PML is over-expressed in ccRCC tissues and cell lines. On these bases, we hypothesized that PML might play pro-tumorigenic functions in ccRCC, and that similarly to TNBC, this may be mediated by modulation of HIFα transcriptional activity. Also, the characterization of the role of PML in ccRCC will not only help us elucidate a previously unexplored involvement of PML in this tumor context, but also open new therapeutic opportunities for ccRCC treatment, by using ATO that is currently used as first line therapy in APL patients (Lo-Coco *et al*, 2013; Lo-Coco *et al*, 2016).

With these assumptions, we structured this project in three aims:

Aim 1 – Evaluate the pro-oncogenic and pro-metastatic role of PML in RCC and identify the PML-dependent transcriptional signature;

Aim 2 – Test the physical and functional interactions of PML with HIFα oncogenic proteins in ccRCC;

Aim 3 – Test the effect of PML pharmacological targeting with arsenic trioxide in ccRCC.

In addressing these questions, we aim to fill the following gaps of knowledge: i) to gain molecular insights into the role of PML in ccRCC, and ii) to assess the efficacy of ATO for ccRCC treatment in pre-clinical testing.

3. RESULTS

3. 1 Aim 1- Evaluate the pro-oncogenic and pro-metastatic role of PML in different RCC subtypes

It has been reported that the *PML* gene is expressed at variable levels in cancer tissues, displaying both down- and up-regulation. This evidence, strongly suggests a dual role of PML in tumorigenesis, either tumor-suppressive or tumor-promoting depending on the tumor context (Gurrieri *et al*, 2004; Carracedo *et al*, 2012a; Martín-Martín *et al*, 2016; Ponente *et al*, 2017; Arreal *et al*, 2020; Amodeo *et al*, 2017; Gentric *et al*, 2019).

In 2014, work investigating the post-translational regulation of PML via phosphorylation-induced proteasomal degradation reported that PML is down-regulated in ccRCC via inhibition of the protein phosphatase SCP1 (Lin *et al*, 2014). 36 ccRCC and adjacent normal kidney tissues were analyzed by immunohistochemistry (IHC), and PML was found significantly down-regulated with respect to normal tissue (Lin *et al*, 2014).

These data are in stark contrast to a preliminary and unpublished analysis performed in collaboration with Dr. Sabina Signoretti at the Brigham and Women's Hospital in Boston on 56 ccRCC samples and 5 normal kidney cortexes, where we detected up-regulation of PML in the majority of cancer samples, and correlation of high PML expression with Fuhrman nuclear grade, a predictor of aggressive disease (Figure 7 A-C).

Moreover, western blot (WB) analysis clearly showed that PML is over-expressed in a number of ccRCC cell lines when compared both to normal cells of kidney origin (i.e., HEK-293T cells), cancer cells where it was described as down-regulated (i.e., prostate cancer) (Bernardi *et al*, 2006), as well as tumor cells where PML was found highly expressed (i.e., chronic myeloid leukemia) (Ito *et al*, 2008) (Figure 7 D).

Therefore, we first aimed to: i) further test whether ccRCC is characterized by PML over-expression; ii) to evaluate the involvement of PML in ccRCC pathogenesis by performing *in vitro* and *in vivo* phenotypic characterization of a panel of human RCC cells in response to PML silencing; iii) to unravel PML-dependent transcriptional programs.
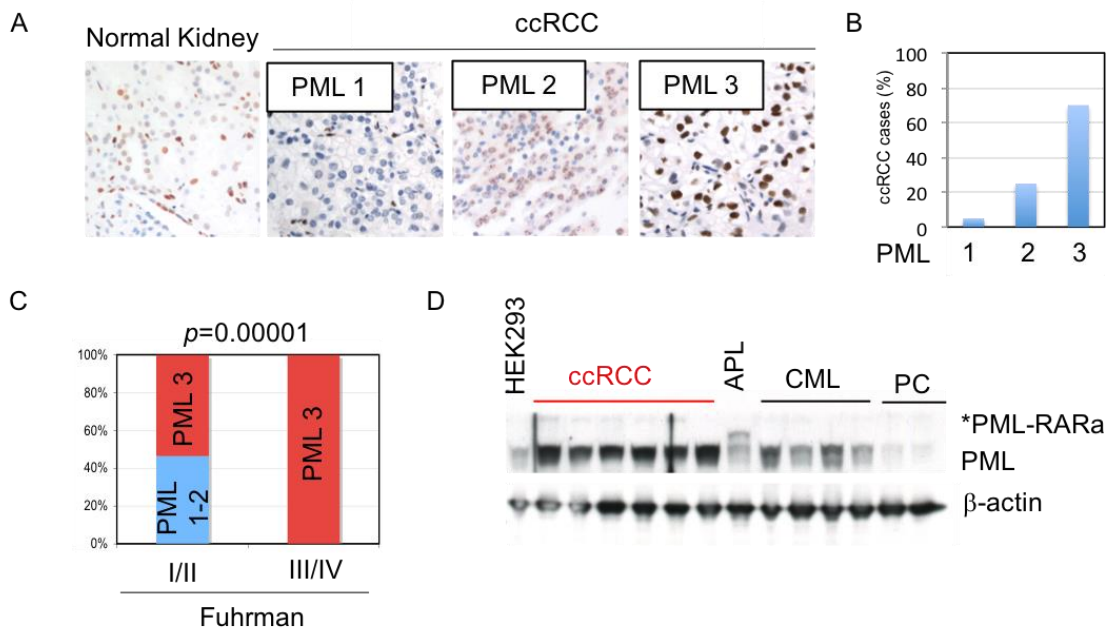
Figure 7. PML protein expression in ccRCC. (***A*** *and* ***B***) *Evaluation of PML expression in normal kidney cortex (n=5) and in ccRCC (n=56), representative examples of three expression levels. (****C****) Correlation of high PML expression with Fuhrman grade. (****D****) Western blot (WB) analysis of PML in the indicated cell lines. APL: acute promyelocytic leukemia; AML: chronic myeloid leukemia; PC: prostate cancer. The asterisk indicates expression of the PML-RARα fusion protein in APL cells. HEK-293 cells represent normal kidney cells.*

3.1.1 PML is over-expressed in ccRCC at mRNA and protein levels

To unbiasedly assess PML expression in ccRCC samples, we took advantage of available transcriptomic and proteomic data by The Cancer Genome Atlas and the Clinical Proteomic Tumor Analysis Consortium of the National Cancer Institute. Specifically, to get insights about *PML* mRNA levels, we consulted The Cancer Genome Atlas Kidney Renal Clear Cell Carcinoma (TCGA-KIRC) data set (Creighton *et al*, 2013), and to expand our examination we included The Cancer Genome Atlas Cervical Kidney Renal Papillary cell carcinoma cohort (TCGA-KIRP) (Creighton *et al*, 2013). To query for *PML* mRNA expression in ccRCC and pRCC data collections, we used the ULACAN on line tool (Chandrashekar *et al*, 2017). We found that PML mRNA was over-expressed in both ccRCC and pRCC samples, with a three-fold increase of Transcript Per Million (TPM) ($p<1\times10^{-12}$) in ccRCC (Figure 8A), and a two-fold increase of TPM in the pRCC group ($p<1.9\ 10^{-12}$) (Figure 8B), in comparison to the normal individuals. However, analysis of point mutations and copy number alteration of the *PML* gene by using cBioPortal (Cerami

et al, 2012; Gao *et al*, 2013) revealed that PML is mutated with very low frequency (0.25%) in ccRCC patients included in the TCGA-KIRK dataset (data not shown).

To understand whether the increased expression of PML mRNA corresponds to an over-expression of the protein, we interrogated the National Cancer Institute's Clinical Proteomic Tumor Analysis Consortium Kidney Renal Clear Cell Carcinoma dataset (CPTAC-KIRK) (Clark *et al*, 2019) by using the UALCAN tool (Chandrashekar *et al*, 2017). Consistently with transcriptomic data, we found that the PML protein is over-expressed in the CPTAC-KIRK group with respect to normal kidney tissue (Figure 8C). We did not evaluate PML protein levels in KIRP dataset because this was not included in the CPTAC data collection (Clark *et al*, 2019).
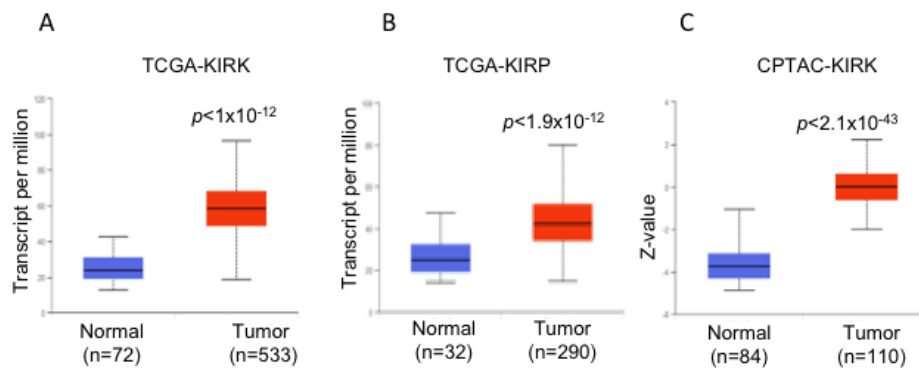
Figure 8. PML mRNA and protein expression in TCGA-KIRK and TCGA-KIRP data sets. PML mRNA abundance expressed as TPM in tumor (n=533) and normal (n=72) samples of the TCGA-KIRK datasets (A) and in tumor (n=290) and normal (n=32) samples of the TCGA-KIRP cohort (B). (C) PML protein levels in the CPTA-KIRK dataset including ccRCC tumor (n=110) and normal (n=84) tissues, are expressed as Z-value. Data shown in A-C were obtained from UALCAN.

3.1.2 PML over-expression correlates with unfavorable clinical outcomes in ccRCC

To test the clinical significance of PML over-expression in ccRCC and pRCC, we analyzed the expression of PML protein and primary transcript in ccRCC samples subdivided accordingly to tumor grade (indicated by Fuhrman nuclear Grade 1-4) (Figure 9A and B). PML expression does not increase along with tumor grade in these cohorts of patients (Figure 9A and B). Nonetheless, we found that PML represents an unfavorable prognostic marker in the TCGA-KIRK cohort (Creighton *et al*, 2013), as shown by the lower survival probability of patients displaying high expression of PML mRNA in

comparison with those displaying low/medium expression (*p*=0.013) (Figure 9C). In contrast, the survival probability of patients affected by pRCC does not correlate with *PML* expression levels, neither positively nor negatively (*p*=0.24) (Figure 9D).
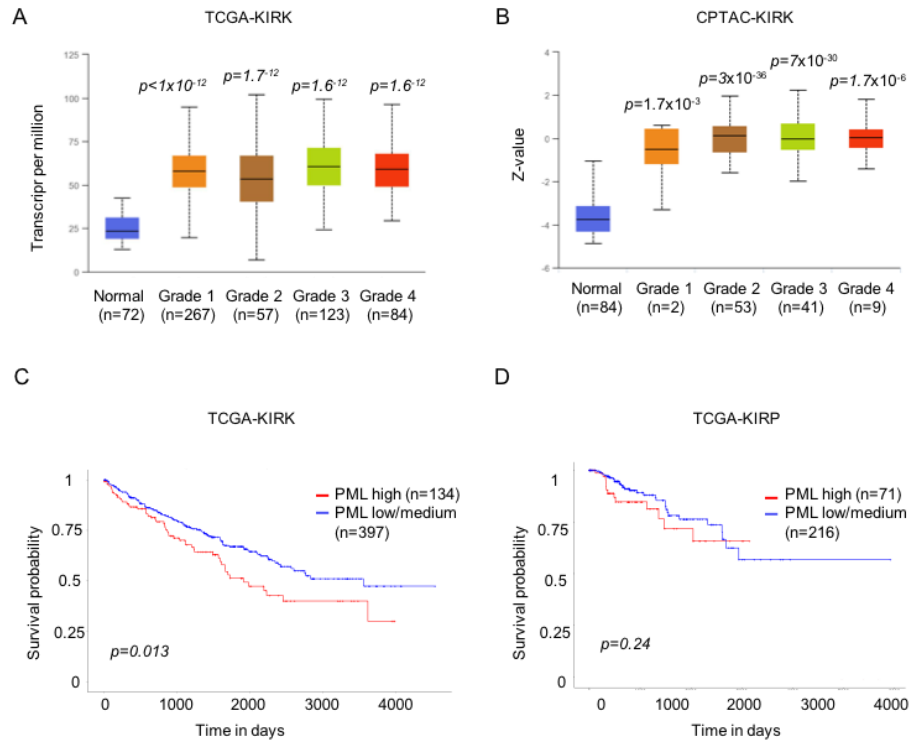
Figure 9. PML over-expression correlates with ccRCC bad patients prognosis. (A) Distribution of PML protein levels in ccRCC with different Fuhrman nuclear Grade in the TCGA-KIRK dataset. (B) Distribution of PML protein levels in ccRCC with different Fuhrman nuclear Grade in the CPTAC-KIRK dataset. (C and D) Kaplan-Meyer curves showing survival probability (time expressed in days) of patients affected by ccRCC (C) and pRCC (D) stratified on the basis of PML low/medium and PML high expression. TCGA-KIRK and KIRP data available on UALCAN online tool were used for the analysis.

In summary, preliminary data obtained from publicly available datasets indicate that PML is over-expressed in RCC patients, both at the mRNA and protein levels (Figure 8A and B). Also, PML expression levels positively correlates with bad patients' prognosis, specifically in the ccRCC subtype, where PML is overexpressed at higher levels than pRCC (Figure 8A and B). Thus, the expression and mutational profiles of PML in RCC patients led us to hypothesize that PML is required to sustain tumorigenesis and to speculate that, given the lack of significant mutational burden in the *PML* gene (data not shown), PML may be regulated downstream oncogenic pathways active in these tumor types. In this respect, in our laboratory it was previously demonstrated that PML is

positively regulated by HIF1α in hypoxic conditions and in TNBC (Ponente *et al*, 2017). Therefore, it is possible that at least part of PML upregulation occurs downstream activation of hypoxia responsive pathways in renal cancer.

3.1.3 PML plays a critical role in ccRCC proliferation, cell cycle progression, and colony formation capabilities

To investigate the role of PML in ccRCC, as a starting point we decided to characterize the phenotype of a panel of human RCC cell lines representative of pRCC and ccRCC in response to PML knock-down (Figure 10A). We selected the ACHN cell line as a model of pRCC. ACHN cells are VHL proficient cells in which HIFα are subjected to the oxygen-dependent pathway degradation. Three ccRCC cell lines were chosen as representative of the heterogeneous genetic background of the disease: i) Caki-1 cells, which are *VHL* proficient, express low levels of HIF1α and HIF2α and are subjected to oxygen-dependent regulation of HIFα proteins; ii) RCC4 cells, which are *VHL* null and constitutively express both HIF1α and HIF2α; iii) A498 cells, which are *VHL* null and express only HIF2α (Brodaczewska *et al*, 2016) (Figure 10A).

Initially, we sought to adopt constitutive lentiviral transduction of short hairpin RNA (shRNA) to knock-down PML expression. However, we observed that stable PML-silenced ccRCC cell lines could not be obtained, as after viral infection and selection we were not able to expand the populations of PML-silenced cells with a clear cell phenotype, while ACHN cells could grow *in vitro* even upon PML silencing (data not shown). We postulated that such dramatic response to PML constitutive knock-down represented a growth addiction of ccRCC cells to PML expression and that chronic and prolonged PML silencing was deleterious to ccRCC cells. Therefore, we applied a doxycycline-inducible system to suppress PML expression (Wiederschain *et al*, 2009), with the assumption that acute PML silencing induced by pulsing cells with doxycycline would be less impactful. On this basis, we transduced RCC cells with a shRNA against PML (hereafter as shPML) and with a shRNA with a scramble control sequence (hereafter shCtrl). As shown in Figure 10, 96 hours after doxycycline treatment, quantitative real time PCR (qRT-PCR) and WB analyses revealed that PML silencing was robust both at the protein (Figure 10B) and RNA level (Figure 10C) in all the cell lines examined.

A

Cell line	RCC type	VHL status	HIFα expression
ACHN	pRCC	+/+	HIF1α ; HIF2α
Caki-1	ccRCC	+/+	HIF1α ; HIF2α
RCC4	ccRCC	-/-	HIF1α ; HIF2α
A498	ccRCC	-/-	HIF2α
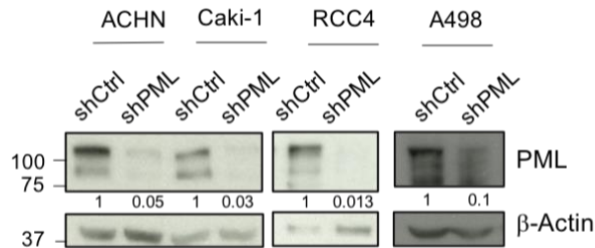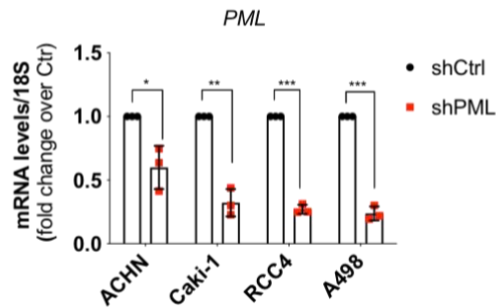
Figure 10. Validation of PML silencing in RCC cell lines. (A) Human RCC cell lines listed on the basis of RCC subtype, VHL status and HIFα expression. (B) WB showing PML expression in shCtrl and PML-silenced cells (ACHN, Caki-1, RCC4 and A498 cell lines) upon 96 hours of doxycycline incubation. β-Actin was used as loading control. Western blots are representative of three independent experiments of three biological replicates. Numbers represent densitometric analysis of bands intensity expressed as fold change over the respective shCtrl condition. (C) qRT-PCR showing PML mRNA relative expression following shPML expression induced by doxycycline. Data are expressed as mean ± SD of three independent experiments. Statistical significance was calculated with Student's t-test (*p<0.05, **p<0.01, ***p<0.001).

To understand the nature of PML dependency by ccRCC cell lines as evidenced by their response to PML silencing, we performed a series of phenotypic assays, including proliferation and focus forming assays in adherent conditions, and cell cycle analysis. As shown in Figure 11A, the proliferative rate of ACHN cells (belonging to the pRCC subtype) remained unchanged upon PML silencing. However, PML knock-down specifically affected the proliferation capability of ccRCC cell lines (Caki-1, RCC4 and

56

A498) (Figure 11A), suggesting that PML might exert pro-tumorigenic functions particularly in these RCC subtype. RCC cells were further challenged with a proliferation assay that measures the formation of foci of cancer cells starting from single cells upon plating at high dilution (focus forming assay). The increased stringency of this assay revealed that PML silencing also affected focus forming capacity of ACHN pRCC cells, although ccRCC cells were affected more profoundly (Figure 11B).
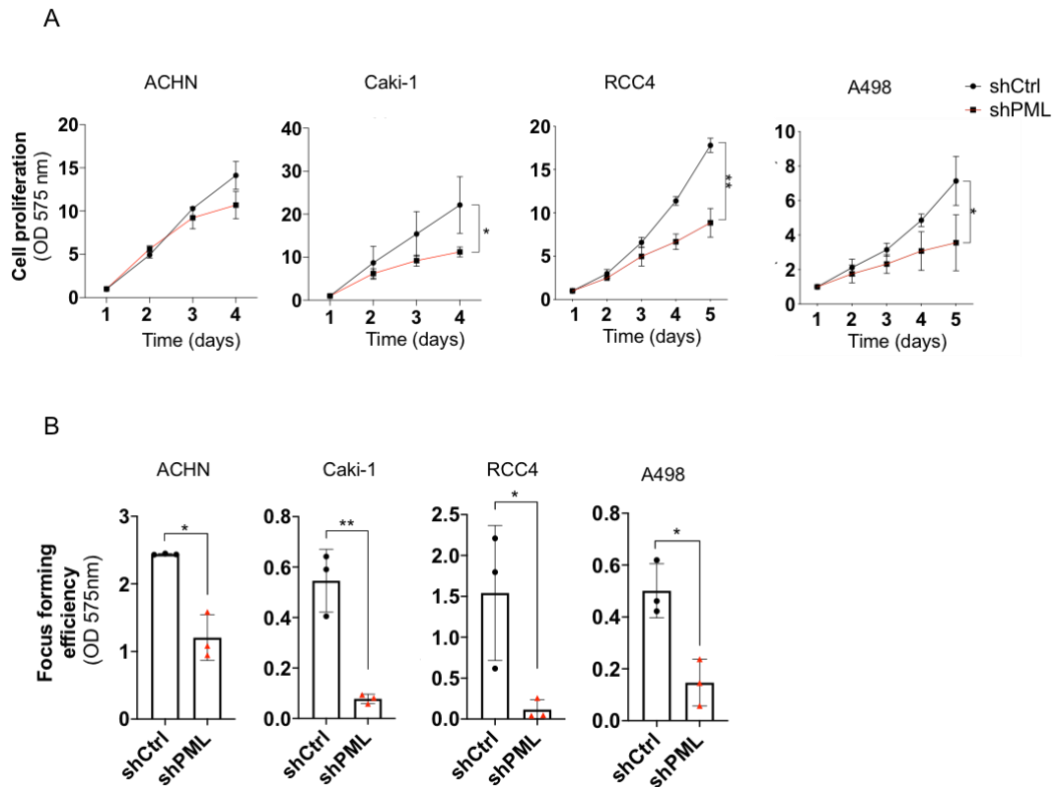
Figure 11. PML knock-down inhibits cell proliferation and focus forming efficiency of RCC cells. (A) Proliferation curves of the indicated RCC cell lines expressing shCtrl and shPML constructs upon incubation with doxycycline for the indicated time points. Values represent a ratio of crystal violet optical density (OD) at 575nm over day 1. (B) Focus forming assay performed in shCtrl and shPML RCC cell lines (14 days of culture). Focus forming efficiency was measured by crystal violet optical density (OD) at 575nm. Data represent the mean values ± SD of at least three independent experiments. Statistical significance was calculated with Student's t-test (*p<0.05, **p<0.01, ***p<0.001).

To understand if the reduced cell proliferation observed in response to PML knock-down was due to cell death, we evaluated the extent of apoptosis or necrosis by measuring the percentage of annexin positive cells and by trypan blue exclusion assay respectively. Surprisingly, we found that PML silencing did not induce apoptosis or necrosis in RCC cells (Figure 12A and B).
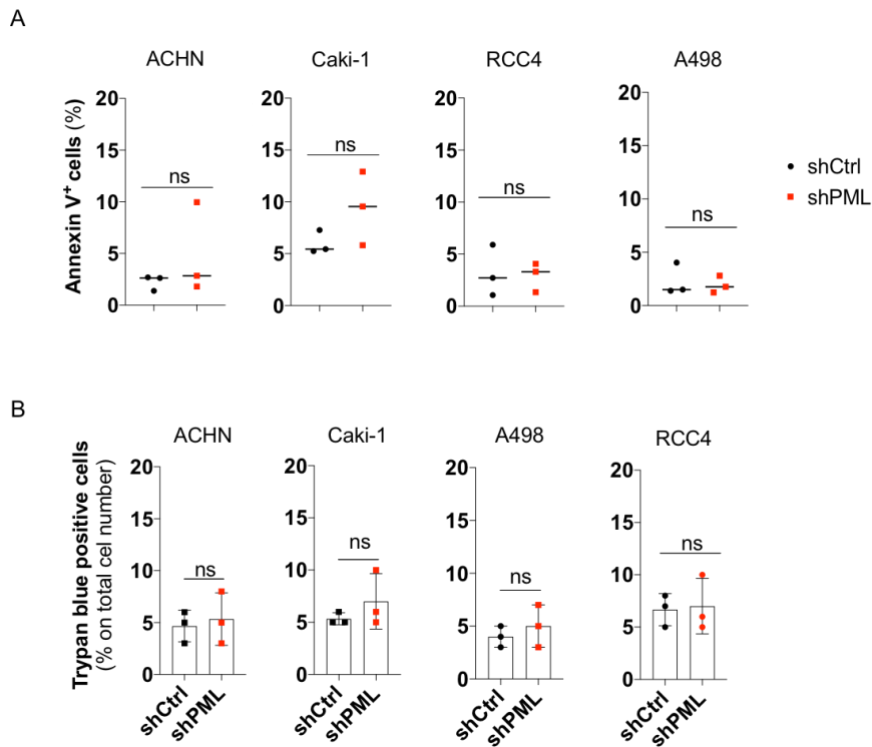
Figure 62. PML knock-down does not elicit cell death. *(**A**) Fluorescence activated cell sorting (FACS) analysis showing the percentage of Annexin V positive cells in shCtrl and shPML cells of the indicated cell lines. Data are presented as single values of each independent experiment and the bars represent the mean. (**B**) Trypan blue exclusion assay showing the percentage of trypan blue positive cells in shCtrl and shPML of the indicated cell lines. Data represent the mean values ± SD of at least three independent experiments. Statistical significance was calculated with Student's t-test (ns=p>0.05).*

Next, to understand whether reduced cell numbers upon PML knock-down was due to defects of cell cycle progression, we performed Bromo-deoxy Uridine (BrdU) uptake assays to identify actively proliferating cells in the S phase, coupled to Propidium Iodide (PI) staining to measure the percentage of cells distributed in G1 and G2/M phases. Interestingly, we found that all the ccRCC cell lines displayed ~50% increase in the percentage of cells in the G1 phase, indicating a severe growth arrest caused by PML silencing (Figure 13B-D). This phenotype was specific to ccRCC cell lines, as we did not detect any significant difference in cell cycle distribution in ACHN shPML cells (Figure 13A), in line with what we have previously observed, namely no reduced proliferation unless in challenging cell culture conditions of single cell growth.
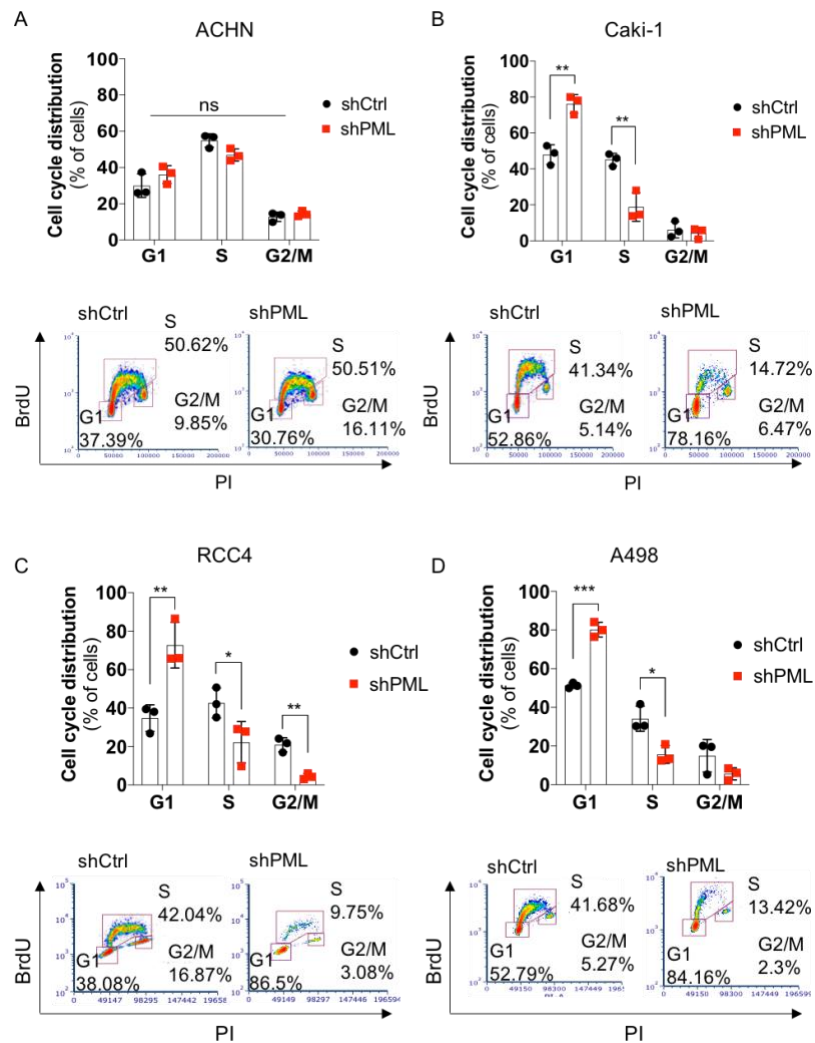
*Figure 13. PML expression sustains ccRCC cells cell cycle progression. FACS cell cycle analysis of ACHN (**A**), Caki-1 (**B**), RCC4 (**C**) and A498 (**D**) cell lines showing the percentage of cells distribution in cell cycle phases, following the induction of shCtrl and shPML constructs by doxycycline addition to culture media (96 hours incubation). Representative scatter plots are reported for each cell line. Bar plots show mean ± SD of three independent experiments. At the bottom, representative scatter plots are reported for each cell line. Statistical significance was calculated with Student's t-test (*p<0.05, **p<0.01, ***p<0.001).*

These results led us to speculate that PML might promote cell cycle progression and proliferation specifically in ccRCC cells, thus playing tumor-promoting functions in this tumor type. In order to corroborate these findings, and to convincingly demonstrate that PML regulates these processes, we used a second shRNA to knock-down PML expression (shPML#2) in RCC4 and A498 cell lines, which displayed the most significant phenotype in response to PML knock-down. Use of shPML#2 recapitulated all the results obtained with the other shRNA: impaired cell proliferation, diminished focus forming capacity and

cell cycle arrest, without impinging on cell survival on both RCC4 (Figure 14A) and A498 cells (Figure 14B).
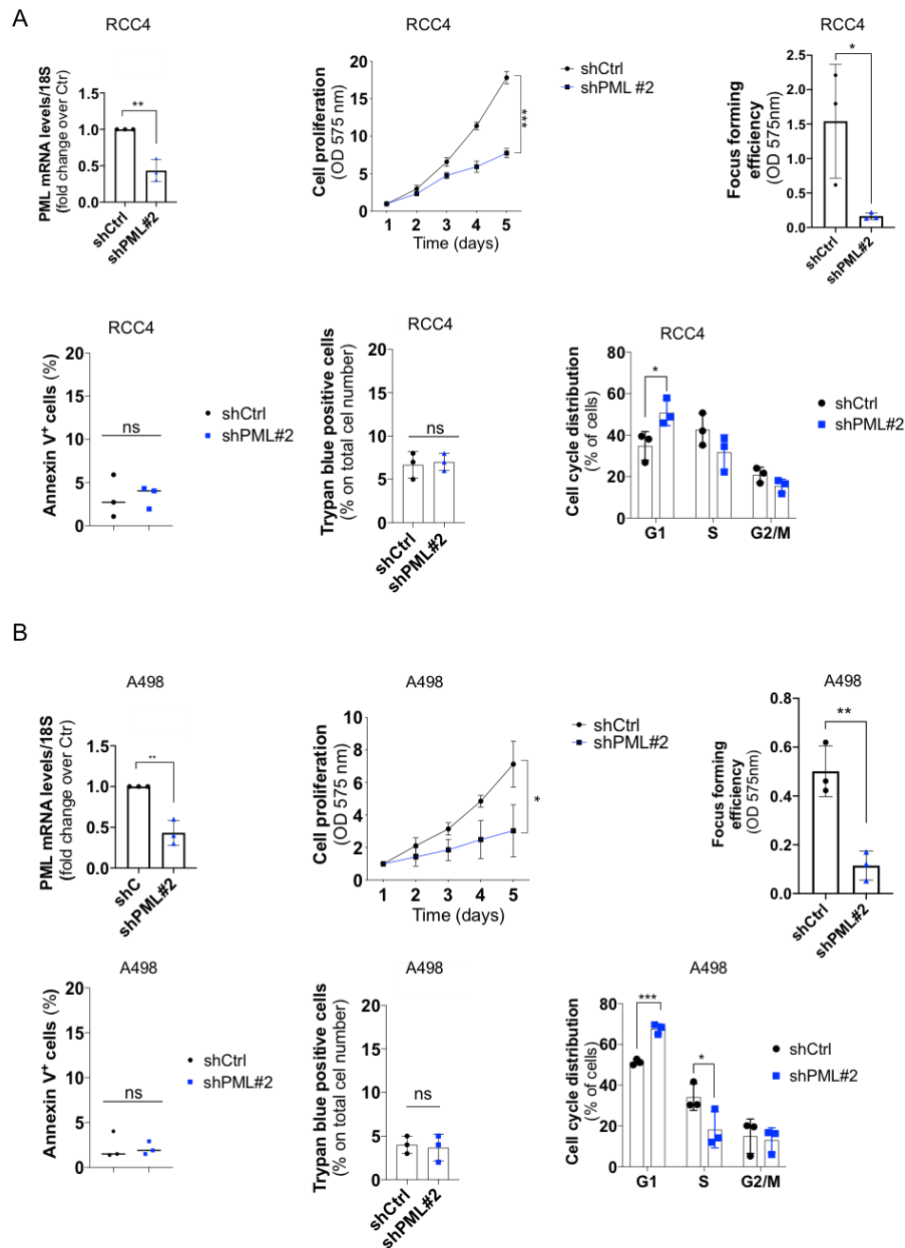
***Figure 14. Validation of PML pro-proliferative functions with a second shRNA. A** and **B** panels represent RCC4 and A498 cell lines respectively. From left to right: qRT-PCR showing PML expression following shPML#2 induction; proliferation curves. Values represent a ratio of crystal violet optical density (OD) at 575nm over day 1; focus forming assays (14 days of culture) measured by crystal violet optical density (OD) at 575nm; FACS analysis showing the percentage of Annexin V positive cells; trypan blue exclusion assay showing the percentage of trypan blue positive cells; FACS analysis showing the percentage of cell distribution in the cell cycle phases. In all experiments, cells were treated with doxycycline for 96 hours, Data are presented as single values of each independent experiment and the bars represent the mean. Statistical significance was calculated with Student's t-test (*p<0.05, **p<0.01, ***p<0.001).*

3.1.4 PML loss-induced cell cycle halt correlates with p53 and p21 up-regulation

At a molecular level, cell cycle progression is finely regulated by the action of cyclins and cyclin-dependent protein kinases, as well as their inhibitors, including p21, and checkpoint tumor-suppressor genes like p53 (Herranz & Gil, 2018). Because we found that PML is intimately involved in promoting cell cycle progression and cell proliferation in ccRCC cells, we evaluated whether the G1 arrest induced by loss of PML correlated with induced protein expression of p53 and p21. Interestingly, we observed that PML silencing led to a robust up-regulation of both p53 and p21 that was specifically conserved in ccRCC cell lines and not in ACHN cells (Figure 15). These results suggest that PML knock-down severely impairs cell cycle progression by up-regulating p53 and p21 in a cell-line specific manner.
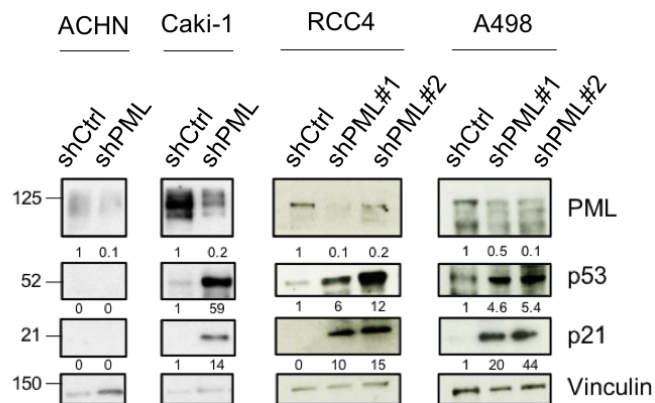
Figure 15. p53 and p21 expression is inhibited by PML in ccRCC cell lines. *WB analysis showing p53 and p21 protein expression upon PML silencing in ACHN, Caki-1, RCC4 and A498 cell lines. Vinculin was used as a loading control. WB are representative of three independent experiments. Numbers represent densitometric analysis of bands intensity expressed as fold change over the respective shCtrl condition.*

3.1.5 Ectopic PMLI over-expression in murine RenCa cell line promotes focus forming efficiency

To validate these findings via additional experiments, we planned to overexpress PML in a RCC model system that did not show constitutive PML over-expression. To this aim, we selected the murine ccRCC RenCa cell line where immunofluorescence (IF) experiments did not reveal PML overexpression, unlike in human ccRCC cells lines (Figure 16).
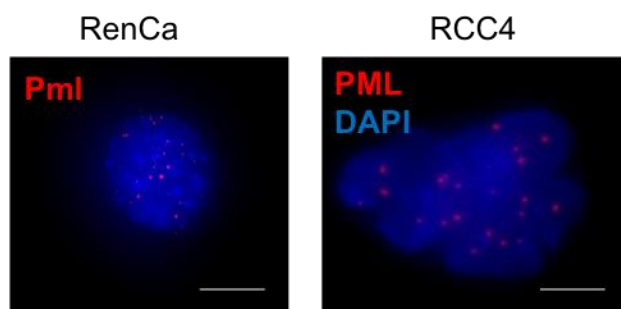
16. Murine RenCa cell line express Pml at lower levels in comparison to human RCC4 cell line. *Representative IF images showing murine Pml expression in RenCa cells and in human RCC4 cell line. 60x magnification, scalebar 1μm.*

To perform these experiments, we selected PML isoforms I and IV because accumulating evidence is revealing isoform-specific functions of PML in cancer. PMLI and PMLIV are the more extensively studied isoforms, and have been shown to exhibit at times opposite functions in certain type of tumors. Specifically, PMLIV over-expression in breast cancer cells leads to reduced cell proliferation and tumor-sphere formation, while PMLI elicits the opposite phenotype, resulting in cell expansion (Sachini *et al*, 2019; Alhazmi *et al*, 2020). With this in mind, we asked if PMLI or PMLIV over-expression may induce the opposite phenotype as compared to PML knock-down, namely promote cell proliferation and focus formation. RenCa cells were transfected with plasmids encoding PMLI-eGFP, PML-IV-eGFP, or eGFP alone and single cell sorting was performed to isolate GFP⁺ cells form the mixed population (data not shown) and obtain monoclonal cell lines stably expressing eGFP, PMLI or PMLIV. This approach allowed us to select only those clones showing low/moderate PML overexpression, with a number and size of PML-NBs that resembled endogenous PML in RCC4 that over-express the oncogenic protein (Figure 17B). These clones had to be carefully selected, as the majority of single cell clones displayed massive PML expression, with the formation of large PML-NBs that may induce artifactual results (not shown).

Thus, upon mild PML over-expression, we observed that both PMLI and PMLIV induced morphological remodeling of RenCa cell lines, which grew in a disordered manner in comparison to RenCa-eGFP cells and displayed a mesenchymal-like morphology (Figure 17A). Neither PMLI nor PMLIV over-expression induced significant changes in cell proliferation (Figure 17C and D), however RenCa eGFP-PMLI clones exhibited increased colony forming efficiency (Figure 17D), suggesting that even PML mild

overexpression promotes growth advantage in a ccRCC cell line and this is particularly evident when measuring single-cell induced proliferation. Moreover, in line with recent data in a breast cancer cell line (Alhazmi *et al*,2020), induction of ccRCC proliferation appear specific for PMLI, although we tested only 2 of the 7 PML isoforms. In sum, although preliminary, these data confirm that PML exerts pro-oncogenic functions in ccRCC and suggest that these functions may be isoform-specific.
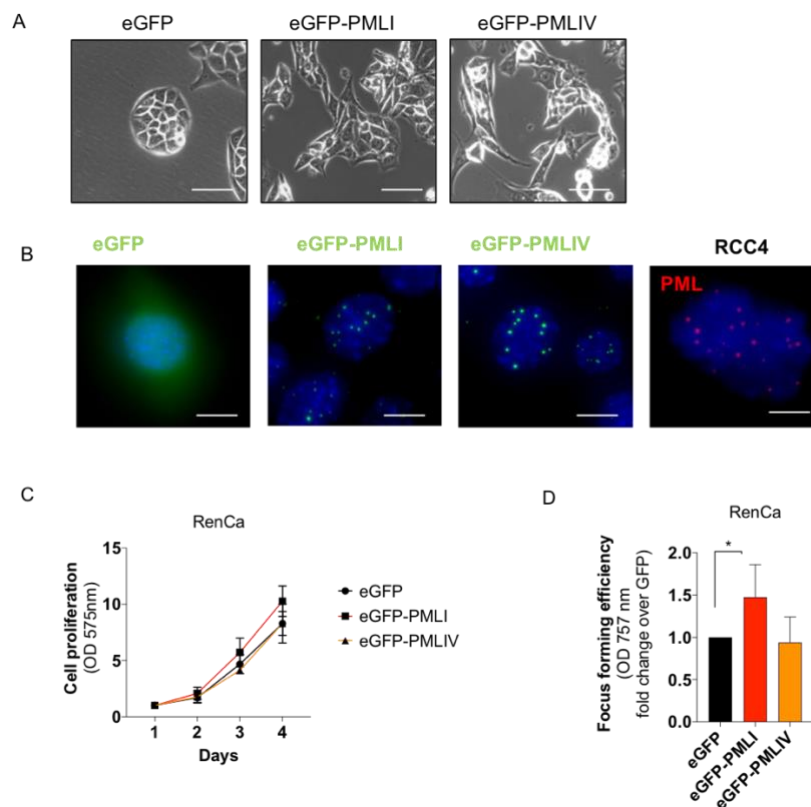
*Figure 17. PMLI and PMLIV over-expression in RenCa cells. (**A**) Representative images showing the impact of PMLI and PMLIV on RenCa morphology (20x magnification, scalebar 10 μm). (**B**) Representative fluorescence images showing the levels of eGFP expression in different RenCa clones and IF to detect endogenous PML in RCC4 cells (60x 1μm scalebar) (**C**) Proliferation assays of RenCa clones the indicated constructs. Values represent a ratio of crystal violet optical density (OD) at 575nm over day 1. (**D**) Focus forming assay showing colony forming efficiency of RenCa expressing the indicated constructs. Data represent the mean values ± SD of at least three independent experiments. Statistical significance was calculated by the Student's t-test (*p<0.05).*

3.1.6 PML knock-down leads to morphological changes reminiscent of cell senescence

When performing FACS analysis to measure cell cycle progression upon PML knock-down, we noticed that PML silencing also induced morphological differences that could

be visualized by flow cytometry. Specifically, all ccRCC cells displayed increased cell size (measured as forward scatter FSC-A values) and granularity (measured as size scatter SSC-A values) when compared to cells expressing a control shRNA. These observations are in line with a similar effect described when depleting PML from TNBC cells lines, where this phenotype was associated to the induction of cellular senescence (Arreal *et al*, 2020). Conversely, pRCC cells ACHN did not show significant differences in terms of cell size and granularity (Figure 18), consistently with a less severe impairment of proliferation and no major defects in cell cycle progression (Figures 11 and 13).
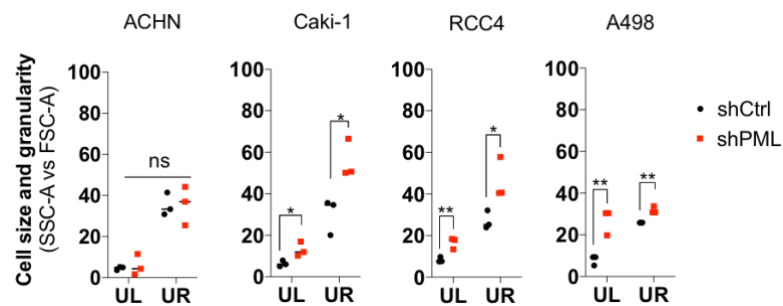
Figure 18. PML silencing leads to increased cell size and granularity of ccRCC cell lines. *Plots showing the distribution of cells in the upper left (UL) and upper right (UR) quadrants obtained following FACS analysis of physical parameters of cell granularity (SSC-A) and cell size (FSC-A). Data are presented as single values of three independent experiment and the bars represent the mean. Statistical significance was calculated with Student's t-test (*p>0.05; **p<0.01).*

Accordingly, the morphology of ccRCC cells appeared significantly changed upon PML knock-down, with the following common alterations in Caki-1, and more markedly in RCC4 and A498 cell lines: i) increased deposition of granular material in the perinuclear cytoplasmic space; ii) cell flattening; iii) appearance of vacuolar-like cytoplasmic structures (Figure 19A-C). Similar morphological alterations (increased cell size and granularity) in concomitance to cell cycle halt are typical features of senescent cells (Gosselin *et al*, 2009; Degtyarev *et al*, 2014). Moreover, increased intracellular granularity might result from increased lysosomal activity, which in senescent cells promotes recycling and degradation of cellular constituents (Gosselin *et al*, 2009; Degtyarev *et al*, 2014; Herranz & Gil, 2018). Therefore, we measured expression of senescence associated β-Galactosidase (SA β-Gal) by X-gal staining, which is an indicator of lysosome functionality in senescence cells (Dimri *et al*, 1995).
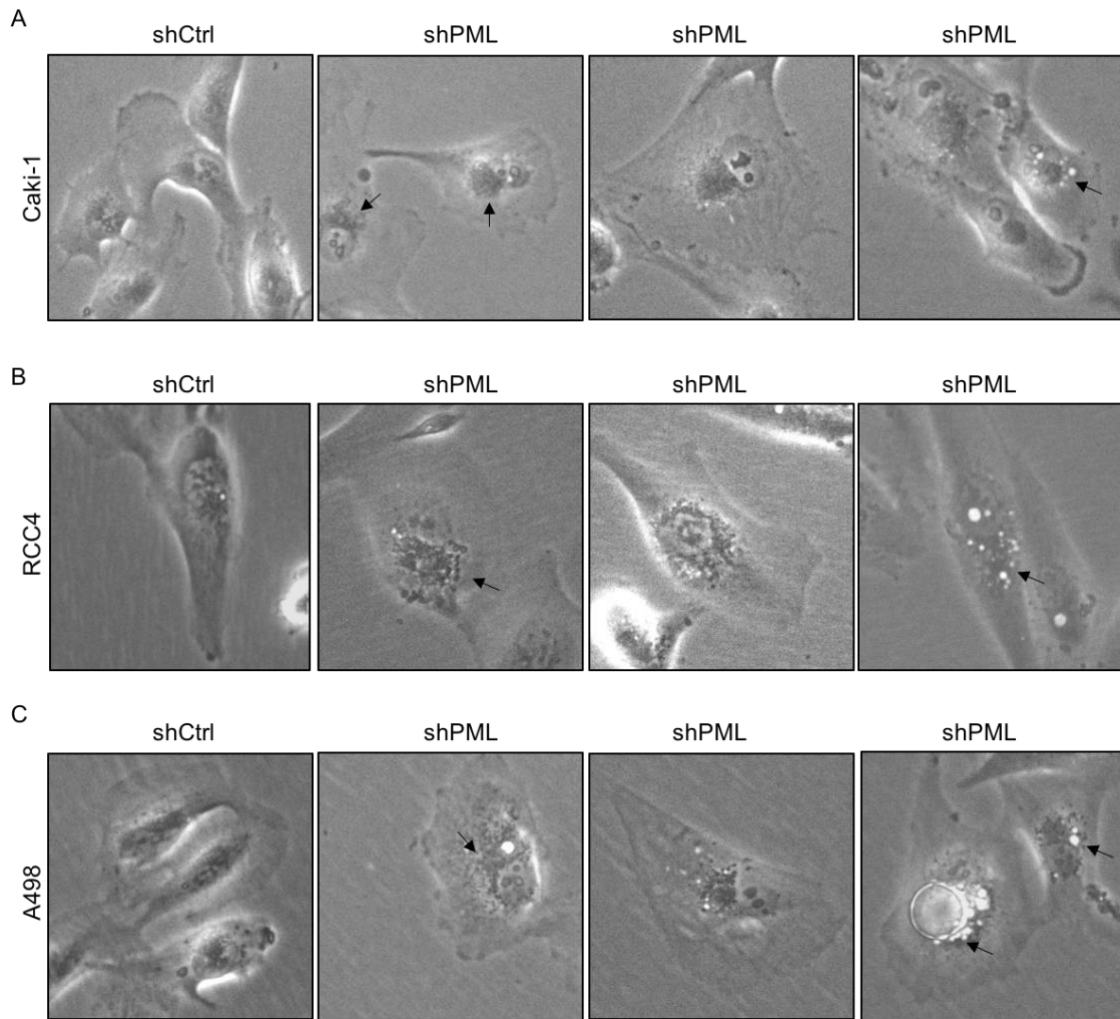
Figure 19. Morphological alterations in ccRCC cells following PML silencing. Representative light phase contrast microscopy images (20x magnification) of Caki-1 (A), RCC4 (B), A498(C) cell lines, following 96 hours of PML knock-down. (A-C) From left to right: shCtrl cells; shPML cells showing increased perinuclear deposition of granular material indicated by the arrows; shPML cells representative of cell flattening; shPML cells displaying the presence of vacuolar-like intracytoplasmic structures indicated by the arrows.

As a positive control, we treated shCtrl Caki-1, RCC4 and A498 cells with Nutlin-3 (hereafter Nut-3), a compound that stabilizes p53 and was reported to induce senescence in human ccRCC cells (Polański *et al*, 2014). Surprisingly, X-gal positive cells were not detected upon PML silencing, unlike upon Nut-3 treatment (Figure 20A-C).

To further assess induction of cellular senescence, phosphorylated γH2A.x (p-γH2A.x) was measured, as this is another marker of senescence (Rodier *et al*, 2011) and its deposition at DBSs was reported to increase following PML silencing in ovarian cancer cells (Liu *et al*, 2017). However, PML silencing did not induce p-γH2A.x foci in ccRCC

cells, which rather appeared depleted upon PML silencing in both RCC4 and A498 cells (Figure 21).
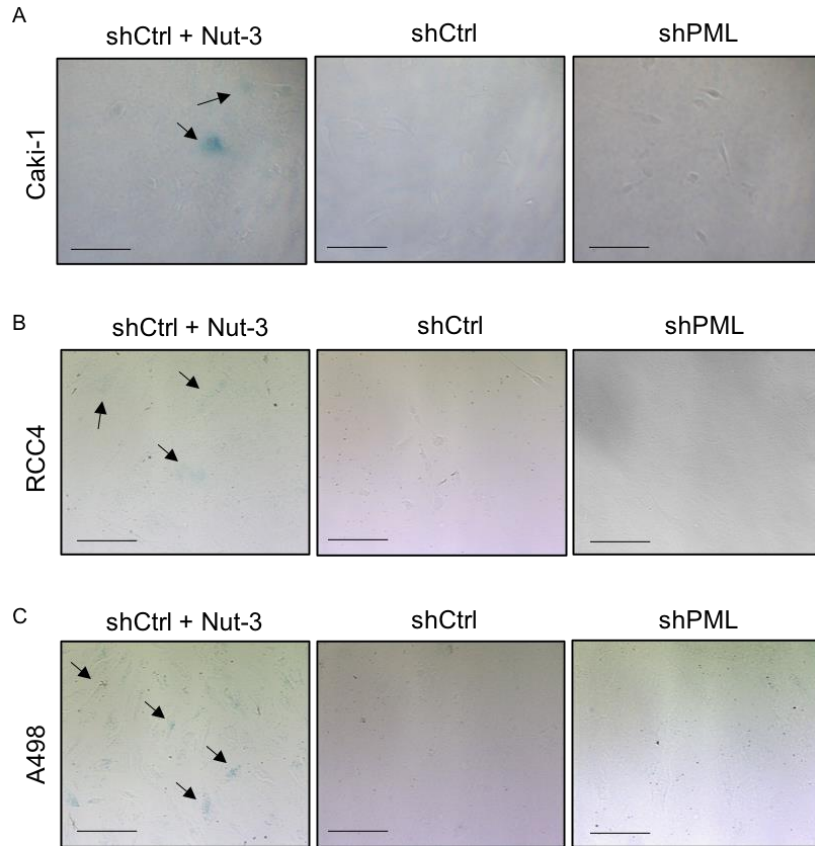
Figure 20. PML silenced cells are not SA β–Gal positive. *Representative images of X-gal staining (20x magnification, scalebar 20 μm) in shCtrl and shPML of Caki1 (**A**), RCC4 (**B**) and A498 (**C**) cells. SA β-Gal positive cells are indicated by arrows.*
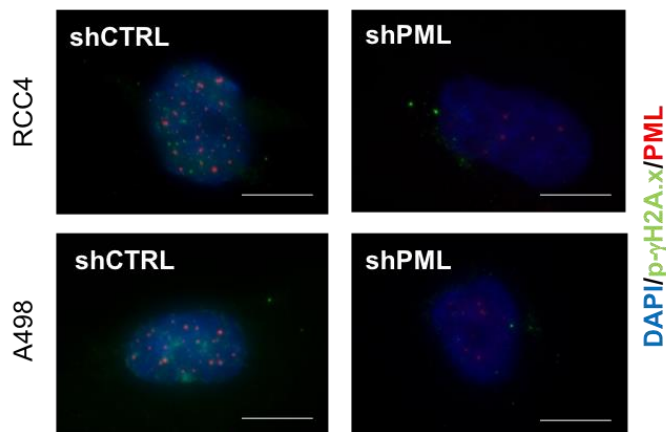
Figure 21. p-γH2A.x foci accumulation upon PML silencing. *Representative IF images of p-γH2A.x foci (green) in RCC4 and A498 cell lines following PML knock-down (60x magnification,*

scalebar 1μm). Cells were stained for PML (red) to visualize PML silenced cells. Nuclei were counterstained with DAPI (blue).

Taken together, these results indicate that although PML knock-down leads to a severe stall of the cell cycle, up-regulation of p53 and p21, and increased in cell size and granularity in ccRCC cell lines, this phenotype is not accompanied by classical markers of senescence, like accumulation of SA β-Gal positive cells and p- γH2A.x foci. These data are in contrast with a recently described phenotype occurring in TNBC cells upon PML depletion, where cell cycle inhibition was accompanied by features of senescence (Arreal *et al*, 2020).

3.1.7 Morphological analysis of PML silenced cells by transmission electron microscopy (TEM)

To better understand the nature of the granular deposits and vacuolar-like structures commonly observed by light phase contrast microscopy in ccRCC cell lines, we investigated cell morphology by transmission electron microscopy (TEM) in RCC4 and A498. Interestingly, we found that the ultrastructural intracellular architecture was profoundly affected in both RCC4 and A498 cells by PML silencing, with RCC4 and A498 shPML cells showing both common and cell-line specific features, that are summarized in Figure 22.

Observation	RCC4	A498
Lysosomes and other degradative structures	Increased	Increased
Membrane invaginations	Yes	Yes
Mirochondria	Big, swelled	-
Glycogen deposits	Increased	-
Lipid droplets	-	Increased
Endoplasmic reticulum	-	-
Golgi apparatus	-	-

Figure 22. List of common and cell type-specific ultrastructural alteration due to PML silencing observed in RCC4 and A498 cell lines. Increased number of lysosomes and degradative structures, together with the formation of large membrane invaginations, were observed in both cell lines. In addition, RCC4 shPML cells displayed bigger, swelled mitochondria, and increased glycogen deposits, in comparison to RCC4 shCtrl cells, while A498 cells had increased deposition of lipid droplets in comparison to A498 shCtrl cells. In both cell lines neither the endoplasmic reticulum, nor the Golgi apparatus were affected by PML silencing.

In particular, the common ultrastructural alterations found in RCC4 and A498 cells upon PML silencing included: i) an increased content of degradative structures, which may include phagosomes and lysosomes at different stages of maturation and processing of intra-organelle contents (Figure 23A and B, arrows); ii) formation of large invaginations of the cellular membrane that appear like intracytoplasmic organelles but are empty of intracellular contents (Figure 25, asterisks). Cell line-specific alterations were: i) appearance of swelled and big mitochondria (Figure 23A, asterisks), and increased glycogen deposition in RCC4 cells (Figure 26, arrows); ii) high presence of lipid droplets (LD) in A498 cells (Figure 27).
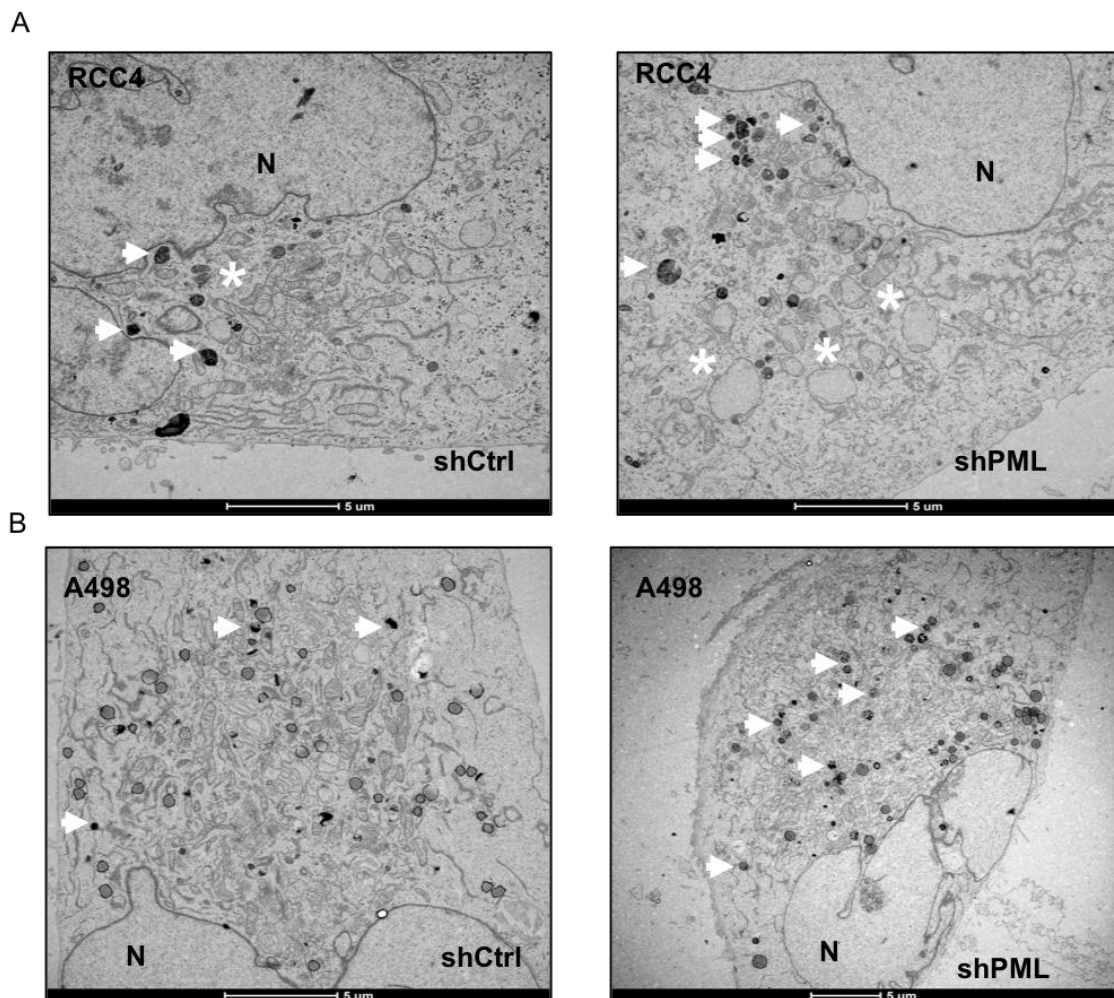
Figure 23. PML silencing leads to increased content of degradative structures in both RCC4 and A498 cells. Representative TEM images show increased number of degradative structures in both RCC4 (A) and A498 shPML cell lines (B) in comparison with shCtrl condition. Degradative structures are indicated by white arrows. Darker or lighter coloration indicates molecular density and different stages of the degradative process, with lighter organelles representing initial

Because TEM did not reveal any major difference in ER distribution and representation in either cell line, to evaluate whether the increase in perinuclear granular material that was observed by light phase contrast microscopy (Figure 19) was due to increased degradative structures, we performed immunofluorescence (IF) staining for the membrane lysosomal markers LAMP1 and LAMP2. Notably, LAMP1 and LAMP2 contents in RCC4 (Figure 24A) and A498 (Figure 24B) cells were severely increased upon PML silencing, and they displayed a perinuclear localization that is consistent with the location of the granular material observed by light contrast phase microscopy (Figure 19). These observations suggest that the increased granularity observed by microscopy as well as FACS analysis in ccRCC cells upon PML silencing may represent increased lysosomal content. This is consistent with previous reports showing that increased lysosomal content contributes to increase cytoplasmic granularity, measured by FACS analysis (Gosselin *et al*, 2009; Degtyarev *et al*, 2014).

Notably, IF staining of membrane lysosomal markers allowed to exclude that the intracytoplasmic vacuolar-like structures evident by light phase contrast microscopy (Figure 18) originate form lysosomes. Rather, as shown in Figure 24A, in RCC4 shPML cells LAMP2 positive lysosomes appear excluded and displaced from hollow cytoplasmic structures like the one marked with a white asterisk in Figure 24A, thus further revealing the presence of big and mysterious cytoplasmic vacuoles that appear empty and are not involved in the recycling and/or degradation of cellular constituents.

To attempt to understand the nature of these big cytoplasmic vacuoles appearing in both ccRCC cell lines in response to PML knock-down, we turned to a more detailed analysis of TEM images. In collaboration with electron microscopy and cellular anatomy expert Carlo Tacchetti of Vita Salute San Raffaele University, we concluded that these structures are unlikely to represent intracellular vacuoles, as they are empty of intracellular contents, are surrounded by a single membrane, and sometimes contain microvilli-like evaginations on their surface or at their interior (Figure 25). Therefore, we hypothesized that these structures represent profound cytoplasmic invaginations of the cell membrane that surround an empty space, which may perhaps give origin to complete invaginations that

become visible as large cytoplasmic vacuoles by light phase contrast microscopy (Figure 19). Interestingly, microvilli in the apical cytoplasmic membrane are a distinctive tract of
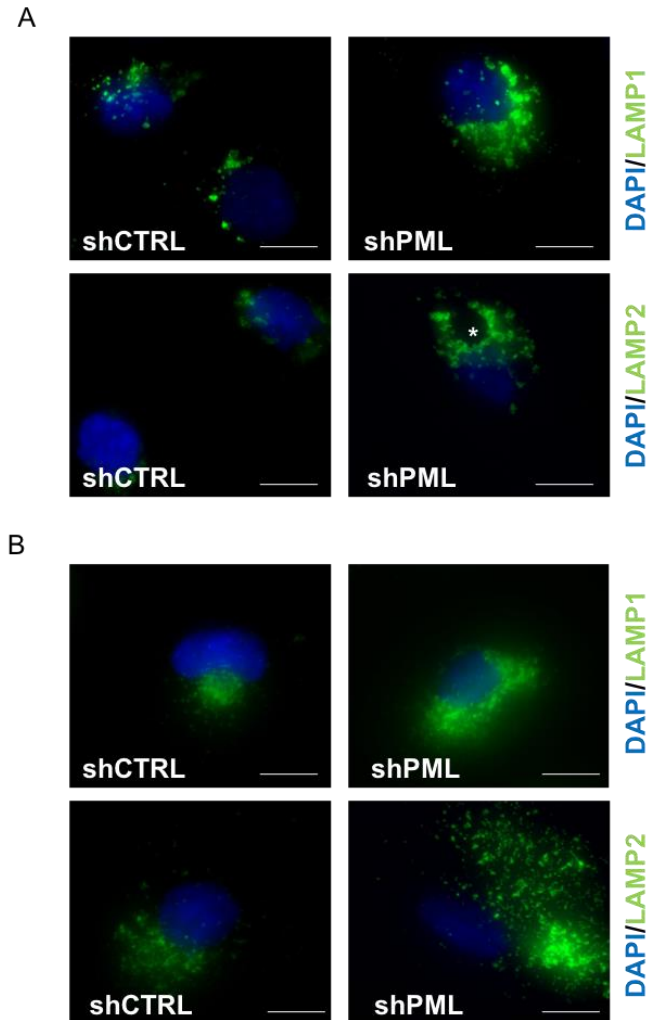
Figure 24. PML regulates lysosomal content in RCC4 and A498 cells. *Representative IF images of LAMP1 and LAMP2 (green) in RCC4 (**A**) and A498 (**B**) cell lines following PML knock-down (60x magnification, scalebar 1 µm). Nuclei were counterstained with DAPI (blue). Asterisk in (**A**) marks an intracellular vacuolar-like structure.*

kidney proximal tubular cells, epithelial cells specialized in absorption of water, ions and other organic nutrients including glucose, lactate and aminoacids (Verlander, 1998; Sekiya *et al*, 2013). These results led us to speculate that PML silencing might elicit a transition of RCC4 and A498 cells form an anaplastic state to a kidney proximal tubular epithelial-like morphology, in a morphological change representative of an aberrant differentiation process. However, a complete morphological characterization of these

structures cannot be derived from the analysis of a single cellular section, like the on obtained by TEM, or microscopy examination of cells by light phase contrast microscopy in 2D. Therefore additional types of studies will be necessary to define the complete morphological changes or ccRCC cells upon PML silencing.
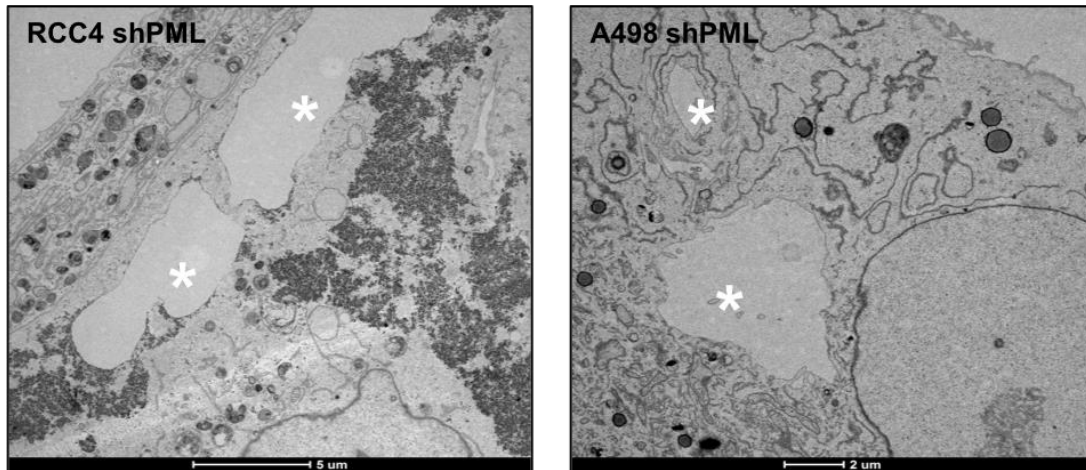
Figure 25. Membrane invaginations in RCC4 and A498 cells caused by PML silencing.
Representative TEM images showing the formation of gross and empty membrane invaginations
(indicated by white asterisks) in both RCC4 and A498 shPML cells.

Beside these common structural changes, as previously stated TEM analysis revealed that PML knock-down leads to cell line-specific alterations in RCC4 and A498 ultrastructural morphology. In particular, within RCC4 shPML cells we observed bigger, swelled mitochondria (Figure 23A, asterisks) and increased glycogen (Figure 26, arrows), in comparison to RCC4 shCtrl cells. Of note, glycogen deposits were found to distinctively accumulate in proximity of the membranes delineating the empty organelles that we have just discussed. Because glycogen deposits tend to accumulate proximal to the plasma membrane in hepatocytes and skeletal muscle cells, where they provide a storage site for internalized glucose (Prats *et al*, 2011) this observation further suggests that the empty intracellular vacuoles observed upon PML silencing derive from the cytoplasmic membrane, which is by definition in direct contact with the extracellular environment.

Finally, specifically in A498 cells, we found an increased number of LD, which are identified in TEM as small, homogeneously stained cytoplasmic vacuoles delimited by a dark membrane (Figure 27). To further validate that such effect existed and was specific for A498 cells, we performed Oil red O (ORO) staining to detect intracellular neutral lipids. Notably, ORO staining confirmed an increase in cytoplasmic LD following PML

knock-down only A498 cells, and further confirmed that these structures are excluded from, and are different from, the big vacuoles that characterize shPML ccRCC cell lines (Figure 28B).
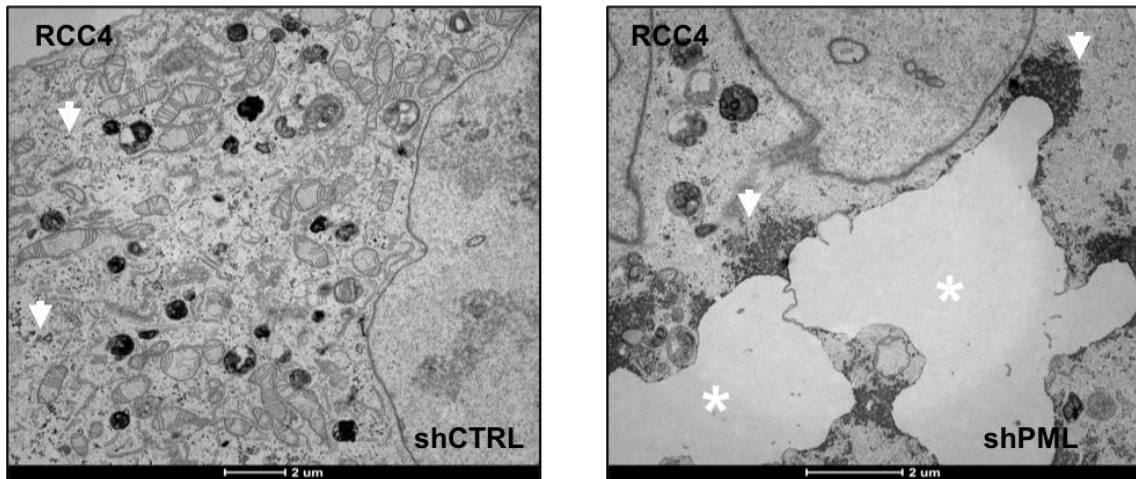
Figure 26. RCC4 cell-specific morphological alterations due to PML knock-down. *Representative TEM images showing increased glycogen deposits (indicated by white arrows) in the proximity of the membrane of empty intracellular vacuoles (indicated by white asterisks) in RCC4 shPML cells, in comparison to shCtrl cells.*
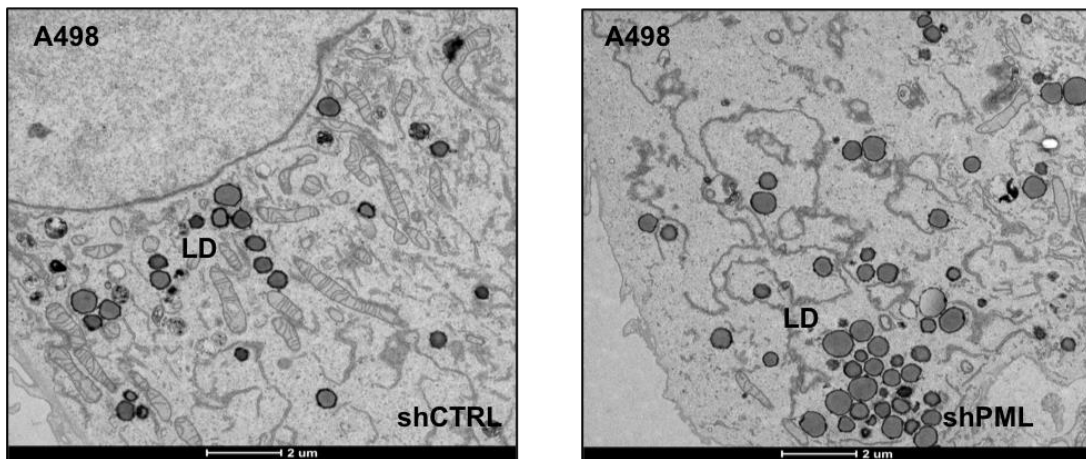
Figure 27. A498 cell-specific morphological alterations due to PML knock-down. *Representative TEM images showing increased LD content in A498 shPML cells, in comparison to shCtrl cells.*

A

shCtrl   shPML

RCC4

B

shCtrl   shPML
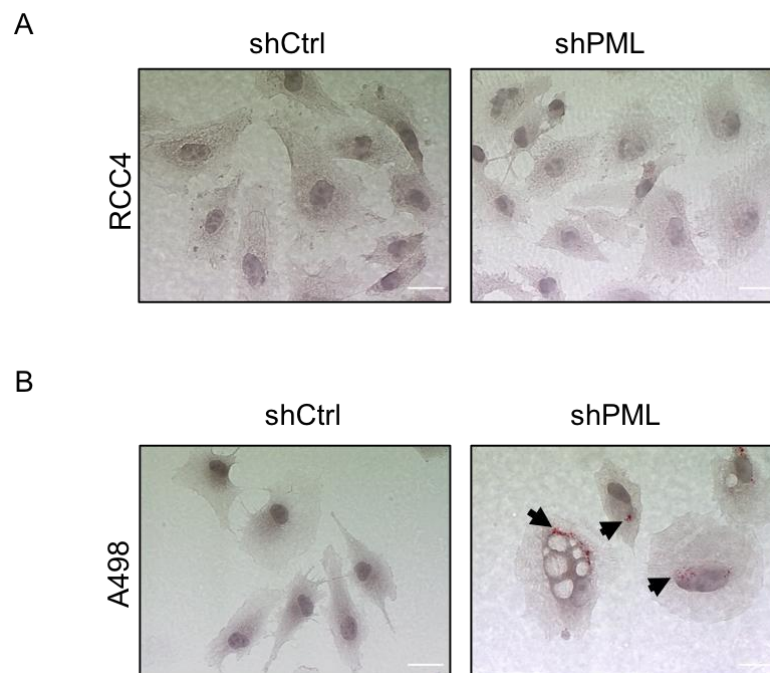
A498

Figure 28. PML inhibits lipid droplets deposition in A498 cell line. Representative images of ORO staining in RCC4 (A) and A498 (B) cell lines upon PML silencing. Neutral lipids where stained with ORO and the cell nucleus was counterstained with hematoxylin. Magnification 40x scale bar 10 μm.

In conclusion, analysis of ccRCC cellular morphology by TEM revealed that: i) PML negatively regulates the accumulation of degradative structures and in particular of lysosomes, that contribute to increase cell granularity; ii) PML regulates cell polarization and its down-regulation leads to morphological change akin aberrant differentiation.

3.1.8 PML does not regulate cell migration and invasion of ccRCC cells

Previous work in our laboratory demonstrated that PML promotes metastatic dissemination of TNBC cells and *in vitro* features of metastasis, like cell migration, invasion and EMT (Ponente *et al*, 2017). To test whether this was also evident in ccRCC, we performed wound healing and Matrigel invasion assays to specifically measure migratory and invasive phenotypes in all RCC cell lines upon PML silencing (ACHN, Caki-1, RCC-4 and A498). Contrary to the phenotype that we had described in TNBC (Ponente *et al*,2017), we did not observe any significative defect or increase in cell motility or cell invasion upon PML silencing in any of the cell lines analyzed. Representative examples of RCC4 cells are reported in Figure 29. *In vivo*, we did not find

metastatic foci of Caki-1 and A498 cells in control tumors, and silencing of PML did not cause metastasis.
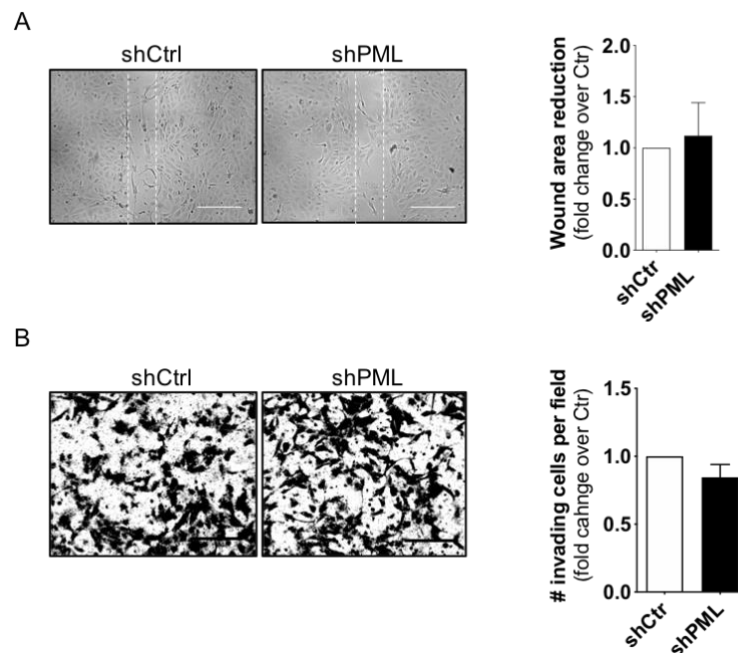
Figure 29. PML silencing does not affect cell motility. (A) Representative images of wound healing assay acquired with 10x magnification (scale bar=20 μm) and bar plot representing wound area reduction after 24 hours from scratch application of one of three independent experiments (B) Representative images of transwell invasion assay of one of at least three independent experiments (20x magnification, scalebar 10 μm) and bar plot showing the number of invading cells per field. Data are presented as the mean values ± SD. Statistical significance was calculated by Student's t-test.

In conclusion, analysis of the role of PML in ccRCC pathogenesis *in vitro* revealed that PML appears to display clear tumor-promoting functions in this context, with a predominant effect on cell proliferation and morphological changes that may represent reactivation of aberrant differentiation programs. Conversely, PML does not promote cell migration and metastatic features in this tumor type, unlike in TNBC (Ponente *et al*, 2017).

3.1.9 Unraveling the PML-dependent transcriptional program in ccRCC cells

The results described so far point to a crucial function of PML as a pro-oncogenic factor in ccRCC by displaying functions that appear more pronounced than in other tumor types where PML has been described as an oncogene, first and foremost TNBC (Carracedo *et al*, 2012a; Martín-Martín *et al*, 2016; Arreal *et al*, 2020). Also, we observed an important function of PML in determining cell morphology features that are not easy to interpret.

To gain functional insights into the function/s of PML in ccRCC, we interrogated the transcriptional program mediated by PML in this tumor context. We thus performed RNA-sequencing (RNAseq) upon PML knock-down in RCC4 cells, as this cell line has been previously studied to identify HIF transcriptional targets and allowed us to do comparative analyses.

Global changes in RNA expression in RCC4 cells upon PML silencing are shown in Figure 30. We found that 1695 coding genes were differentially expressed in response to PML knock-down. These 820 up-regulated (log2FC>0, FDR<0.05) and 875 down-regulated (log2FC<0, FDR<0.05) genes.
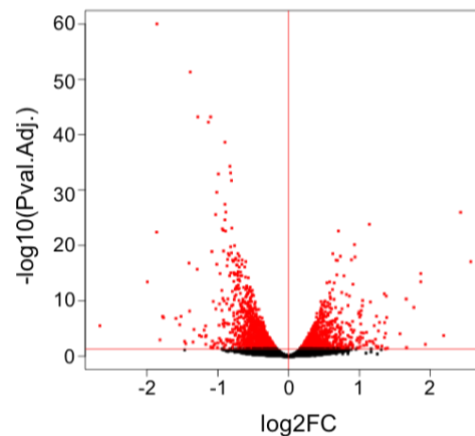
Figure 30. Differential gene expression analysis following PML silencing in RCC4 cell line.
Volcano plot depicting differentially expressed genes between shCtrl and shPML RCC4 cells. Red dots represent statistically significant differentially expressed genes (FDR<0.05), calculated by row count values. Black dots represent genes whose expression was not significantly altered.

To describe the main functional categories regulated by PML in ccRCC, we performed functional enrichment analysis of the 821 down-regulated and 876 up-regulated genes separately with the EnrichR online tool (Kuleshov *et al*, 2016). Functional enrichment analysis of down-regulated genes in response to PML silencing (i.e., genes positively regulated by PML) showed that the top 100 most enriched terms and pathways (AdjPval<0.1) where homogeneously and mostly related to proliferation-associated cellular processes (Figure 31). Specifically, the top 100 enriched terms were subjected to supervised clustering, and we identified eight major clusters: i) response to infection; ii) DNA replication; iii) DNA damage; iv) cell cycle; v) DNA repair; vi) mismatch repair; vii) nucleotide excision; viii) DNA synthesis (Figure 31).

Figure 31. Functional categories activated by PML. *Heatmap displaying the top 100 terms and pathways enriched in genes down-regulated upon PML silencing. Terms were grouped by performing supervised hierarchical clustering of functional categories. Enrichment analysis was performed by using EnrichR online tool. The following datasets were included: KEGG, MSigDB_Hallmark, Reactome, GO_Biological Process, GO_Molecular Function and GO_Cellular Component. The terms used to perform supervised hierarchical clustering shown in the heatmap were filtered for their statistical significance indicated by Adjusted Pvalue (AdjPval)<0.1.*

This analysis further demonstrates the fundamental role of PML in regulating ccRCC cell proliferation and cell cycle progression. The main functional category was related to cell cycle regulation, and included important *bona fide* cell cycle effectors like *CDK1*, *E2F*, *Cyclin E*, *CDC245*, *BUB3* and *POLE* and other pro-proliferative genes like *PCNA* and *FOXL1*. Positive transcriptional regulation of these gene categories was not previously reported for PML, thus suggesting that PML may be directly involved in regulating proliferation specifically in ccRCC cells. Interestingly, another member of the Forkhead transcription factor (FOX) family, FOXM1, was reported to be inhibited by PMLIV over-expression along with PCNA in TNBC cells, thus inhibiting cell growth and focus forming capacity (Sachini *et al*, 2019). These results suggest that PML might modulate similar targets across different tissues, albeit in opposite manners. Also, the down-

regulation of genes involved in DNA replication (*RFC5, RPA1, TOP3A, PRIM2,* and *POLE4)* and repair (*MSH2, RFC5, RFC3*) was not previously reported as a consequence of PML genetic manipulation, suggesting that PML regulation with respect to genes involved in DNA synthesis and repair might be tissue-specific. Intriguingly, the same gene sets down-regulated in response to PML silencing, namely DNA replication, cell cycle, cell cycle check-point and DNA repair process, including *CD1*, *TOP2A*, *CDK1*, *CDK2*, *BLM*, *E2F,* and *BRCA1* genes, were identified as the most significantly regulated genes upon HIF2α pharmacological targeting with the novel small molecule inhibitor Belzutifan (Cheng *et al*, 2016), suggesting that PML and HIF2α may synergies to promote ccRCC cell proliferation.

However, we cannot exclude that such regulation might occur as a consequence of the non-proliferative state of PML-silenced cells, which do not require the activation of DNA synthesis and repair pathways, in line with the depletion of p-γH2A.x foci that we observed following PML knock-down (Figure 21).

Finally, the down-regulation of gene sets involved in response to viral infections, which comprehends genes encoding nucleoporins (NUPs) that counteract viral genome entry in the nucleoplasm (Shen 2021), is consistent with the vast amount of literature demonstrating that PML is a viral restriction factor (Neerukonda, 2021; Everett, 2001). Nonetheless, PML regulation of viral genome entry in host cells was not reported as a transcriptionally regulated mechanism, thus expanding the involvement of PML in counteracting viral infections.

The same analysis was performed for the up-regulated genes in response to PML knock-down (i.e., genes negatively regulated by PML). In this case, we found more heterogeneous gene sets (Figure 32) that functional hierarchical clustering analysis grouped in more heterogeneous categories (Figure 32). Specifically, the top 100 enriched terms and pathways (AdjPval<0.1) clustered in the following categories: i) ribosomal proteins; ii) glycolysis; iii) semaphorin signaling; iv) cholesterol biosynthesis; v) neutrophil activation; vi) extracellular matrix (ECM) remodeling; vii) lysosome; viii) and a more heterogeneous cluster indicating the up-regulation of other pathways related to interleukin (IL) signaling, endosome trafficking, stress-response and inflammation.

In analyzing these results, we found that some gene terms are coherent with the phenotype caused by knocking-down PML expression. First and foremost, the up-regulation of

lysosomal gene families correlates with the increased number of lysosomes and other degradative structures observed by TEM and by IF in RCC4 and A498 cells (Figures 23 and 24).
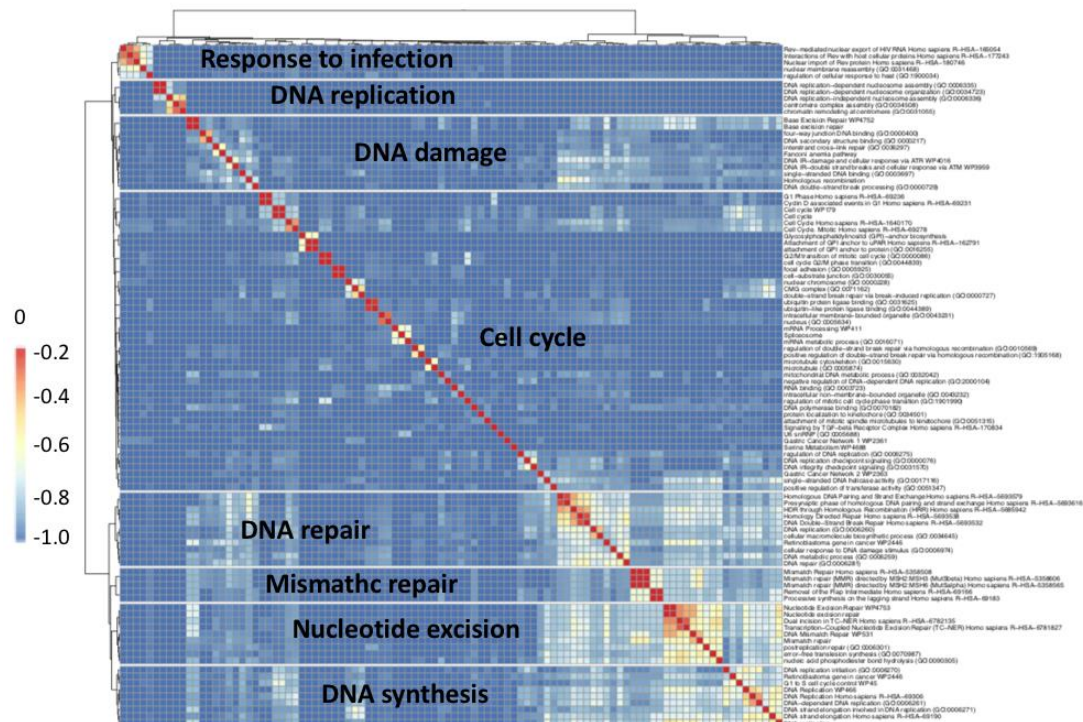

Figure 32. Functional categories suppressed by PML. Heatmap displaying the top 100 terms and pathways up-regulated upon PML silencing. Terms were grouped by performing supervised hierarchical clustering of functional categories. Enrichment analysis was performed by using EnrichR online tool. The following datasets were included: KEGG, MSigDB_Hallmark, Reactome, GO_Biological Process, GO_Molecular Function and GO_Cellular Component. The terms used to perform supervised hierarchical clustering shown in the heatmap were filtered for their statistical significance indicated by Adjusted Pvalue (AdjPval)<0.1.

We found that *LAMP1* and *LAMTOR* lysosomal membrane proteins, and ATPases regulating lysosome acidification are transcriptionally up-regulated in response to PML knock-down. Intriguingly, the transcriptional regulation of genes encoding lysosomal structural proteins by PML was not previously reported. However, cytoplasmic PML was found to localize at mitochondrial associated membranes (MAMs), modulating autophagy (Missiroli *et al*, 2017), a cellular process that delivers cellular component to lysosome for degradation (Yim & Mizushima, 2020). Despite this, since here we observe that PML regulates the expression of lysosomal factors, our findings further expand PML-dependent regulation of lysosomal dynamics. Other terms are coherent with functions of PML reported in the literature. For example, the involvement of PML in suppressing

cholesterol biogenesis has been reported in tissues including normal liver, muscle and white adipose tissue (Cheng *et al*, 2013), as well as prostate cancer, where PML negatively regulates the activity of SREBP2 transcription factor, which we found included in gene families clustering in the "Cholesterol biosynthesis" category (Figure 32). Interestingly, negative regulation of cholesterol metabolism by PML was suggested to prevent diet-induced obesity (Kim *et al*, 2011) and inhibit metastatic behavior in prostate cancer (Chen *et al*, 2018), two roles that fit with systemic and cell-intrinsic tumor suppressive functions of PML, in contrast with PML acting as an oncogene in ccRCC. However, in ccRCC tissues expression of cholesterol biosynthetic enzymes was reported to be repressed when compared to normal tissues (Riscal *et al*, 2021). Therefore, although a clear role for intracellular cholesterol synthesis in ccRCC remains to be established, our data suggest that PML may participate to suppression of cholesterol biosynthetic pathways in this tumor context. Consistently, we found that several SREBP2 target genes that are reported to be regulated by PML in prostate cancer (Chen *et al*, 2018) are up-regulated in response to PML silencing in ccRCC cells, including *SREFBP2* itself and *HMGCR, HMGCS, ELOVL6,* and *IDI1*.

In addition, our RNAsequencing analysis revealed that PML silencing elicits a complex stress response in ccRCC, which comprehends up-regulation of a variety of pro-inflammatory pathways and ECM remodeling factors, including *MMP9, LOXL2*, *LOXL4*, *MMP1* and *ADAMTS1*. Of note, this is in contrast with what we have previously demonstrated in TNBC, where PML positively regulates the expression of ECM degradation proteins, thus enhancing breast cancer cell invasion (Ponente *et al*, 2017). However, increased production of other ECM remodeling factors*,* was described in TNBC cells upon PML silencing (Arreal *et al*, 2020), and these features were associated to induction of cellular senescence (Herranz & Gil, 2018; Kirkland & Tchkonia, 2020). In this context, proteomic analysis of the secretome of PML-silenced TNBC cells revealed that their senescence-associated secretory phenotype (SASP) does not fully resemble the canonical SASP but is particularly enriched of ECM remodeling factors (Arreal *et al*, 2020), probably due to the high heterogeneity and tissue specificity of SASP (Hernandez-Segura *et al*, 2017). Therefore, our data are consistent with the SASP phenotype induced by PML silencing in TNBC cells (Arreal *et al*, 2020) and further

suggest that in ccRCC cells PML may also induce senescence, albeit not accompanied by classical senescence markers.

Another intriguing result of our transcriptomic data is the upregulation of glycolysis. In this respect, PML loss induced the over-expression of *HK2*, *GAPDH*, *ENO1, GPI, PFKP*, which are *bona fide* HIF1α-target genes (Ray & Semenza, 2010). We had previously identified PML as a transcriptional co-activator of HIF1α in TNBC (Ponente *et al*, 2017) and unpublished RNA-sequencing results demonstrate that glycolytic genes are down-regulated upon PML suppression in TNBC cells (data not shown). These counterintuitive observations indicate that PML regulation with respect to HIF1α transcriptional activity might be tissue specific. Furthermore, it was reported that increased glycolysis can be found in association with SASP in senescent cells (Dörr *et al*, 2013), further suggesting that PML inhibition in ccRCC cells might induce the acquisition of a non-canonical senescent-like phenotype. The role of semaphorin and interleukin signaling pathways as well as increased protein synthesis pathways are less clear and will need validation and further investigation.

In summary, profiling changes of the transcriptomic profile of ccRCC cells upon PML silencing partly confirmed the phenotypes that were identified via morphological and functional characterization, and further extended our analysis to include other pathways that appear specifically regulated by PML in this tumor context, including lysosome dynamics and metabolic reprogramming.

Since our transcriptomic analysis is strongly indicating that PML might be intimately involved in metabolic reprogramming in ccRCC, we expanded our findings to clinical data. Specifically, co-expression analysis was performed between *PML* mRNA abundance and mRNA levels of genes involved in glycolysis and cholesterol biosynthesis in the TCGA-KIRK dataset using cBioPortal (Cerami *et al*, 2012; Gao *et al*, 2013). Interestingly, we found an inverse correlation between PML and some glycolytic genes including, *PDK1*, *PGK1*, and *BNIP3* (Figure 33A-C)
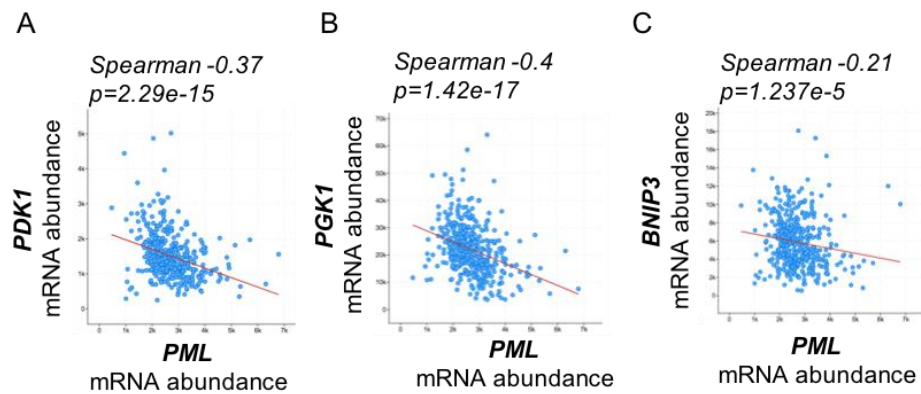
Figure 33. Co-expression analysis between PML and glycolytic genes. *Spearman's correlation analyses between PML mRNA abundance and PDK1 (**A**), PGK1 (**B**), BNIP3 (**C**) in the TCGA-KIRK dataset. Data were retrieved by using cBioPortal.*

Similarly, co-expression analysis between PML and genes involved in cholesterol biosynthetic process showed inverse correlation with *HMCGR*, *HMGCS1* and *IDI1* (Figure 34A-C). Notably, these are well-established SREBP2 target genes (Chen *et al*, 2018) that are known to be repressed in ccRCC as opposed to normal kidney tissue (Riscal *et al*, 2021).
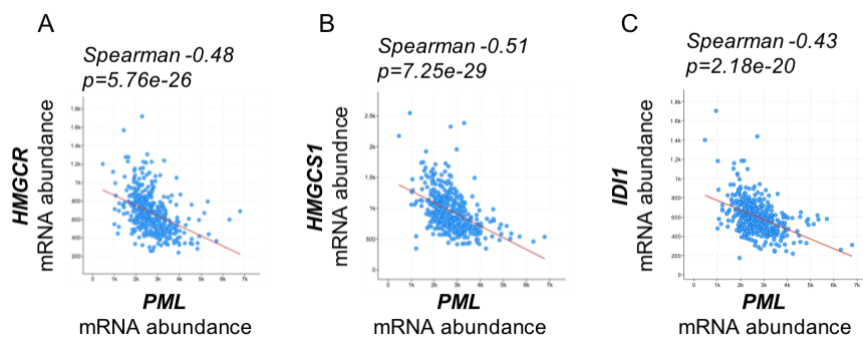
Figure 34. Co-expression analysis between PML and genes of cholesterol synthesis. *Spearman's correlation analyses between PML mRNA abundance and HMGCR (**A**), HMGCS1 (**B**), IDI1 (**C**) in the TCGA-KIRK dataset. Data were retrieved by using cBioPortal.*

Taken together, co-expression analyses revealed that PML is involved in the suppression of glycolysis and cholesterol anabolic pathways, unraveling a possible pro-oncogenic metabolic role of PML in ccRCC.

3.1.10 PML expression sustains *in vivo* tumor growth

In order to validate PML involvement in ccRCC pathogenesis in *in vivo* settings, we injected subcutaneously inducible shCtrl and shPML ccRCC cells in immunocompromised mice. For these experiments, we selected Caki-1 and A498 cells as they were reported by previously published literature to engraft in immunocompromised mice, while RCC4 cells did not (Brodaczewska *et al*, 2016).

After cell implantation, we measured tumor growth weekly and started doxycycline administration when tumor masses originating from each cell line reached approximately 200 mm^3 (Figure 35). A498 and Caki-1 tumors took different periods of time to engraft and reach the size of 200 mm^3 (9 and 5 weeks, respectively) (Figure 35, left panels). From these time points, doxycycline was administered daily through oral gavage, in order to induce PML silencing *in vivo* for the indicated periods of time (Figure 35, left panels). 2-3 weeks after doxycycline administration, tumors derived from both A498 and Caki-1 cells started to show reduced *in vivo* growth in the presence of the PML silencing shRNA, and this difference became more pronounced as control tumors grew bigger (Figure 35, left panels). The experiment was interrupted at 5 weeks post doxycycline administration due to tumor sizes in control animals (Figure 35, left panels). At this time point, tumors originated from shPML ccRCC cells were significantly smaller and displayed lower weight than control tumors (Figure 35, middle panels). These data clearly indicate that PML silencing delays *in vivo* tumor growth. To univocally show that such effects were due to PML down-regulation, we performed immune histochemistry (IHC) to visualize PML protein expression, which confirmed that PML knock-down was robust (Figure 35, right panels).
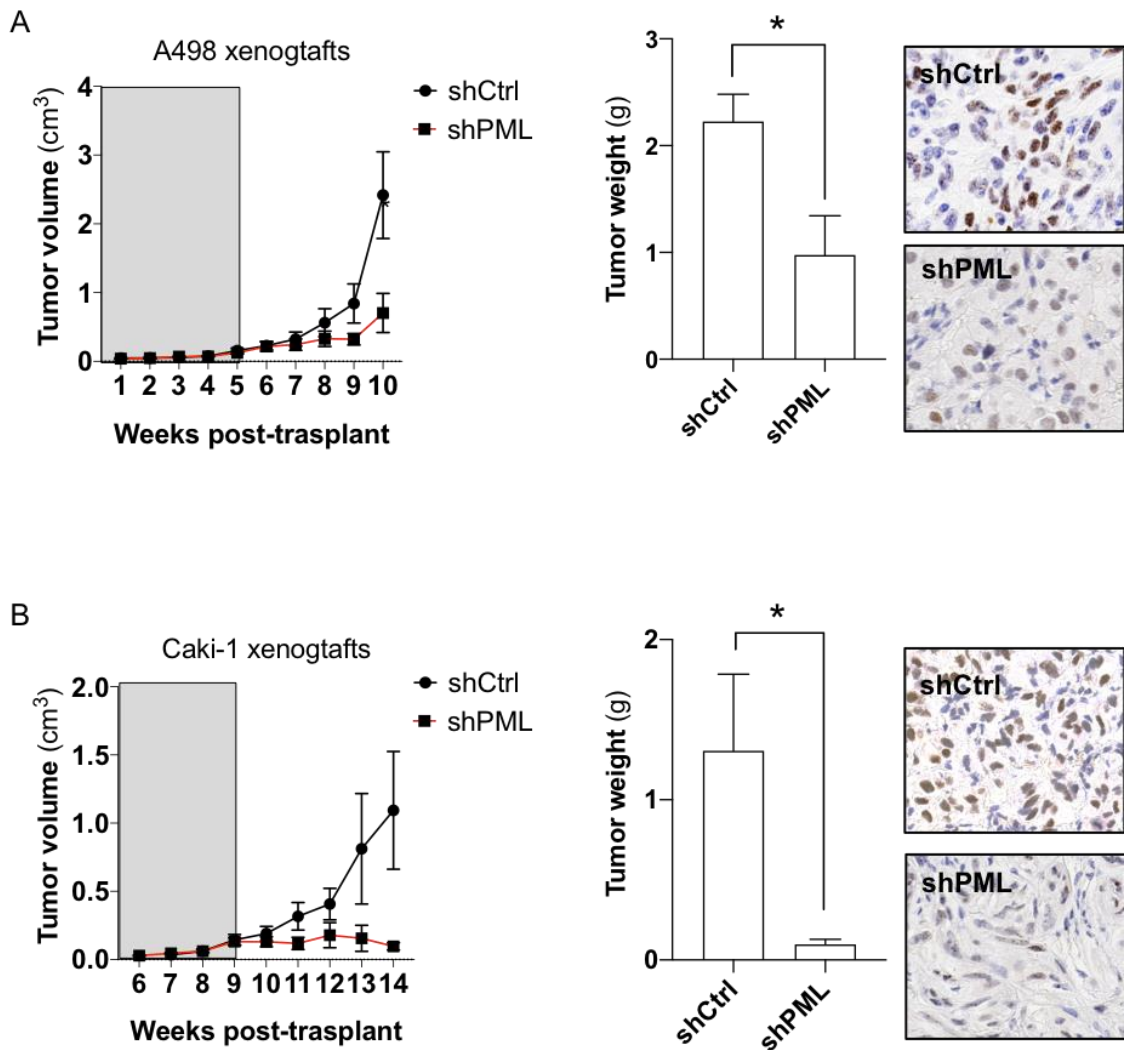
Figure 35. PML silencing impairs tumor expansion in vivo. (A) Growth curve of tumors (n=4 per experimental group) generated by A498 cells (shCtrl and shPML) and tumor weight at sacrifice. Doxycycline was administered from week 9 to 14 from implantation. On the right, representative images of PML IHC in one sample each of shCtrl and shPML tumors. Images were taken at 60x magnification. (B) Growth curve of tumors (shCtrl n=6, shPML n=5) generated by Caki-1 cell (shCtrl and shPML) and tumor weight at sacrifice. Doxycycline was administered from week 5 to 10 from implantation. On the right, representative images of PML IHC in one sample each of shCtrl and shPML tumors. Images were taken at 60x magnification. Data are expressed as mean ± SEM. Statistical significance was calculated with Student's t-test (*p<0.05).

In order to assess whether the reduced volume and weight caused by PML depletion was due to diminished cell proliferation, we performed IHC for the proliferation marker KI67 in shCtrl and shPML tumors. We found that the number of proliferative cells decline in the shPML condition (Figure 36), and this was particularly evident in the Caki-1 model (Figure 36A). In contrast, KI67 in the A498 model was not significantly reduced upon PML silencing in comparison to shCtrl condition, perhaps because control tumors were

very large and showed reduced proliferation and large necrotic areas due to tumor over-growth (Figure 36B).
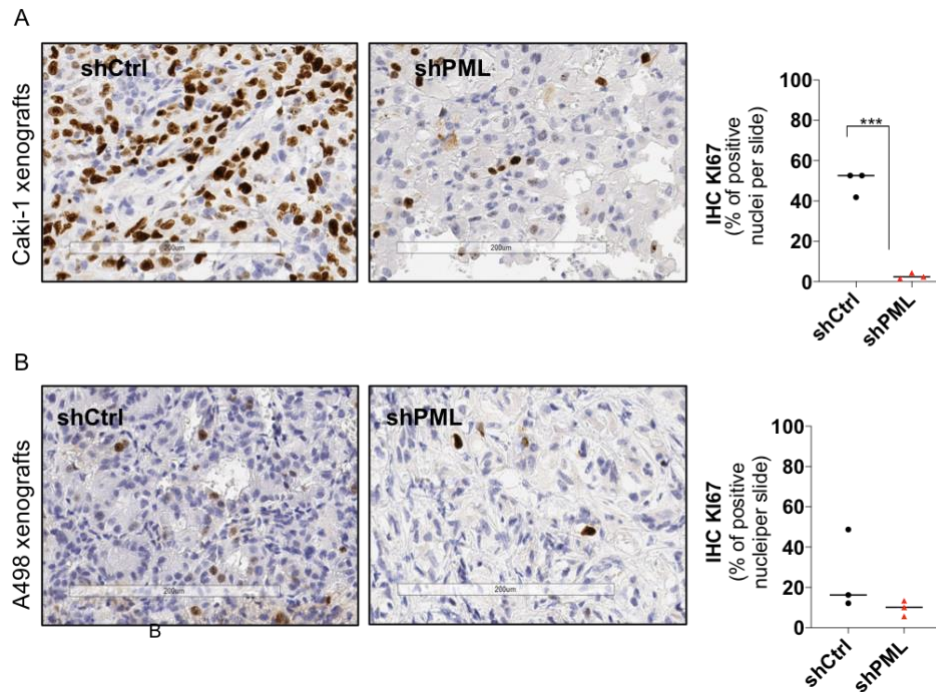
Figure 36. KI67 staining of Caki-1 and A498 xenografts. (A) Representative images of IHC staining for KI67 performed in 3 out of 6 samples for each experimental condition of mice transplanted with Caki-1 (A) or A498 (B) shCtrl or shPML cells. The graphs (right panel in A and B) represents the percentage of KI67 positive nuclei. The quantification was performed by scanning the entire tissue slides. Images were acquired at 60x magnification (200 μm scalebar). Data are presented as single values of each experiment and the bars represent the mean. Statistical significance was calculated with Student's t-test (***p<0.001).

Additionally, in collaboration with the pathologist Roberta Lucianò of San Raffaele Hospital, we performed hematoxylin and eosin (H&E) staining and pathology evaluation of tumor architecture and tumor staging, according to nucleolar grade, in 3-4 representative tumors/cohort. Tumors derived from both A498 and c Caki-1cells were generally of high grade, with prevalent scoring of grade III-IV (Figure 37A and 38A). Also, they often displayed areas of sarcomatoid and rhabdoid differentiation (Figure 37B and 38B, left panels), which are typical of high-grade ccRCC (Elias *et al*, 2021). Tumor grade was not statistically different upon PML silencing in A498 tumors (Figure 37A). However, morphological features of sarcomatoid and rhabdoid differentiation were under-represented in A498 shPML samples (n=1 grade III, n=3 grade III/IV and n=1 grade IV), and these tumors presented areas of distinctive clear cell morphology, with

cells displaying clear cytoplasm, while control tumors had more anaplastic features
(Figure 37B).
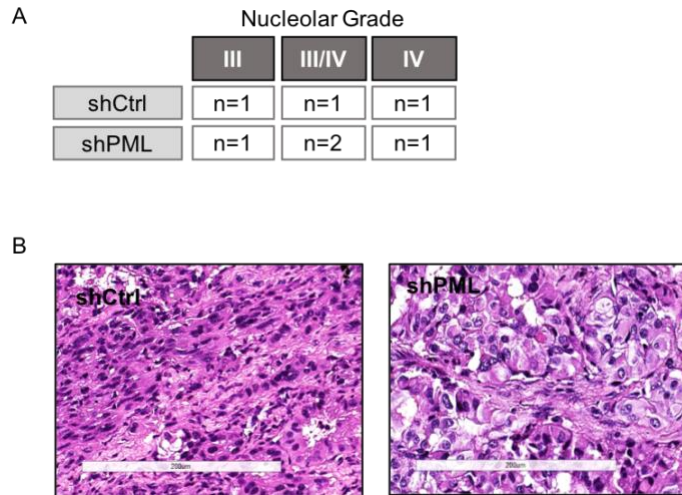
Figure 37. Evaluation of A498 tumor architecture and tumor staging. (A) Table showing the micro-anatomopathological staging of A498 xenografts according to nucleolar grade. (B) Representative H&E staining of tumor xenografts derived from A498 shCtrl and shPML cells (60x magnification, 200 μm scalebar).

The same analysis was performed in three out of six shCtrl and shPML Caki-1 tumors per group and produced more significant results. Masses arising from shCtrl Caki-1 cells where high-grade tumors (n=1 grade III/IV, n=2 grade VI) (Figure 38A), displaying rhabdoid architecture (Figure 38B). In contrast, 2/3 small masses derived from shPML Caki-1 cells barely displayed tumor cells and were mostly characterized by fibrotic tissue (Figure 38B). In these samples, we found signs of remission, as suggested by the presence of stromal activated fibroblasts and scarce abundance of morphological features of tumor cells. Only one tumor had clearly defined cancer cells with grade III/IV (Figure 38A).

A

	Nucleolar Grade		
	III	III/IV	IV
shCtrl	n=0	n=1	n=2
shPML	n=0	n=1	n=0

B
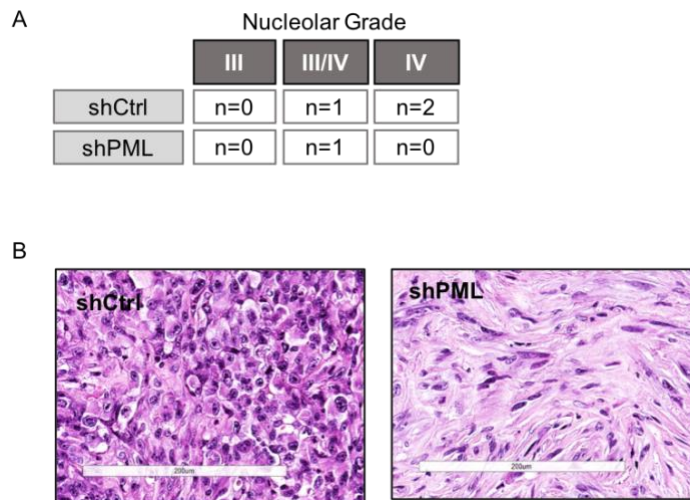
Figure 38. Evaluation of Caki-1 tumor architecture and tumor staging. (A) Table showing the micro-anatomopathological staging of Caki-1 xenografts according to nucleolar grade. (B) Representative H&E staining of tumor xenografts derived from Caki-1 shCtrl and shPML cells (60x magnification, 200 µm scalebar).

To understand whether mesenchymal-like cells in these tumors represented an inflammatory stroma or tumor cells with EMT features, we performed immunohistochemical staining for the human epithelial marker cytokeratin 8/18 (Figure 38, right panel). Caki-1 shCtrl tumors showed low, cytoplasmic staining for cytokeratin 8/18, while shPML Caki-1 tumors showed two distinct types of staining: few scattered positive cells in areas of fibrosis (Figure 39, left panel) and a stronger staining of cytokeratin 8/18 in the few areas of morphological tumor cells in comparison to shCtrl tissue (Figure 39, compare the left panel to the middle panel).

This observation further suggests that PML silencing may lead to the acquisition of an epithelial-like phenotype, which may define less aggressive tumors that somehow undergo a process of differentiation, as suggested by the morphological vacuolization of ccRCC cells in vitro. Along these lines, we observed features of cytoplasmic vacuoles in some areas of Caki-1 shPML tumors (Figure 40, indicated by the arrows in the boxes). This was not observed in shPML A498 cells, in contrast to *in vitro* findings, perhaps due to the fact that A498 cells grow more rapidly *in vivo* and when the experiment was arrested when tumors were in general bigger, necrotic and profoundly anaplastic, than Caki-1-derived tumors,.

In summary, these data clearly indicate that: i) PML has a strong tumor-promoting capacity in ccRCC, and that similar to *in vitro* setting, acute *in vivo* silencing of PML

induces a strong growth arrest, which is accompanied by tumor features of reduced anaplasia; ii) since PML regulates cell polarization, its silencing might lead to the development of more differentiated tumors.
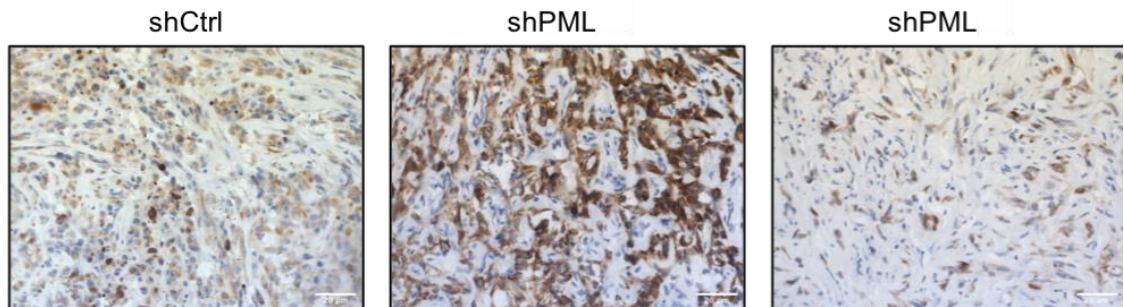
Figure 39. IHC of cytokeratin 8/18 in Caki-1 xenografts. *Representative images if IHC staining for the epithelial marker cytokeratin 8/18 of one shCtrl (left panel) and two shPML samples (middle and right panels). 20x magnification, scale bar 20 μm.*
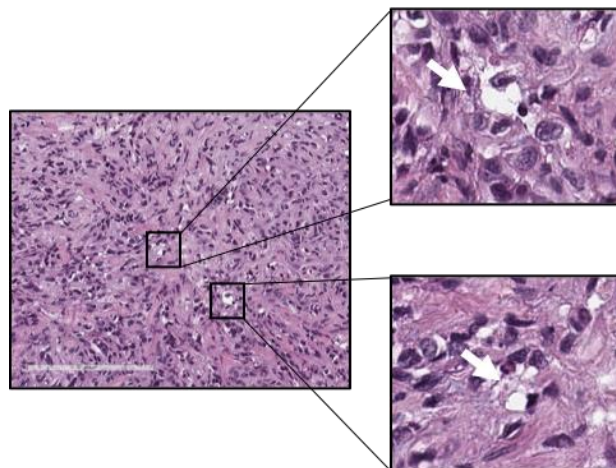
Figure 40. Cytoplasmic vacuolation observed upon PML silencing in Caki-1 model. *Left panel, representative H&E staining of tumor xenografts derived from shPML Caki-1 cells (60x magnification, 200 μm scalebar); right panel, enlargement of the indicated area in the left panel. Arrow indicates cytoplasmic vacuolation.*

3.2 Aim 2- Test physical and functional interaction of PML with HIFα oncogenic proteins in ccRCC

It was previously demonstrated that PML cooperatively regulates the expression of a specific subset of HIF1α pro-metastatic target genes in TNBC, suggesting that PML

could be physically associated to HIF1α onto their regulatory regions (Ponente *et al*, 2017). However, here we found that PML pro-metastatic functions are not conserved in ccRCC, since PML knock-down does not affect the migratory or invasive behaviors of ccRCC cells (Figure 29). In contrast, the transcriptomic data obtained in Aim 1 indicate that PML suppresses gene categories related to glycolysis, a molecular process that is prominently activated by HIF1α (Rey & Semenza, 2010). This evidence led us to speculate that PML might act as a HIF1α co-repressor in ccRCC cells, rather than a co-activator, in an opposite manner as it does in TNBC (Ponente *et al*, 2017). Furthermore, in Aim 1 we demonstrated that PML positively regulates proliferation, a cellular function that is largely attributed to HIF2α, especially in the context of ccRCC (Biswas *et al*, 2010). Therefore, we did not exclude that a functional PML/HIFα axis existed also in ccRCC and we aimed to test the following hypothesis : i) that functional interactions between PML and HIFα subunits occur in ccRCC; ii) that PML modulates HIFα transcriptional programs via direct protein-protein interaction.

3.2.1 PML regulates the expression of *bona fide* HIFα genes

To evaluate the functional crosstalk of PML/HIF1α and PML/HIF2α, we took advantage of RCC4 cells that constitutively express both HIF1α and HIF2α due to VHL deletion. Firstly, we measured the expression of HIF1α pro-metastatic target genes that were positively co-regulated by PML and HIF1α in TNBC, including *ZEB2*, *PLOD1*, *WIPF1* and *LOX* (Ponente *et al*, 2017). However, unlike TNBC cells, the expression of HIF1α pro-metastatic targets was not inhibited upon PML silencing in RCC4 cells (Figure 41A). Rather, PML knock-down led to the slight up-regulation of some of these genes, and a more significant up-regulation of HIF1α target genes involved in glycolysis (Figure 41B), in validation of the results obtained upon RNA-sequencing where glycolytic pathways were found up-regulated upon PML suppression (Figure 32), and inversely correlated with PML in the TGCA-KIRK dataset (Figure 33). These data thus suggest that rather than promoting pro-metastatic HIF1α functions, PML may antagonize HIF1α transcriptional activity with respect to genes involved in glycolysis in ccRCC.
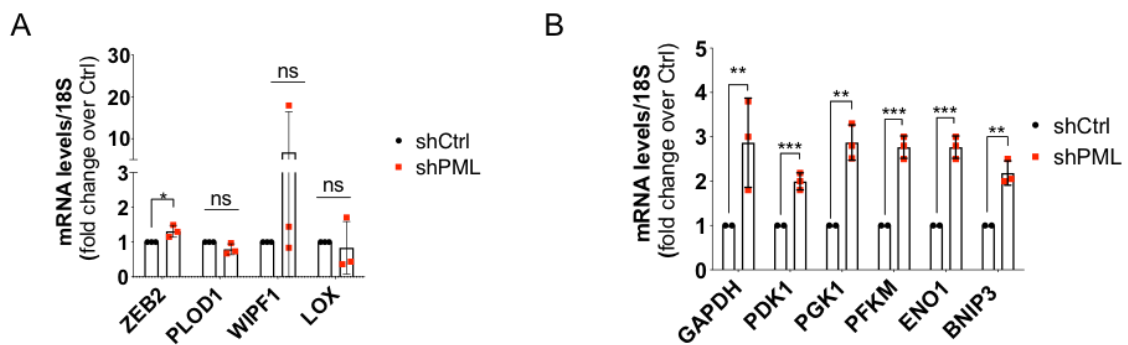
Figure 41. Expression levels of HIF1α target genes following PML knock-down. *qRT-PCR showing the fold change in expression of HIF1α pro-metastatic (**A**) and glycolytic (**B**) target genes in RCC4 cells following PML silencing. Data represent mean values ± SD of three independent experiments. Statistical significance has been calculated by Student's t-test (*p<0.05; **p<0.01; ***p<0.001).*

Since we found that PML is fundamental for ccRCC proliferation and this function has been prominently attributed to HIF2α (Biswas *et al*, 2010), we asked whether PML might specifically cooperate with HIF2α to such process. We evaluated the expression levels of a small subset of HIF2α target genes, including genes involved in proliferation (*CD1* and *NDRG1*) and self-renewal (*Oct4*, *SOX2*) (Forristal *et al*, 2010; Cho *et al*, 2016). In contrast to what we observed with respect to HIF1α targets, and in agreement with PML pro-tumorigenic function in ccRCC cells, PML silencing led to a significant down-regulation of HIF2α regulated genes (Figure 42). These data are in addition to PML positive regulation of a series of newly described HIF2α target genes, including *CD1*, *TOP2A*, *CDK1*, *CDK2*, *BLM*, *E2F* and *BRCA1*, which were identified upon HIF2α targeting with a specific inhibitor (Chen *et al*, 2016) and we found down-regulated by RNA-sequencing upon PML knock-down. Taken together these findings suggest that in ccRCC, PML may exert opposite functions in the regulation of HIFα targets compared to TNBC.

Intriguingly, along with the negative and positive regulation of HIF1α and HIF2α-target genes, we observed that PML knock-down led to specific and opposite regulation of the mRNA and protein amounts of HIF1α and HIF2α, via increasing HIF1α and decreasing HIF2α expression (Figure 43A and B).
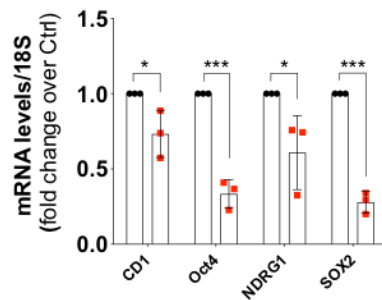
Figure 42. Expression levels of HIF2α target genes following PML knock-down. qRT-PCR showing the fold change in expression of HIF2α targets genes in RCC4 cells, following PML silencing compared to shCtrl cells. Data represent mean values ± standard deviation (SD) of three independent experiments. Statistical significance has been calculated by Student's t-test (*p<0.05; ***p<0.001).
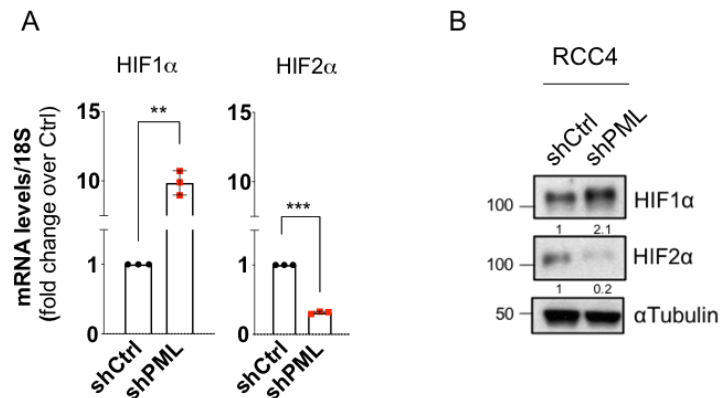
Figure 43. PML inhibits and enhances the expression of HIF1α and HIF2α respectively. (A) qRT-PCR showing HIF1α and HIF2α levels relative to 18S in RCC4 cells, following the induction of shPML. Data represent mean values ± SD of three independent experiments. (B) WB analysis showing HIF1α and HIF2α proteins expression upon PML silencing in RCC4 cell line. αTubulin was used as a loading control. WB is representative of two independent experiments of two biological replicates. Numbers represent densitometric analysis of bands intensity expressed as fold change over shCtrl condition. Statistical significance has been calculated by Student's t-test (**p<0.01; ***p<0.001).

Taken together, these results suggest that PML regulates HIFα in a dichotomic manner, by inhibiting HIF1α glycolytic target genes and promoting modulation of HIF2α target genes involved in cells proliferation.

3.2.2 PML and HIFα transcriptional programs are partially overlapping

To investigate in more detail the functional crosstalk between PML and HIFα transcription factors and evaluate whether PML shares co-regulated gene sets with HIF1α or HIF2α, we overlapped the PML-dependent transcriptional signature that we obtained

via RNA-sequencing with: i) available HIF1α and HIF2α ChIP-sequencing data from the RCC4 cell line (Smythies *et al*, 2019); ii) RNA-sequencing data obtained from RCC4 cells reconstituted for VHL expression and exposed to hypoxic conditions to identify HIFα target genes (Smythies *et al*, 2019).

Firstly, we annotated HIF1α and HIF2α ChIP-sequencing peaks, and identified 3001 genes bound by HIF1α, and only 249 genes by HIF2α in RCC4 cells. These data are surprising, as functional studies indicate that HIF2α is a crucial oncogene in ccRCC (Shen *et al*, 2011). However, HIF2α-specific antibodies may be less efficient than HIF1α-specific antibodies, thus explaining this incongruency. Then, we overlapped HIF1α associated genes with genes positively (hereafter shPML_Down) or negatively (hereafter shPML_Up) regulated by PML (Figure 44A and C). In line with the hypothesis that PML inhibits HIF1α target genes in ccRCC, we found no overlap between shPML_Down and HIF1α ChIP-sequencing peaks (Figure 44A) but we found that 124 genes bound by HIF1α are also suppressed by PML (Figure 44C). We performed the same analysis by overlapping PML-regulated genes with HIF2α targets but we found only a small overlap between PML and HIF2α peaks, with 9 and 14 genes shared between shPML_Down, shPML_Up and HIF2α, respectively (Figure 44B and D).
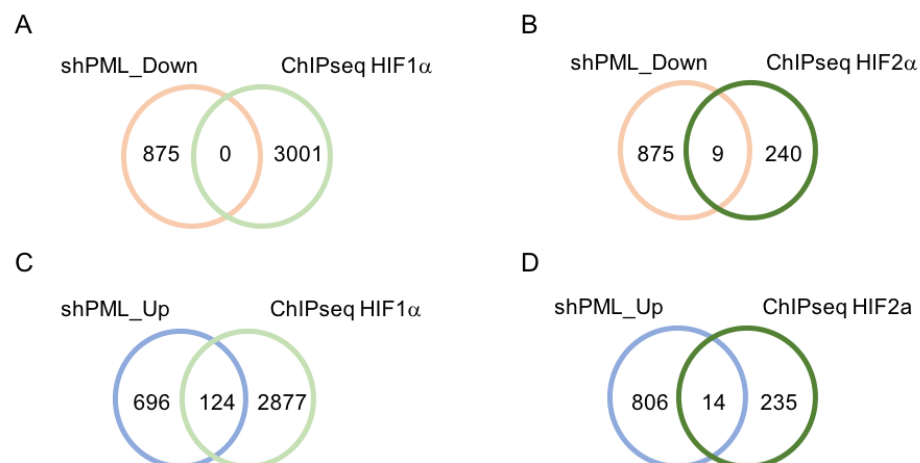
Figure 44. Overlap analysis of PML-regulated genes with genes bound by HIF1α or HIF2α. *Venn diagrams showing PML-HIF1α (**A** and **C**) and PML-HIF2α (**B** and **D**) commonly regulated/bound genes. (**A**) 0 genes positively regulated by PML and bound by HIF1α in RCC4 cells. (**B**) 9 genes are positively regulated by PML and bound by HIF2α. (**C**) 124 genes are inhibited by PML expression and bound by HIF1α. (**D**) 14 genes are inhibited by PML expression and bound by HIF2α.*

To get insights of PML and HIFα co-regulated molecular pathways, we performed functional enrichment analysis of gene lists obtained from this analysis. Consistently, we found that PML suppresses the expression of HIF1α-dependent metabolic pathways, including glycolysis and fatty acid synthesis (Figure 45A). Moreover, we observed an enrichment in terms related to the mTORC1 pathway (Figure 45A), which is in line with previous studies demonstrating that PML inhibits mTORC1 activity, resulting in the suppression of HIF1α (Berardi *et al*, 2006). Surprisingly, the same analysis performed by using genes repressed by PML and bound by HIF2α retrieved the same terms and pathways found in shPML_UP and HIF1α overlap (Figure 45B). This is due to the fact that the 14 genes regulated by PML and bound by HIF2α are shared in the ChIP-sequencing data of HIF1α and HIF2α (13 out of 14 HIF2α-regulated genes, not shown), thus suggesting that HIF1α and HIF2α play partially redundant functions in RCC4 cells.
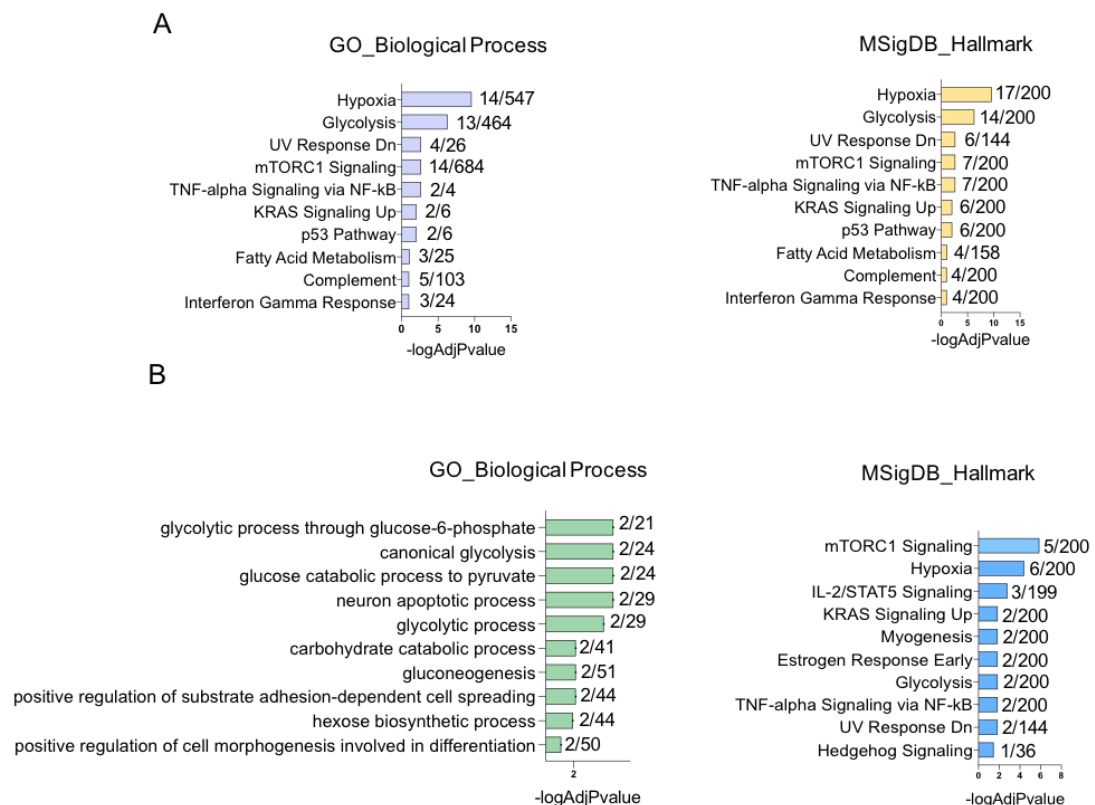
***Figure 45. Functional enrichment analysis of HIF1α and HIF2α target genes repressed by PML.** (**A**) Functional enrichment analysis for differentially expressed genes that are regulated by PML and bound by HIF1α. (**B**) Functional enrichment analysis for differentially expressed genes that are positively regulated by PML and bound by HIF2α. Top 10 terms with*

AdjPval<0.01 are shown. Analyses were performed with EnrichR tool and GO_Biological Process and MSigDB_Hallmark datasets were used. Number represents the overlap between gene lists used as input, and the number of genes belonging to each category.

Due to the paucity of HIF2α bound genes, functional enrichment analysis of genes that are positively regulated by PML and associated to HIF2α (Figure 44B) produced less than 10 statistically significant terms, with no more than one gene annotated in each category. Therefore, we excluded this condition from further evaluations.

To expand the map of PML involvement in hypoxic responses beyond the regulation of genes that are directly bound by HIFα proteins, we performed additional overlap analysis by using available RNA-sequencing data obtained from RCC4+VHL cells grown in hypoxic condition (24 hours at 0.5% pO2) (Smythies *et al*, 2019). We obtained a list of deregulated genes in hypoxic versus normoxic conditions starting from the raw data, and we overlapped the lists of genes de-regulated following PML knock-down and up-regulated in hypoxic conditions (Figure 46).
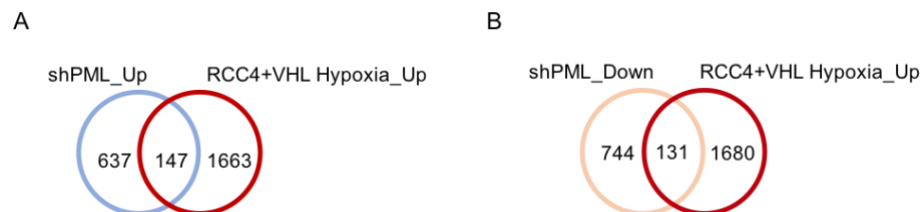
Figure 46. Overlap analysis of PML and hypoxia-dependent gene expression. (A) Venn diagrams showing the PML and hypoxia commonly regulated genes. (A) 147 genes are negatively regulated by PML and up-regulated upon hypoxia exposure. (B) 131 genes are positively regulated by PML and hypoxia.

As shown by the functional enrichment analysis (Figure 47), the 147 genes repressed by PML and up-regulated in hypoxia (Figure 46A) were again associated to glycolysis, inflammation and mTORC1 pathway (Figure 47A), further supporting an inhibitory function of PML towards glycolytic pathways in hypoxia and the activation of the mTOR signaling pathway. Interestingly, the enrichment analysis of the 131 genes positively regulated by PML and up-regulated upon hypoxia exposure revealed that PML promotes the expression of genes that are annotated in pro-proliferative pathways, like E2F targets, G2/M checkpoint and inhibition of apoptosis (Figure 47B), further suggesting that PML

might promote HIF2α-mediated pro-survival pathways. Again, and unexpectedly, we found the term glycolysis between the genes whose expression is positively regulated by PML. However, in this case, we found enrichment of different genes (like *PAXIP1*, *PGM2*, *IRS2*, *GPC4* and *HS2ST* and *CDK11*) which are not directly bound by HIF1α and are different from those observed in Figure 44A (not shown), suggesting that PML regulates the expression of a wider group of glycolytic genes also including non-classical direct targets of HIF1α.

Taken together, the results suggest that PML inhibits the expression of HIF1α targets regulating glycolysis and promotes the activation of pro-proliferative pathways that may be HIF2α-dependent. Moreover, this analysis revealed that the transcriptional signature mediated by PML in ccRCC is prominently HIFα-independent.
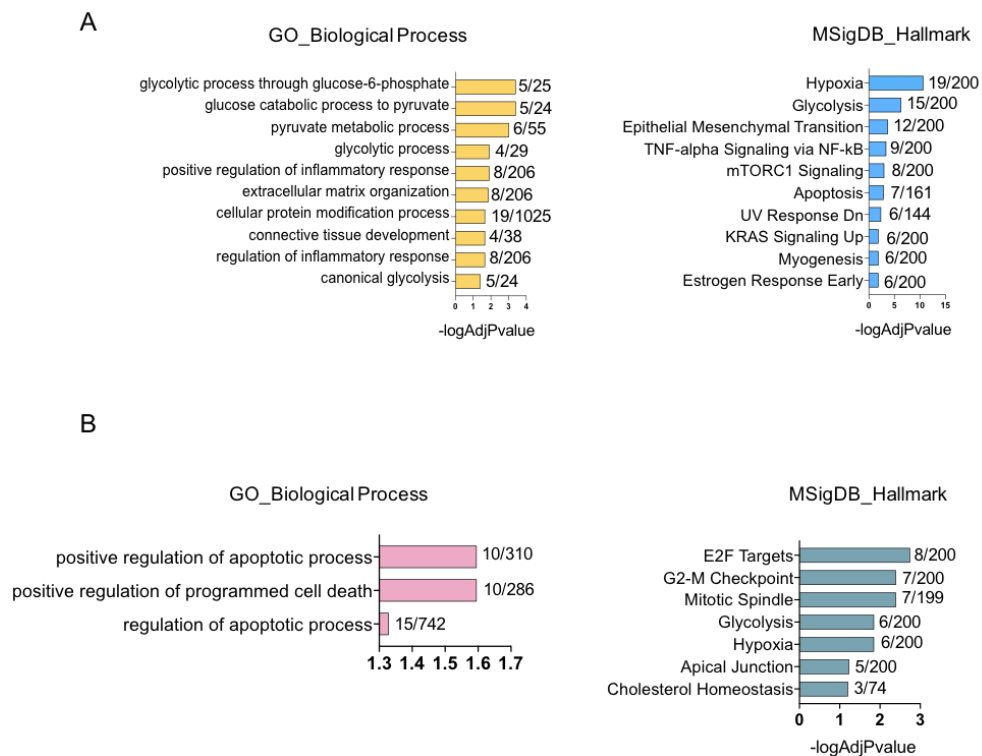
Figure 47. Functional enrichment analysis of PML and hypoxia regulated genes. (A) Functional enrichment analysis for differentially expressed genes that are commonly up-regulated by PML and hypoxia. (B) Functional enrichment analysis of genes whose expression is positively regulated by PML and hypoxia. Top 10 terms with AdjPval <0.01, are shown. Analyses were performed with EnrichR tool and GO_Biological Process and MSigDB_Hallmark datasets were used. Number represents the overlap between gene lists used as input, and the number of genes belonging to each category.

3.2.3 PML and HIFα subunits physically interact in ccRCC cells

The results obtained so far, indicate that PML is a modulator of HIFα expression (inhibiting HIF1α and sustaining HIF2α) and that it is endowed with fundamental pro-proliferative functions, at least in part by activating the expression of HIF2α targets involved in proliferation (*CD1* and *NDRG1*, *TOP2A*, *CDK1*, *CDK2*, *BLM*, *E2F* and *BRCA1*) and self-renewal (*Oct4* and *SOX2*), cellular processes that are mostly attributed to HIF2α in ccRCC (Biswas *et al*, 2010). This prompted us to test whether the PML-dependent modulation of the transcriptional activity of HIF2α is the result of protein-protein interactions. To this aim, we performed co-immunoprecipitation (Co-IP) assays followed by WB to detect PML-HIF2α protein complexes. Preliminary experiments revealed a weak co-immunoprecipitation in whole cell extracts that was difficult to validate (data not shown), also due to the scarce quality of some of the antibodies used in these experiments. Therefore, to conclusively establish whether these proteins interact, and interact in the transcriptionally active form of HIF2α, we focused on the chromatin-bound nuclear fraction. Specifically, we used a protocol that allowed us to fractionate a soluble fraction (hereafter SF) containing both cytoplasmic and nuclear soluble proteins, and an insoluble nuclear fraction containing chromatin-bound proteins (hereafter CH) (Vertegaal *et al*, 2004). A498 cells were included in this analysis for further validation, as they express HIF2α alone (Brodaczewska *et al*, 2016).
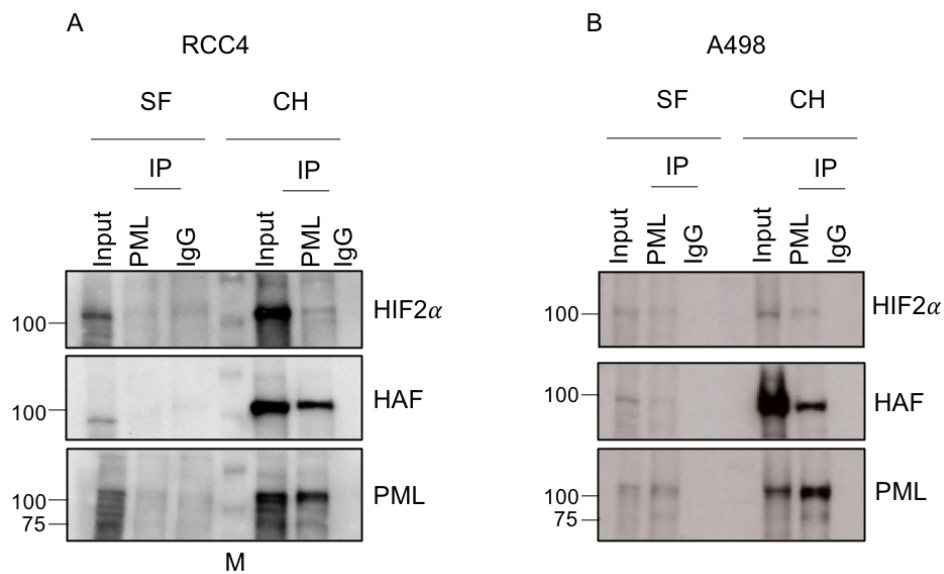
Figure 48. PML-HIF1α and PML-HIF2α are chromatin-bound protein complexes. *Co-IP experiment performed by immunoprecipitating PML in the soluble (SF) and chromatin-bound*

*(CH) fractions in RCC4 (**A**) and A498 (**B**) cell lines, followed by WB to detect PML, HIF2α and HAF co-immunoprecipitating proteins. Whole cell lysates were subjected to IP with anti-PML antibody, or with IgG, and then stained with anti HIF1α, HIF2α, or HAF antibodies. M; molecular weight marker.*

We observed that PML co-immunoprecipitated the HIF2α protein in both RCC4 and A498 cells in the CH fraction, albeit at low levels. Interestingly, we found that PML co-immunoprecipitated more significantly the HIF2α transcriptional co-activator HAF in the CH fraction (Figure 48A and B) in both the cell lines included in the analysis.

Importantly, HAF is a transcriptional co-activator that acts specifically upon HIF2α in ccRCC cells (Koh *et al*, 2015), suggesting that PML might modulate its transcriptional activity via direct or indirect physical association with HIF2α, and via the recruitment of its transcriptional co-activator. Intriguingly, HAF is a negative regulator of HIF1α protein stability (Koh *et al*, 2015), suggesting an alternative possible mechanism at the basis of PML-mediated balancing of HIFα protein levels.

To validate these data, we performed immunofluorescence analysis. By IF, PML is prominently distributed into PML-NBs in the interchromatin space. However, it was previously reported that regulation of transcription factors activity by PML can occur both inside (Ferbeyre *et al*, 2000; Ulbricht *et al*, 2012) and outside PML-NBs (Zhong *et al*, 2000; Martin *et al*, 2012). With this in mind, we asked whether the PML-HIF2α protein complex that we detected by Co-IP assay reflected their association within the PML-NBs. To address this point, we performed proximity ligation assay (PLA) coupled to PML IF to visualize PML-HIF2α protein complexes distribution with respect to PML-NBs in RCC4 cells. We included RCC4 cells expressing exogenous VHL (hereafter RCC4+VHL) as a control of the specificity of PLA signals. We measured protein-protein interaction between PML and HIF2α and found 4.5 PML-HIF2α dots per nuclei in RCC4 cells, which diminished by ~50% when VHL expression was re-constituted and HIF2α degradation was re-established (Figure 49A and B), thus demonstrating the specificity of PML-HIF2α PLA interactions. A similar number of PLA interaction loci between PML and HAF were detected in RCC4 cells, but this number increased to 7.5 loci/cell upon VHL reconstitution (Figure 49A). This result could be due to the fact that RCC4+VHL cells express higher PML levels in comparison to RCC4, as shown by PML IF (Figure 49) and western blot (data not shown), although we do not know the mechanism leading

to this upregulation. These observations indicate that PML interacts in a similar way with HIF2α and HAF, albeit we do not know whether there are found in the same complex. Interestingly, we did not detect any co-localization or proximity between PML-HIF2α and PML-HAF interaction foci with the PML-NBs (Figure 49), thus suggesting that such protein complexes are formed outside the PML-NBs. Similar results were obtained in TNBC cells, where PML acts as a transcriptional co-activator of HIF1α and establishes a similar number of interaction foci, which however occur outside of the PML-NBs (data not shown). Therefore these data suggest that PML might modulate the transcriptional activity of HIF2α via binding to this protein in its DNA-associated forms, but this occurs outside the PML-NBs and may be mediated by nucleoplasmic PML moieties.
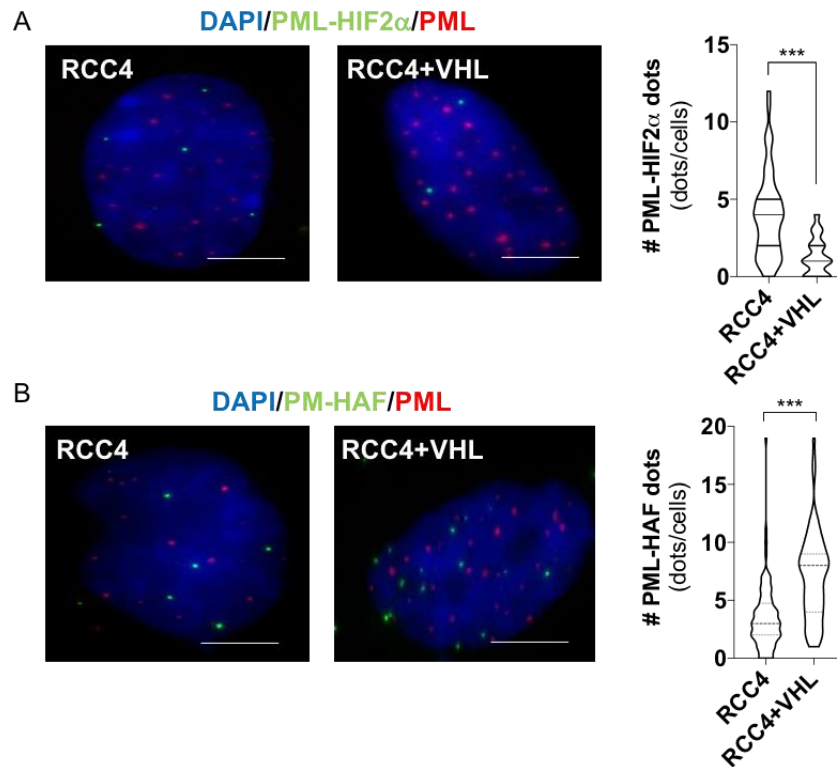
Figure 49. PML-HIF2α and PML-HAF complexes localize outside PML-NBs. Representative images of one out of three independent experiments of PLA assay coupled to IF. Green dots consist of PML-HIF1α (A) or PML-HAF (B) protein complexes visualized as PLA dots. PML was immuno-stained to visualize PML-NBs (red dots), in RCC4 and RCC4+VHL cell lines. Violin plots (right panels in A and B) are presented as single values indicating the number of nuclear PLA dots per cell, the bar represents the means. Images were acquired in 60x, scale bar 1µm. Statistical significance were calculated by Student's t-test (***p<0.001).

In conclusion, the results obtained so far suggest that: i) the transcriptional programs orchestrated by PML and HIFα transcription factors in ccRCC are only partially overlapping; ii) PML inhibits the expression of glycolytic HIF1α target genes; iii) PML enhances expression of pro-proliferative HIF2α-target gene ; iv) PML regulates HIF1α and HIF2α in opposite ways, by inhibiting HIF1α and promoting HIF2α expression; v) PML interacts with HIF2α and its transcriptional co-activator HAF on chromatin.

3.3 Aim 3- Test the effect of PML pharmacological targeting with arsenic trioxide in ccRCC

Arsenic trioxide (ATO) is currently used as first line therapy for APL patients, thanks to its ability to induce PML-RARα fusion protein degradation via direct binding to PML moiety (Lo-Coco *et al*, 2013; Lo-Coco *et al*, 2016). Moreover, PML targeting with ATO inhibits metastatization in TNBC (Ponente *et al*, 2017), disrupts glioma stem cells and tumor growth *in vivo* (Zhou *et al*, 2015), and causes cell cycle arrest in myeloma (Park *et al*, 2000), head and neck (Kotowski *et al*, 2012) and in A498 cells (Hyun Park *et al*, 2003), thus expanding the therapeutic potential of ATO to the treatment of solid tumors. Since we observed that PML plays fundamental tumor-promoting functions, here we aimed to test the therapeutic potential of ATO in ccRCC, and to evaluate whether PML pharmacological targeting induces anti-proliferative effects, both *in vitro* and *in vivo*, possibly recapitulating the antiproliferative effects that we achieved by its knock-down through genetic manipulation.

3.3.1 Non-cytotoxic doses of ATO impair focus forming efficiency of ccRCC cells

In order to test whether similar to PML silencing, ATO treatment blunted ccRCC growth by eliciting cytostatic effects via PML degradation, we treated ACHN, Caki-1, RCC4 and A498 wild type cells with increasing doses of the drug. To avoid cell death, we used lower concentrations than the 1 μM ATO dosage used in APL cells (Zheng *et al*, 2006; Lallemand-Breitenbach *et al*, 2008, Subastri *et al*, 2018), and measured cell viability through trypan blue exclusion assay (Figure 50A). Of note, none of the doses of ATO that we tested were cytotoxic (Figure 50A), and efficiently induced PML degradation (Figure 50B). Intriguingly, focus forming assays showed severe dose-dependent

cytostatic effect, except papillary ACHN cells, (Figure 50C). Of note, decreased proliferation was also evident at the lowest dose used in this assay, suggesting that ccRCC cells might be particularly sensitive to ATO treatment.
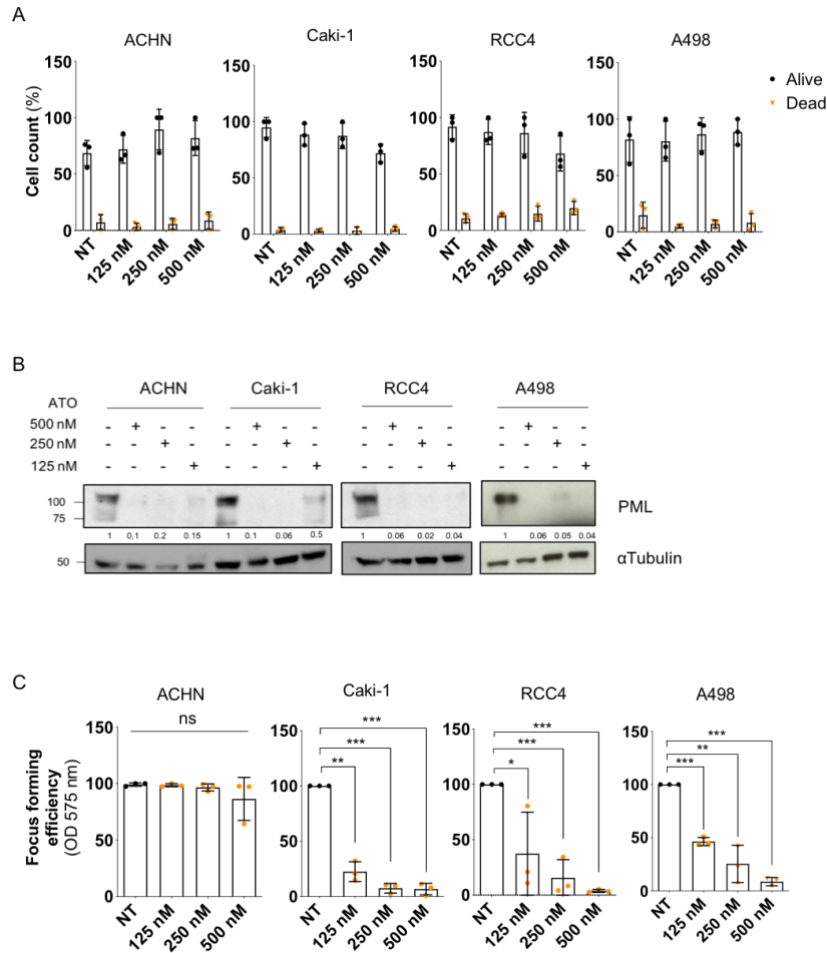
Figure 50. Non-cytotoxic doses of ATO efficiently degrade PML protein and inhibit ccRCC cells focus forming efficiency in a dose-dependent manner. (A) Trypan blue exclusion assay was performed in the indicated cell lines upon 48h of increasing ATO concentrations. (B) WB analysis of PML protein degradation following 48 hours of ATO treatment at the indicated doses. (C) Focus forming assay performed in the indicated cell lines, following 48h incubation with ATO at the indicated concentration. Focus forming efficiency was measured by crystal violet optical density (OD) at 575nm, and data are presented as percentages over respective non-treated (NT) conditions. Data represent the mean values ± SD of three independent experiments. Statistical significance was calculated with Student's t-test (*p<0.05, **p<0.01, ***p<0.001).

3.3.2 ATO inhibits A498 cells *in vivo* tumor growth

The results obtained so far strongly suggest that ATO exerts a cytostatic effect in ccRCC cell lines by inducing PML degradation at non-cytotoxic doses. This prompted us to test the efficacy of ATO treatment *in vivo*. We subcutaneously injected A498 cell line in the

flank of immunocompromised mice and once tumor volumes approached 200 mm^3, we started daily intraperitoneal injection of ATO (4 mg/Kg) at a concentration that is the mouse equivalent of the concentration used to treat APL patients. Importantly, at the time of sacrifice, mice subjected to ATO treatment displayed delayed tumor growth in comparison to the control cohort, suggesting that ATO achieved its cytostatic effects *in vivo* (Figure 51).
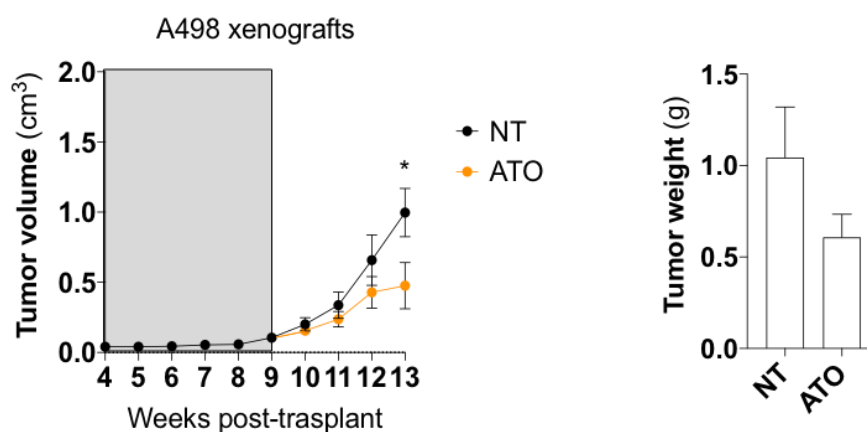
Figure 51. In vivo ATO administration impairs tumor growth. *Left panel shows growth curve of A498 xenografts before and during ATO administration ATO intraperitoneal injections (4 mg/Kg) were performed from week 9 to 13 from implantation. Right panel shows box plots of tumors weight at sacrifice of NT and ATO cohorts (n=6 per group). Data are expressed as mean ± SEM. Statistical significance was calculated with Student's t-test (*p<0.05).*

The data collected in the last aim of this work, indicate that ATO preclinical testing, *in vitro* and *in vivo*, showed anti-proliferative effects in ccRCC cells.

On these bases, since PML is an unfavorable marker of patients' clinical outcome, it might represents an attractive new pharmacological target, and ATO might be repurposed as cytostatic drug in ccRCC therapy.

4. Discussion

Since its discovery in APL, the PML protein attracted great research interest and the initial characterization of its cellular functions in hematological malignancies revealed its tumor-suppressive roles. Later studies further corroborated such evidence, showing that PML is frequently downregulated in various solid tumors. Nonetheless, a large body of literature in the last decade is showing that an inflexible definition as a tumor-suppressor is unrealistic for PML, a protein endowed with tumor-promoting functions in a wide spectra of cancer subtypes. Thus, it is becoming accepted that such dualistic functions of PML may reside in its role as a stress-responsive factor and in the fact that PML finely tunes multiple cellular processes, whose outcome may be tissue and cell-type specific.

The oncogenic functions of PML have been particularly investigated in TNBC, where it is over-expressed and mediates a multitude of tumorigenic pathways that include the regulation of FAO and cancer stem cells maintenance as well as promoting metastasis by enhancing the expression of HIF1α pro-metastatic target genes (Arreal *et al*, 2020; Martín-Martín *et al*, 2016; Ponente *et al*, 2017).

Importantly, HIF1α and its paralogue HIF2α, are crucial oncogenic drivers in ccRCC, and a preliminary and unpublished analysis of PML protein expression that was performed before the beginning of this study on ccRCC tissues and cell lines, had shown that PML is up-regulated in ccRCC, leading us to hypothesize that PML might synergizes with HIFα in promoting ccRCC oncogenesis. In contrast to our results, a different study reported that the PML protein is rather down-regulated in ccRCC, where it was shown to play tumor-suppressor functions (Ching *et al*, 2014). However, the effects of PML knock-down alone were not reported in this publication, and an independent study later reported that *PML* mRNA expression along with that of well-established oncogenes (*LRP1, CDK2, CDK4* and *PLAU*) correlates with tumor stage, lymph node and distant metastasis in ccRCC (Li *et al*, 2019). Here, we validated our preliminary data by observing that PML is over-expressed in the TCGA-KIRK and CPTAC-KIRK datasets at the mRNA and protein level respectively, and importantly we observed that PML over-expression correlates with worse patients outcome in ccRCC, further corroborating our hypothesis that PML may favor tumor progression in this tumor type, perhaps similarly to its function

in TNBC, where it promotes metastatic dissemination in concert with HIF1α (Ponente *et al*, 2017).

To test this hypothesis and to systematically characterize the functions of PML in ccRCC, we analyzed the phenotype elicited by PML knock-down in a panel of four human RCC cell lines belonging to the papillary and clear cell phenotype and characterized by distinct genetic alterations representative of ccRCC molecular types. Unexpectedly, we observed that the main phenotype associated to PML silencing was not a reduction of cell migration and invasion, in contrast to what we had previously demonstrated in TNBC (Ponente *et al*, 2017), rather the most evident phenotype was a reduction of cell proliferation through the regulation of cell cycle progression. This consequence of PML knock-down was so evident that it precluded the isolation of cell populations with stable PML silencing, unlike TNBC cells, which could be established in our laboratory upon constitutive PML silencing and showed a minor proliferation defect (data not shown). Inducible PML knock-down in ccRCC cells led to an abrupt and profound growth arrest correlated with the up-regulation of the tumor-suppressors p53 and p21. This occurred specifically in ccRCC cell lines and not in papillary ACHN cells, however, when pRCC cells were challenged in single-cell proliferation assays, PML silencing caused impaired focus forming capacity also in ACHN cells, although to a minor extent in comparison to ccRCC cells. Conversely, increasing the expression of PML isoform I to levels similar to human ccRCC cells in a murine RCC cell line that does not exhibit PML over-expression, was sufficient to increase focus forming efficiency, further supporting an important role of PML in promoting proliferation in renal cancer. Critical regulation of cell proliferation by PML in ccRCC was further supported by transcriptomic data, showing that PML promotes the expression of genes that are directly involved in proliferation and cell cycle progression like *PCNA*, *E2F*, *CDK1*, *CDC245*, *BUB3* and *POLE*. Additionally, our findings were corroborated by *in vivo* studies with two ccRCC models, showing that PML knock-down delays tumor growth, in some cases leading to features of tumor regression. Notably, a recent study performed in TNBC cells demonstrated that inducible inhibition of PML expression leads to growth arrest and senescence (Arreal *et al*, 2020). In line with these data, PML knock-down led to the acquisition of similar senescent-like morphological features also in ccRCC cells, including increased cell size and increased cell granularity that may be caused by increased accumulation of lysosomes (Kwon *et al*,

2019). However, we failed to detect two well-established senescence markers following PML knock-down in ccRCC cells, namely SA β-Gal positive cells and deposition of p-γH2A.x foci, in contrast to what was shown in TNBC and ovarian cancer cells (Liu *et al*, 2017; Arreal *et al*, 2020). Nonetheless, transcriptomic analysis revealed that similarly to TNBC cells PML loss leads to the downregulation of *LMNB1*, a structural component of nuclear envelope that is suppressed in cells undergoing senescence (Freund *et al*, 2012; Arreal *et al*, 2020). Also, we found that the expression of another marker of nuclear integrity, *HMGB1* (Lee *et al*, 2019) was reduced in response to PML silencing. These data may appear in contrast with the depletion of p-γH2A.x foci that we observed upon PML targeting. However, PML inhibition in ccRCC cells led to a major suppression of genes involved in DNA synthesis and repair, possibly as a consequence of the robust proliferation arrest, thus suggesting that the senescent-like phenotype that we observe in ccRCC cells is not elicited by DNA damage, but by other factors. Altogether, these pieces of evidence prompt us to speculate that the growth arrest triggered by PML loss is strongly reminiscent of cellular senescence. In line with this hypothesis, PML silencing in ccRCC appears to also upregulate expression of genes that belong to a SASP signature defined in TNBC cells by proteomic studies. Specifically, proteomic analysis of the supernatant of PML silenced TNBC cells revealed that SASP associated to PML knock-down is particularly enriched in ECM remodeling factors, thus not fully resembling the classical SASP (Arreal *et al*, 2020). This is probably due to the highly tissue and cell-type specificity of SASP composition (Hernandez-Segura *et al*, 2017). We confirmed that also in ccRCC PML silencing led to transcriptional upregulation of *MMP9*, *LOXL2*, *LOXL4*, *MMP1* and *ADAMTS1*, similarly to the secreted proteome of TNBC cells (Arreal *et al*, 2020). Although these ECM remodeling factors may also promote pro-invasive features, PML knock-down does not affect migratory or invasive capacity of ccRCC cell lines, suggesting that in this context they may also be produced as part of a senescent secretome. Moreover, similarly to senescent TNBC cells, we observed up-regulation of the pro-inflammatory cytokines *CXCL8* (aka *IL8*) and *IL6*, whose presence in SASP is conserved among different tissues (Hudgins 2018). Albeit a complete characterization of the PML-associated secretome is still lacking, altogether these data suggest that PML depletion induces growth arrest and senescence in ccRCC cells and this phenotype lacks classical

senescence markers and may represent a late, inflammatory type of senescence (Kirkland & Tchkonia, 2020).

Beside the defect in cell proliferation, important differences in cell morphology were induced by PML silencing. Specifically, such phenotypic alterations included: increased cell size and granularity, cell flattening and the formation of cytoplasmic vacuolar-like structures. While increased flattening and granularity are typical features of senescent cells, the presence of large cytoplasmic vacuoles was more difficult to interpret. To elucidate their nature, we performed cell morphology investigation by TEM. These studies suggested that the large cytoplasmic vacuoles that can be easily observed by light microscopy upon PML silencing may represent dramatic invaginations of the cell membrane, as they are empty of cytoplasmic content and may present microvilli-like structures in their internal surface, typical of proximal tubular epithelial cells. These data suggest that PML silencing may lead to a transition from an anaplastic and undifferentiated state to a kidney epithelial-like morphology in ccRCC cells. Although intriguing, this hypothesis needs to be further studied since 2D culture does not allow a full characterization of cell morphology. Therefore, 3D systems will be helpful to univocally describe the involvement of PML in the regulation of kidney cell polarization. Along with the functional and morphological characterization of ccRCC cells depleted of PML, to gain molecular insights into the functions of PML in this tumor context where it has been poorly studied, we characterized the transcriptional profile of ccRCC cells upon PML depletion. Surprisingly, this analysis revealed that PML down-regulation severely impinges on the expression of genes regulating glycolytic metabolism, a biological process that has been largely attributed to HIF1α. Specifically, we found that PML repressed the expression of *bona fide* HIF1α-target genes regulating glycolysis. Of note, some of these genes (*PDK1*, *PGK1* and *BINIP3)* inversely correlated with PML expression in the TCGA-KIRK dataset. In contrast, PML promotes the expression of HIF2α targets involved in cell proliferation and self-renewal, thus suggesting that the oncogenic functions of PML in ccRCC might result from a synergy between HIF2α and PML. In line with this hypothesis, the top gene categories down-regulated upon PML silencing in our experiments matched with the same gene sets identified upon HIF2α pharmacological inhibition in PDX mouse models of ccRCC (Chen *et al*, 2016). Consistently, we found that PML interacts with both HIF2α and its transcriptional co-

activator HAF (Koh *et al*, 2015) in their chromatin-bound conformation, thus revealing a novel PML interactor that might provide the basis of PML-dependent positive regulation of HIF2α activity. Intriguingly, we demonstrated that PML-HIF2α and PML-HAF, protein complexes localize outside PML-NBs. Similar results were obtained when investigating PML-HIF1α interactions in TNBC cells (data not shown), thus suggesting that PML-dependent transcriptional regulation of HIFs signaling is mediated by nucleoplasmic PML moieties. Finally, we observed that in ccRCC PML regulates the balance between HIFα proteins, by promoting HIF2α expression while inhibiting HIF1α. Taken together these data strengthen the functional cross-talk between PML and hypoxia signaling via HIFα genes that we had previously defined in TNBC (Ponente *et al*, 2017), but also suggest that there may be a strong tissue-specific component to the regulation of HIFα factors by PML, as PML appears to promote or repress the activities of HIFα in different tissues, and to impinge on the regulation of different sets of target genes.

Within the gene categories suppressed by PML, besides glycolytic genes and ECM remodeling factors, we found the enrichment of genes involved in cholesterol biosynthetic processes. Of note, these transcriptional alterations are considered typical of highly proliferative cancer cells (Giacomini *et al*, 2021; Hanahan & Weinberg, 2011), and their upregulation in growth arrested ccRCC cells upon PML loss may appear counterintuitive. Nonetheless, enhanced glucose catabolism and cholesterol biosynthesis are common features of senescent cells, because although non-proliferative these cells maintain high metabolic activity (Herranz & Gil, 2018; Kwon & Hong, 2019). A mechanistic explanation of this phenomenon is still lacking, but it is believed that ATP moieties from glycolysis fuel protein synthesis of SASP factors (Dörr *et al*, 2013). Interestingly, it was reported that this may contribute a targetable vulnerability of senescent cells, by leading to excessive proteotoxic stress due to ER over-loading (Dörr *et al*, 2013). Along these lines, preliminary experiments performed in the laboratory revealed that tunicamycin (an inhibitor of N-glycosylation causing ER proteotoxic stress) is synthetically lethal with PML silencing on RCC4 cells (not shown). However, additional experiments are needed to validate these data across ccRCC cell lines,

Cholesterol biosynthetic genes regulated by PML in ccRCC included the transcription factor *SREBF2* and its target genes *HMGCR*, *HMGCS*, *ELOV6*, and *IDI1*. Our data are in line with previous evidence obtained in different cells and tissues where PML was

similarly found to suppress cholesterol anabolic pathways. PML inhibits cholesterol biosynthesis in liver, white adipose tissue and in skeletal muscle (Chang *et al*, 2013), as well as in a mouse model of prostate cancer, via suppression of SREBP2 transcriptional program (Chen *et al*, 2018). Of note, in this last study suppression of cholesterol biosynthesis was linked to PML tumor suppressive functions in prostate cancer, and was suggested to lead to inhibition of metastasis (Chen *et al*, 2018). However, previous work in ccRCC patients samples has revealed that the cholesterol biosynthetic pathway is suppressed in ccRCC when compared to normal kidney tissue, rendering ccRCC cells auxotroph for such nutrient (Qi *et al*, 2021). Consistently, an inverse correlation was reported between cholesterol biosynthetic genes (*HMGCR*, *FDFT1*, *DHCR24*, *SQLE,* and *LSS*) and genes involved in extracellular cholesterol up-take (*SCARB1*, *VLDLR,* and *CD34*), which are upregulated in ccRCC (Riscal *et al*, 2021). We here report that PML over-expression is inversely correlated with a subgroup of SRBP2 target genes in the TGCA-KIRK dataset (*HMGCR*, *HMGCS1,* and *IDI1*), thus suggesting the possibility that PML might be involved in the acquisition of cholesterol autotrophy in ccRCC, a context where PML is over-expressed and plays fundamental oncogenic functions. In this scenario, PML inhibition might lead to a cholesterol overload, with possible detrimental consequences on ccRCC cells proliferation. In line with this, it was shown that kidney epithelial cells display proliferative defects when challenged with cholesterol (Honzumi *et al*, 2018). Also, cholesterol biosynthesis has been implicated in senescence, by promoting *de novo* assembly of cell membranes to increase organelles biogenesis, including lysosome and biomass, thus resulting in increased cell size (Saxton & Sabatini, 2017; Kotas *et al*, 2017).

On the basis of this evidence, we hypothesize that senescence induction by PML inhibition might be due to the re-activation of *de novo* cholesterol anabolism that, coupled to its uptake from the microenvironment, could lead to a senescence-like phenotype triggered by lipotoxicity. To test this hypothesis, we will measure the effect of cholesterol inhibitors like statins on PML silenced cells and will perform rescue experiments to test whether SREBP2 silencing may inhibit growth arrest induced by PML loss in ccRCC.

In summary, albeit inducible PML silencing leads to a similar senescent-like growth arrest in TNBC and ccRCC cells, the mechanism of this process may be different as in TNBC it was suggested that senescence is triggered via PML-dependent transcriptional

regulation of c-Myc (Arreal *et al*, 2020). In contrast, we did not find c-Myc deregulation in ccRCC cells, thus prompting us to investigated alternative mechanisms including regulation of cholesterol biosynthesis.

Finally, having demonstrated important tumor-promoting functions of PML in ccRCC via *in vitro* and *in vivo* studies, we propose that PML may represent a new pharmacological target in this disease, an hypothesis that we have begun testing by using ATO in a preclinical ccRCC model. In these experiments we aim to validate whether PML targeting induces senescence *in vivo*. In this respect, because senescence *in vivo* may contribute to chronic inflammation and fibrosis via SASP production, thus promoting immune evasion and tumor spread (Herranz & Gil, 2018), we will expand our preclinical testing of the pharmacological application of ATO in ccRCC to include combination with senolytic drugs, with the aim to eradicate senescence-like cells that may accumulate as a result of PML pharmacological inhibition. Also, since PML and HIF2α share co-regulated genes that are crucial for cell proliferation, PML-dependent proliferative functions may be mediated by HIF2α, we will also test the efficacy of the pharmacological combination with the HIF2α selective inhibitor Belzutifan that has been recently FDA approved for the treatment of VHL patients with RCC-associated disease (source: FDA website. http://www.fda.gov/cder/approval/index.htm). However, in this respect our data show that PML exerts important oncogenic functions in ccRCC cells irrespective of VHL mutational status, thus suggesting that PML activities extend beyond cooperating with HIFs signaling in this tumor context.

In conclusion, we have found that ccRCC represents a tumor type with a striking non oncogenic addiction to PML, and further mechanistic studies will be necessary to elucidate the full extent of this dependency.

4. MATERIALS AND METHODS

Cell culture

The human RCC cell lines (ATCC) Caki-1 and A498 and murine RCC cells RenCa, were maintained in RPMI-1640 (Lonza). RCC4, RCC4+VHL and ACHN cell lines were maintained in DMEM high glucose (Lonza). HEK293T cells were used for lentivirus preparation and maintained in IMDM (Lonza). All cell media were supplemented with 10% FBS (Carlo Erba) and 100 Ul/ml penicillin and 100 μg/ml (1% Pen-sptep, Lonza). After lentiviral transduction with Tet-pLKO-puro plasmids containing shRNA against PML transcript (shPML and shPML#2) or a scramble sequence (shCtrl) used as control, cell media were supplemented with tetracycline free FBS (Euroclone) to avoid promoter leakiness. To induce PML silencing, cells were treated with 100 ng/ml of doxycycline monohydrate (Sigma) every 48h. All cell lines were grown at 37°C in humidified incubator at 20% O_2 and 5% pCO_2.

Treatments and reagents

Arsenic trioxide (Sigma) was used to treat ACHN, Caki-1, RCC4 and A498 cells at the indicated concentration for 48 hours. For *in vivo* experiments, ATO was administered at 4 mg/Kg through daily intraperitoneal injection until sacrifice.

Doxycycline monohydrate was purchased form Merck (D1822-500MG) and added to cell culture media (100 ng/ml) and cells were incubated 96 hours to achieve PML silencing. Media was changed every 48 hours. For *in vivo* experiments, doxycycline hyclate was purchased form Merck (D9891-1G) administered at 5 mg/Kg through daily oral gavage. Nutlin-3 was purchased by Merck (N6287) and used at 10 nM final concentration. To induce senescence, cells were treated for 6 days.

Lentiviral vectors, virus production and cell lines transduction

To induce PML silencing, we used of Tet-pLKO-puro plasmid expressing shPML (TRCN0000003867) and scramble sequence as a control, was kindly donated by Prof. Arkaitz Carracedo (Biochemistry and Molecular Biology Department, University of the Basque Country (UPV/EHU), Bilbao, Spain). Tet-pLKO-puro plasmid expressing shPML#2 (TRCN0000003868) was sub-cloned from Tet-pLKO-puro form Addgene

(plasmid #21915) following the protocol provided by Dmitri Wiederschain, Novartis Developmental and Molecular Pathways, Cambridge, MA, USA. Briefly, *AgeI* and *EcoRI* restriction sites at the 5' ends of top and bottom shRNA, respectively. 50ng of open Tet-pLKO-puro empty vector were used for ligation. 100 μl Stbl3 bacteria (Invitrogen) were used for transformation of 10 ml of ligation product. Diagnostic digestions to screen for positive colonies were performed using *XhoI* restriction enzyme (NEB).

For viral particle generation, 8×10^6 of HEK293T cells were seeded in p150 petri dishes and grown in IMDM, 10% FBS w/o Pen-Strep. For cell transfection, calcium phosphate based method was used. 32 μg of Tet-pLKO-puro shCtrl, Tet-pLKO-puro shPML, or Tet-pLKO-puro shPML#2, and packaging plasmids (6.25 μg of pRSV-Rev, 12 μg of pMDL-pRRE and 9 μg of pCMV-VSV-G) were used. The day after transfection, the media was replaced and the supernatant containing the lentiviral particles were harvested 24 and 48 hours after. Lentiviral particles were concentrated through ultracentrifugation (20000 rpm 2.20 hours). The viruses were then resuspended in ice cold PBS and stored at -80°C until use.

For lentiviral transduction, human RCC cells were seeded at 80% confluency and the day after, lentiviral particles were added to the media containing 8 μg/ml polybrene (MERK), 10% tetracycline free FBS (Euroclone) and 1% Pen-strep (Lonza). After over-night incubation, the media was changed and the antibiotic selection was applied after 48h form infection. Puromycin concentration was determined for each cell line: 1 μg/ml for ACHN and RCC4, 0.5 μg/ml for Caki-1 and A498 cell lines.

Generation of stable RenCa eGFP-PMLI, eGFP-PMLIV and eGFP clones

eGFP-PMLI and eGFP-PMLIV expression plasmids were gifted by Prof. Andreas Hemmerich (Universität Hamburg, Institute für Laserphysik, Hamburg, Germany). 1 μg of each plasmid was transfected in RenCa cells grown at 80% confluency using Lipofectamine LTX (Invitrogen) following manufacture instructions. FUGW plasmid encoding GFP, was used as control and was provided by Dot. Davide Gabellini (San Raffaele Scientific Institute, Milan, Italy). The day after, the media was changed and after 48h form transfection cells were screened for GFP expression.

Cell sorting was performed on a BD FACSAria Fusion (BD Biosciences) equipped with four lasers: Blue (488 nm), Yellow/Green (561 nm), Red (640 nm) and Violet (405 nm).

100 μm nozzle was used and sheath fluid pressure was at 25 psi. A highly pure sorting modality (4-way purity sorting) was chosen. The drop delay was determined using BD FACS AccuDrop beads. To facilitate high-speed sorting and to prevent clogging of the nozzle, samples were filtered through 35 μm filter (Falcon® 5 ml Round Bottom Polystyrene Test Tube, with Cell Strainer Snap Cap) immediately prior to sorting.

Sorted cells were collected in 96 well plate. Unstained and GFP$^+$ controls have been used to set up compensation. Rainbow beads (SPHEROTM Rainbow Calibration Particles) were used to standardize the experiment and were run before each acquisition.

Co-immunoprecipitation, nuclear fractionation and western blotting

To perform subnuclear fractionation needed to isolate cytoplasmic and nuclear soluble protein and chromatin-bound proteins, we applied the protocol described in Vertegaal *et al*, 2004. In particular, to extract the soluble fraction cells were lysed in CSK buffer (100 mM HEPES, 300 mM sucrose, 3 mM $MgCl_2$, 1 mM EDTA, 0.5% TritonX-100) containing 100 mM NaCl and incubated 20 minutes on ice. After centrifugation (10 minutes 13 000 rpm), the soluble fraction and the pellet, consisting in the insoluble fraction, were separated. The pellet was washed three times in CSK buffer and further fractionated to extract chromatin-bound proteins. In this case, the pellet was treated with CSK buffer containing 50 mM NaCl and 20 U DNaseI (Sigma) and incubated 1h 4°C. Chromatin-bound proteins were solubilized and extracted by adding $(NH_4)_2SO_4$ at 0.25 M final concentration and incubated 30 minutes on ice. The final centrifugation step (10 minutes 13 000 rpm) allowed to separate chromatin-bound protein from the nuclear matrix.

Protein concentration was measured by Bradford protein assay was used (BioRad). Immunoprecipitation of 0.5-1 mg of protein lysate was precleared by incubation with 40 μl of sepharose beads protein G (GE Healthcare) 1h 4°C on a rotatory shaker. After beads removal, immunoprecipitation was performed over-night in 1 ml of final volume (of CO-IP or CSK buffer) using 1 μg of primary anti-PML antibody (refer to Table 1 for antibody information), or normal mouse IgG as negative control were used. The day after, 40 μl of sepharose beads protein G (GE Healthcare) were used to capture primary antibody bound to protein complexes of interest. After 5 washes in CSK buffer, protein complexes and the primary antibody were eluted and partially denatured by adding 4x laemmli buffer

(BioRad) and boiled at 95°C for 5 minutes. The samples, were resolved by SDS-PAGE in 7.5% polyacrylamide gels (BioRad) and transferred to PVDF membranes by using transBlot TurboTM Transfer System (BioRad).

PVDF membranes were blocked in PBS Tween-20 0.1% 5% BSA 1 hour at room temperature and washed three times with PBS Tween-20 0.1% (10 minutes per washing) and finally incubated with primary anti PML, HIF2α and HAF over-night 4°C as indicated in Table 1, diluted in PBS Tween-20 0.1% 1%BSA. Secondary antibodies HRP-conjugated (Table 1) were allowed to hybridize for 1 hour at room temperature in PBS Tween-20 0.1% 1% BSA. Proteins were detected using films (GE Helthcare) and ClarityTM Wester ECL Substrate (BioRad) was used to detect bioluminescence.

Proximity ligation assay (PLA) and immunofluorescence

$20x10^3$ RCC4 or RCC4+VHL cells were plated in 12 well plate on 13 mm coverslip. The proximity between PML and HIF1α, HIF2α or SART1 were detected using Duolink® Proximity Ligation kit purchased form Merk (DUO92101) applying manufacturer's instructions (see Table 1 for the list of primary antibody used).

After PLA, IF was performed to stain PML-NBs and observe PML-HIF2α and PML-HAF localizations. the coverslips were incubated 1 hour at room temperature with anti-PML primary antibody (see Table 1). After tree washes with PBS the glasses were incubated with AlexaFluor546-conjugated secondary antibody (see Table 1) 1 hour at room temperature. Additional three washes in PBS were performed prior to DAPI (Duolink® in Situ Mounting Medium with DAPI) counterstaining and coverslip mounting with Mowiol. 63x images were acquired using Zeiss Axio Imager M2 epifluorescence microscope. Finally, PLA nuclear signals were manually counted after image manipulation: Z-stacks were used to reconstruct the MAX projection (RGB) of cell nuclei by using ImageJ software.

LAMP1 and LAMP2 immunofluorescences were performed by plating $20x10^3$ shCtrl and shPML RCC4 and A498 cell lines in 12 well plate on 13 mm coverslip, after 96 hour of doxycycline treatment. Cells were fixed 5 minutes at room temperature in 4% PFA, and then permeabilized with 0.1% saponin. Prior to primary antibody incubation, cells were blocked in PBS 3% BSA. Anti LAMP1 and LAMP2 antibodies where diluted in PBS 1%BSA, at final concentratations indicated in Table1, overnight 4°C. The day after,

glasses were washed three times in PBS and then incubated 1h RT with Alexa-Fluor 488 anti mouse antibody diluted in blocking solution at final concentration indicated in Table 1. After three additional washes in PBS, nuclei where counterstained with DAPI 10 minutes RT. Then, glasses where washed three times and mounted on a coverslip by using Mowiol.

Murine and human PML in RenCa and RCC4 cells was detected by IF by fixing cells as described above. 10% FBS, 0.05% Tween-20 was used as blocking solution. Anti Pml and anti PML antibodies were diluted in 1%FBS 0.05% Tewwn-20 in PBS at final concentrations indicated in Table 1, and incubated 1h at room temperature. After three washes, glasses were incubated 1 hour room temperature with AlexaFluor 546 antibodies at final concentration indicated in Table 1. After three washes in PBS, DAPI was added and incubated 10 minutes room temperature. After three additional washes in PBS, glasses were mounted on a coverslip with Mowiol.

63x images mages were acquired using Zeiss Axio Imager M2 epifluorescence microscope. Z-stacks were used to reconstruct the MAX projection (RGB) by using ImageJ software.

Proliferation assay

For cell proliferation assays, 25×10^3 ACHN and Caki-1 cells, 5×10^3 RCC4, A498 and RenCa cells were pleated in triplicates in 12 well plate, one plate per each time point. After 24h of plating, one plate was fixed with PBS 4% PFA and stained using 0.1% crystal violet staining solution (98 ml distilled water, 2 ml methanol and 0,1 g Crystal Violet) and considered as Day1. In the other plates, the media was removed and substituted with media containing doxycycline to induce PML silencing. The media was changed every 48h hour to guarantee doxycycline efficacy.

Crystal violet was solubilized using dH_2O 10% acetic acid and cell proliferation was calculated measuring crystal violet absorbance at $\lambda=575$ nm and expressed as OD575.

Focus firming assay

ACHN, RCC4, Caki-1 and RenCa cell lines were plated in triplicate in a 6 wells plate (1×10^3 cells/well) for 14 days to allow them to form colonies. Then, cells were fixed using PBS 4% PFA and stained using 0,1% Crystal Violet Staining Solution. The colony

formation efficiency was evaluated solubilizing Crystal violet using dH_2O 10% acetic acid. Colony forming efficiency was calculated measuring crystal violet absorbance at λ=575 nm and expressed as absorbance OD575.

Wound healing assay

Cell lines have been treated 97 hours and plated in triplicate with 100 ng/ml doxycycline (Sigma) to induce PML silencing and allowed to reach 100% confluency. At this time point, the scratch was made using 20-200 μl micropipette tips and the media was replaced with media w/o FBS to avoid proliferation biases. Three fields were acquired in brightfield using Zeiss Axio Observer Z1 microscope at indicated time points. Wound area reduction was measured using ImageJ software and normalized over shCtrl.

Transwell invasion assay

All RCC human cell lines were treated for 96 hours with 100 ng/ml doxycycline (Sigma) and then were re-plated in the top chamber of the transwell (Costar) coated with 1:1 media and Martrigel at final concentration of 0.125 μg/ml (BD Bioscience). Cells were allowed to invade Matrigel matrix for 48h following FBS gradient (0% in the top chamber, 10% in the bottom chamber) at 37°C and pCO_2 5%.

Prior fixation, non-invading cells were removed from the bottom chamber by using a tampon, then the invading cells were fixed in PBS PFA4% and stained with 0.1% crystal violet. Tree field were acquired in brightfield for each sample using Zeiss Axio Observer Z1 microscope and cells/field were counted by using ImageJ software.

Cell cycle, apoptosis and FACS analysis

ACHN, Caki-1 RCC4 and A498 shCtrl and shPML cells, were pre-treated with doxycycline (100 ng/ml) for 72 hours prior cell cycle analysis or Annexin staining. At this time point, 200×10^3 cells were re-plated and maintained under doxycycline treatment. The day after, cells were pulsed with BrdU (10 μM) for 20 minutes to allow BrdU incorporation by proliferating cells that then were detached, washed once in PBS and then fixed in 70% ethanol and stored at -20°C until FACS analysis.

Cells were washed two times in PBS 1% BSA and subjected to DNA denaturation using 2N NaCl that after 2 minutes was neutralized by adding $Na_2B_4O_7$. BrdU staining was

detected through anti-BrdU AlexaFuor 488 antibody (see Table 1). Hybridization occurred over-night at 4%. DNA was counterstained with PI (Sigma) and RNA digested with RNaseI (Invitrogen) and leaved at 4°C overnight. The day after, cells were washed once in PBS and resuspended in PBS at 100 000/100 µl concentration.

For apoptosis assay, 50×10^3 were plated and maintained 96 hours in doxycycline containing media. Then, apoptosis was evaluated by performing Annexin staining using the PE-Annexin Apoptosis Detection Kit (BD Bioscience) following the manufacturer's instructions.

For all the experiments stained cells were detected by FACS analysis using DB FACSCanto™ II (Becton Dickinson) availble at FRACTAL ISO9001 certified facility at San Raffaele Scientific Institute. Data were analysed with FCS Express Flow Cytometry Software (De novo Software).

Oil Red O staining

The cell line tested were maintained in doxycycline supplemented medium for 96 hour. At 72 hours of doxycycline incubation, 250×10^3 cells were re-plated in p100 mm petri dishes and miniated in doxycycline 24 hours. Cells were washed once in PBS and fixed using 10% formalin (Bio-Optica #05-01-V15P) 30 minutes room temperature. Plates were washed with sterile water and subsequently incubated with 60% isopropanol for 5 minutes. For Oil Red O staining solution preparation, 0.5 mg of Oil Red O Powder form Merck (O0625) were dissolved in 100 ml 90% isopropanol. 3 parts of Oil Red O stock solution were added to 2 parts of deionized water and the solution was allowed to seat at room temperature 10 minutes. Then, the solution was filtered with 3M paper to remove precipitates. Finally, fixed cells were incubated with Oil Red O working solution 20 minutes at room temperature. Cells were rinsed with tap water and nuclei were counterstained with haematoxylin. Neutral lipids staining was evaluated by light contrast phase microscope (Zeiss AxioImager M2m) and representative photographs were acquired with Axiocam MRc5.

Senescence-associated β-Galactosidase staining

The cell line tested were maintained in doxycycline supplemented medium for 96 hour. At 72 hours of doxycycline incubation, 20×10^3 cells were re-plated on the top of 13 mm

coverslip in 12 well plate in triplicate, and miniated in doxycycline 24 hours. At 96 hours of doxycycline induction, cells were fixed with PBS 4% PFA 10 minutes at room temperature. SA β-Gal staining was performed by using Senescence-associated β-Galactosidase staining Kit from Cell Signaling technology following the manufactures' instructions.

Transmission electron microscopy

Cultured cells were fixed as monolayer with 2.5% glutaraldehyde in 0.1M cacodylate buffer pH 7.4 for 1 hour at room temperature. After several washes in cacodylate buffer, cells were postfixed with 1% osmium tetroxide, 1.5% potassium ferrocyanide in 0.1M cacodylate buffer pH 7.4 for 1 hour on ice. After being rinsed in dH2O, samples were en bloc stained in 0.5% uranyl acetate overnight and dehydrated in increasing concentrations of ethanol, and finally embedded in Epon. Samples were cured at 60°C in an oven for 48 houtrs. Epon blocks were sectioned using a Leica EM UC7 ultramicrotome (Leica Microsystems). Ultrathin sections (70 nm) were collected on formvar carbon-coated slot grids, contrasted with 2% uranyl and lead citrate. Samples were observed with a TALOS L120C Transmission Electron Microscope (ThermoFisher Scientific) and images were acquired with a CETA 4x4k CMOS camera (ThermoFisher Scientific).

Xenograft mouse models

The animals used in this study were kept in pathogen-free animal facility and cured in accordance with European Union guidelines. All the applied procedures have been approved by the Institutional Animal Care and Use Committee (IACUC), IACUC number 989. For *in vivo* tumor growth assay, $4x10^6$ A498 and $10x10^6$ Caki-1 expressing doxycycline-inducible shCtrl and shPML constructs, were subcutaneously injected in the right flank of 6-8 weeks old female and male NSG mice, respectively. From transplantation, the mice were maintained in the absence of doxycycline and tumor volumes were measured weekly using a caliper. When the tumor masses arose form shCtrl and shPML cells approached 1 cm^3 of volume, doxycycline hyclate (Sigma) was administered daily through oral gavage (25 mg/Kg) until sacrifice.

To test the *in vivo* efficacy of ATO, $4x10^6$ A498 or $10x10^6$ Caki-1 wild type cells were subcutaneously injected into the right flank of NSG mice. When the tumor masses

approached 1 cm^3, mice were randomly distributed in 2 cohorts. One group was treated with of arsenic trioxide (Sigma) administered intraperitoneally. Tumor diameters were calculated on two sided weekly using a caliper and the formula length x diameter^2 x π/6. The animals were sacrificed at the indicated time points.

Immunohistochemistry and hematoxylin-eosin staining

Formalin-fixed paraffin-embedded consecutive sections (4 μm) were dewaxed and hydrate through graded decrease alcohol series and stained for histology or immunohistochemical characterization (IHC).

For histological analysis in bright-field microscopy, slides were stained using standard protocols for Hematoxylin and Eosin (using Mayer's Hematoxylin, BioOptica #05-06002/L and Eosin, BioOptica #05-10002/L).

For IHC characterizations, slides were immunostained with Automatic Leica BOND RX system (Leica Microsystems GmbH, Wetzlar, Germany). First, tissues were deparaffinized and pre-treated with the Epitope Retrieval Solution (ER1 Citrate Buffer for Ki-67 and PML and ER2 EDTA for Caspase 3,) at 100°C. (see Table1 for antibody specifications). Primary antibodies were developed with Bond Polymer Refine Detection (Leica, DS9800).

Slides were acquired with Aperio AT2 digital scanner at magnification of 20X (Leica Biosystems) and analyze with Imagescope (Leica Biosystem). Immunohistochemical staining of PML and KI67 was quantified using Color Deconvolution Algorithm (Leica) following manufacturer's instruction. For analysis, three different areas of the slides of all samples (1 mm^2 each) were used.

RNA isolation and quantitative RT-PCR (qRT-PCR)

Total RNA from RCC cells was purified using RNeasy mini Kit (Quiagen) and RNA from xenografts was isolated using ReliaPrep RNA Tissue Miniprep System (Promega). cDNA was obtained using Advantage RT-for-PCR Kit (Clontech) and random-hexamer primers were used. To measure the gene expression, RT-PCR was performed by TaqMan assay using a 7900 Fast- Real Time PCR System (Applied Biosystems). All probes for TaqMan assays were purchased from Applied Biosystem. 18S was used as internal

control. The mRNA relative fold change expression (shPML over shCtrl experimental conditions) of the indicated genes, were calculated using $2^{-\Delta\Delta Ct}$ method.

RNAsequencing and analysis

Total RNA from shPML, and shCTRL from RCC4 shCtrl and shPML#1 cells was isolated with QIAGEN RNeasy Plus Micro Kit according to the manufacturer's instructions. RNA-sequencing experiments are representative of two biological replicates, and lentiviral transfections. RNA quality was evaluated with a 2100 Bioanalyzer (Agilent). To generate the libraries, the TruSeq stranded mRNA protocol was used. Libraries were barcoded, pooled and sequenced on an Illumina Nova-Seq 6000 sequencing system. RNA-sequencing experiments were performed generating 30M reads, 100 nucleotide (nt) long, for each run. After trimming, sequences generated within RNASeq experiments were aligned using the STAR aligner (Dobin et al, 2013) and counted with featureCounts (Liao et al, 2014) on the last Gencode (Harrow et al, 2012) release for RNAseq. Differential genes expression was evaluated in R/BioConductor (Huber et al, 2015) using the DESeq2 package (Love et al, 2014). Finally, EnrichR v3.0 (Kuleshov et al, 2016) was used to perform gene set enrichment analysis and find common annotated biological features of DEGs gene and the heatmaps showing the top 100 statistically significant genes (AdjPval<0.1) was generated using Pheatmap package form CRAN. Gene sets were obtained by filtering DEGs with logFC>/< 0.3 and FDR 0.05 while significant gene categories were filtered for Adjusted p-value <0.1.

TCGA-KIRK, TCGA-KIRP and CPTAC-KIRK datasets analysis.

TCGA-KIRK, TCGA-KIRP and CPTAC-KIRK datasets (Creighton et al, 2013; Clark et al, 2019) were explored by using the UALCAN online toll (Chandrashekar et al., 2017; online source: http://ualcan.path.uab.edu) . In this study, the expression analysis of *PML* gene in ccRCC and pRCC tumor samples and normal tissue was obtained. Additionally, patients survival rate correlating with PML expression levels was performed. Alteration frequency of *PML* gene in ccRCC was performed by interrogating TCGA-KIRK (Creighton et al, 2013) database available at cBioPortal (Cerami 2012; Gao 2013; online source: https://www.cbioportal.org). Spearman's correlation analysis between PML

mRNA abundance and the indicated genes in the TGCA-KIRK dataset were retrieved by using cBioPortal (Cerami 2012; Gao 2013; online source: https://www.cbioportal.org).

Statistical analysis

Student's two-tailed t-test was used to determine statistical significance of all the data analyzed, except for data obtained from TCGA, and AML primary samples results that were analyzed by one-way ANOVA. The significance level was set at a p-value of less than 0.05. All analyses were performed using GraphPad Prism version 8.2.1 for macOS (GraphPad Software, San Diego, California, USA, www.graphpad.com).

Table 1. List of antibodies used in the study.

Antibody	Application	Used dilution or concentrations	Specifications
PML	Immunoprecipitation Immunohistochemistry	1 µg 1:100	(PGM3) SC-996
	Western blot	1:1000	NB100-597787
	Chromatin immunoprecipitation	200 µg/ml	SC-71910
HIF1α	Western blot	1:250	BD 610958
	PLA	1:5000	NB100-134
HIF2α	Western blot	1:250	Cell signaling technology (D9E3)#7096
	PLA	1:5000	NB100-122
p53 (DO-1)	Western blot	1:3000	SC-126
p21	Western blot	1:500	SC-6246
HAF	Western blot	1:500	Merck HPA031190
Pml clone 36.1-104	Immunofluorescence	1:1000	Millipore MAB3783
LAMP1	Immunofluorescnece	1:50	Abcam 30687
LAMP2	Immunifluorescence	1:50	Abcam 25631
β-Actin (AC-15)	Western blot	1:10000	SC-69879
Vinculin (7F9)	Western blot	1:10000	SC-73614

Mouse (G3A1) IgG1 Isotype control	Immunoprecipitation	1μg	Cell signaling technology #5415
Goat anti-mouse IgG-HRP	Western blot	1:10000	SC-2005
Mouse anti-rabbit IgG-HRP	Western blot	1:10000	SC-2357
AlexaFluor 488 Goat anti mouse	Immunofluorescence	1:100	ThermoFischer A32732
AlexaFluor 546 Goat ant rabbit	Immunofluorescence	1:100	Thermo Fischer A32731

5. REFERENCES

Alhazmi N, Pai CP, Albaqami A, Wang H, Zhao X, Chen M, Hu P, Guo S, Starost K, Hajihassani O, *et al* (2020) The promyelocytic leukemia protein isoform PML1 is an oncoprotein and a direct target of the antioxidant sulforaphane (SFN). *Biochim Biophys acta Mol cell Res* 1867: 118707

Alimov A, Sundelin B, Wang N, Larsson C & Bergerheim U (2004) Loss of 14q31-q32.2 in renal cell carcinoma is associated with high malignancy grade and poor survival. *Int J Oncol* 25: 179–185

Altabef M, Garcia M, Lavau C, Bae SC, Dejean A & Samarut J (1996) A retrovirus carrying the promyelocyte-retinoic acid receptor PML-RARalpha fusion gene transforms haematopoietic progenitors in vitro and induces acute leukaemias. *EMBO J* 15: 2707–2716

Amodeo V, A D, Betts J, Bartesaghi S, Zhang Y, Richard-Londt A, Ellis M, Roshani R, Vouri M, Galavotti S, *et al* (2017) A PML/Slit Axis Controls Physiological Cell Migration and Cancer Invasion in the CNS. *Cell Rep* 20: 411–426

Aoto T, Saitoh N, Ichimura T, Niwa H & Nakao M (2006) Nuclear and chromatin reorganization in the MHC-Oct3/4 locus at developmental phases of embryonic stem cell differentiation. *Dev Biol* 298: 354–367

Appelhoff RJ, Tian Y-M, Raval RR, Turley H, Harris AL, Pugh CW, Ratcliffe PJ & Gleadle JM (2004) Differential Function of the Prolyl Hydroxylases PHD1, PHD2, and PHD3 in the Regulation of Hypoxia-inducible Factor. *J Biol Chem* 279: 38458–38465

Arreal L, Piva M, Fernández S, Revandkar A, Schaub- Clerigué A, Villanueva J, Zabala-Letona A, Pujana M, Astobiza I, Cortazar AR, *et al* (2020) Targeting PML in triple negative breast cancer elicits growth suppression and senescence. *Cell Death Differ* 27: 1186–1199

Baba M, Hirai S, Yamada-Okabe H, Hamada K, Tabuchi H, Kobayashi K, Kondo K, Yoshida M, Yamashita A, Kishida T, *et al* (2003) Loss of von Hippel-Lindau protein causes cell density dependent deregulation of CyclinD1 expression through Hypoxia-inducible factor. *Oncogene* 22: 2728–2738

Banani SF, Rice AM, Peeples WB, Lin Y, Jain S, Parker R & Rosen MK (2016)

Compositional Control of Phase-Separated Cellular Bodies. *Cell* 166: 651–663

Barsoum IB, Smallwood CA, Siemens DR & Graham CH (2014) A Mechanism of Hypoxia-Mediated Escape from Adaptive Immunity in Cancer Cells. *Cancer Res* 74: 665–674

Bensaad K, Favaro E, Lewis CA, Peck B, Lord S, Collins JM, Pinnick KE, Wigfield S, Buffa FM, Li JL, *et al* (2014) Fatty acid uptake and lipid storage induced by HIF-1α contribute to cell growth and survival after hypoxia-reoxygenation. *Cell Rep* 9: 349–365

Bernardi R, Guernah I, Jin D, Grisendi S, Alimonti A, Teruya-Feldstein J, Cordon-Cardo C, Celeste Simon M, Rafii S & Pandolfi PP (2006) PML inhibits HIF-1α translation and neoangiogenesis through repression of mTOR. *Nature* 442: 779–785

Bernardi R & Pandolfi PP (2003) Role of PML and the PML-nuclear body in the control of programmed cell death. *Oncogene* 22: 9048–9057

Bernardi R & Pandolfi PP (2007) Structure , dynamics and functions of promyelocytic leukaemia nuclear bodies. 8

Bernardi R, Scaglioni PP, Bergmann S, Horn HF, Vousden KH & Pandolfi PP (2004) PML regulates p53 stability by sequestering Mdm2 to the nucleolus. *Nat Cell Biol* 6: 665–672

Beroukhim R, Brunet J-P, Di Napoli A, Mertz KD, Seeley A, Pires MM, Linhart D, Worrell RA, Moch H, Rubin MA, *et al* (2009) Patterns of Gene Expression and Copy-Number Alterations in von-Hippel Lindau Disease-Associated and Sporadic Clear Cell Carcinoma of the Kidney. *Cancer Res* 69: 4674–4681

Berra E (2003) HIF prolyl-hydroxylase 2 is the key oxygen sensor setting low steady-state levels of HIF-1 in normoxia. *EMBO J* 22: 4082–4090

Bhagat M, Palanichamy JK, Ramalingam P, Mudassir M, Irshad K, Chosdol K, Sarkar C, Seth P, Goswami S, Sinha S, *et al* (2016) HIF-2α mediates a marked increase in migration and stemness characteristics in a subset of glioma cells under hypoxia by activating an Oct-4/Sox-2-Mena (INV) axis. *Int J Biochem Cell Biol* 74: 60–71

Birch SE, Kench JG, Takano E, Chan P, Chan A-L, Chiam K, Veillard A-S, Stricker P, Haupt S, Haupt Y, *et al* (2014) Expression of E6AP and PML predicts for prostate cancer progression and cancer-specific death. *Ann Oncol* 25: 2392–2397

Bischof O (2002) Deconstructing PML-induced premature senescence. *EMBO J* 21: 3358–3369

Biswas S, Troy H, Leek R, Chung Y-L, Li J, Raval RR, Turley H, Gatter K, Pezzella F, Griffiths JR, *et al* (2010) Effects of HIF-1 and HIF2 on Growth and Metabolism of Clear-Cell Renal Cell Carcinoma 786-0 Xenografts. *J Oncol* 2010: 1–14

Bracken CP, Fedele AO, Linke S, Balrak W, Lisy K, Whitelaw ML & Peet DJ (2006) Cell-specific Regulation of Hypoxia-inducible Factor (HIF)-1α and HIF-2α Stabilization and Transactivation in a Graded Oxygen Environment. *J Biol Chem* 281: 22575–22585

Brodaczewska KK, Szczylik C, Fiedorowicz M, Porta C & Czarnecka AM (2016) Choosing the right cell line for renal cell cancer research. *Mol Cancer* 15: 83

Brown D, Kogan S, Lagasse E, Weissman I, Alcalay M, Pelicci PG, Atwater S & Bishop JM (1997) A PMLRAR transgene initiates murine acute promyelocytic leukemia. *Proc Natl Acad Sci* 94: 2551–2556

Brugarolas J (2014) Molecular genetics of clear-cell renal cell carcinoma. *J Clin Oncol* 32: 1968–1976

Bushweller JH (2019) Targeting transcription factors in cancer — from undruggable to reality. *Nat Rev Cancer* 19: 611–624

Capitanio U & Montorsi F (2018) Renal cancer. *Lancet* 387: 894–906

Carmeliet P & Jain RK (2011) Principles and mechanisms of vessel normalization for cancer and other angiogenic diseases. *Nat Rev Drug Discov* 10: 417–427

Carracedo A, Ito K & Pandolfi PP (2011) The nuclear bodies inside out : PML conquers the cytoplasm. *Curr Opin Cell Biol* 23: 360–366

Carracedo A, Schafer ZT, Pandolfi PP, Carracedo A, Weiss D, Leliaert AK, Bhasin M, Boer VCJ De, Egia A, Libermann T, *et al* (2012a) A metabolic prosurvival role for PML in breast cancer Find the latest version : A metabolic prosurvival role for PML in breast cancer. *J Clin Invest 2012;122(9)3088-3100* 122: 3088–3100

Carracedo A, Weiss D, Leliaert AK, Bhasin M, de Boer VCJ, Laurent G, Adams AC, Sundvall M, Song SJ, Ito K, *et al* (2012b) A metabolic prosurvival role for PML in breast cancer. *J Clin Invest* 122: 3088–3100

Cassim S, Vučetić M, Ždralević M & Pouyssegur J (2020) Warburg and Beyond: The Power of Mitochondrial Metabolism to Collaborate or Replace Fermentative

Glycolysis in Cancer. *Cancers (Basel)* 12: 1119

Cerami E, Gao J, Dogrusoz U, Gross BE, Sumer SO, Aksoy BA, Jacobsen A, Byrne CJ, Heuer ML, Larsson E, *et al* (2012) The cBio Cancer Genomics Portal: An Open Platform for Exploring Multidimensional Cancer Genomics Data: Figure 1. *Cancer Discov* 2: 401–404

Chandrashekar DS, Bashel B, Balasubramanya SAH, Creighton CJ, Ponce-Rodriguez I, Chakravarthi BVSK & Varambally S (2017) UALCAN: A Portal for Facilitating Tumor Subgroup Gene Expression and Survival Analyses. *Neoplasia* 19: 649–658

Chang C-H, Qiu J, O'Sullivan D, Buck MD, Noguchi T, Curtis JD, Chen Q, Gindin M, Gubin MM, van der Windt GJW, *et al* (2015) Metabolic Competition in the Tumor Microenvironment Is a Driver of Cancer Progression. *Cell* 162: 1229–1241

Chang HR, Munkhjargal A, Kim MJ, Park SY, Jung E, Ryu JH, Yang Y, Lim JS & Kim Y (2018) The functional roles of PML nuclear bodies in genome maintenance. *Mutat Res - Fundam Mol Mech Mutagen* 809: 99–107

Chen M, Zhang J, Sampieri K, Clohessy JG, Mendez L, Gonzalez-Billalabeitia E, Liu X-S, Lee Y-R, Fung J, Katon JM, *et al* (2018) An aberrant SREBP-dependent lipogenic program promotes metastatic prostate cancer. *Nat Genet* 50: 206–218

Chen W, Hill H, Christie A, Kim MS, Holloman E, Pavia-jimenez A, Homayoun F, Ma Y, Patel N, Yell P, *et al* (2016a) antagonist. *Nat Publ Gr* 539: 112–117

Chen W, Hill H, Christie A, Kim MS, Holloman E, Pavia-Jimenez A, Homayoun F, Ma Y, Patel N, Yell P, *et al* (2016b) Targeting renal cell carcinoma with a HIF-2 antagonist. *Nature* 539: 112–117

Cheng X, Guo S, Liu Y, Chu H, Hakimi P, Berger NA, Hanson RW & Kao HY (2013) Ablation of promyelocytic leukemia protein (PML) re-patterns energy balance and protects mice from obesity induced by a western diet. *J Biol Chem* 288: 29746–29759

Chevrier S, Levine JH, Zanotelli VRT, Silina K, Schulz D, Bacac M, Ries CH, Ailles L, Jewett MAS, Moch H, *et al* (2017) An Immune Atlas of Clear Cell Renal Cell Carcinoma. *Cell* 169: 736-749.e18

Cho H, Du X, Rizzi JP, Liberzon E, Chakraborty AA, Gao W, Carvo I, Signoretti S, Bruick RK, Josey JA, *et al* (2016) On-target efficacy of a HIF-2α antagonist in preclinical kidney cancer models. *Nature* 539: 107–111

Clark DJ, Dhanasekaran SM, Petralia F, Pan J, Song X, Hu Y, da Veiga Leprevost F, Reva B, Lih T-SM, Chang H-Y, *et al* (2019) Integrated Proteogenomic Characterization of Clear Cell Renal Cell Carcinoma. *Cell* 179: 964-983.e31

Comprehensive Molecular Characterization of Papillary Renal-Cell Carcinoma (2016) *N Engl J Med* 374: 135–145

Condemine W, Takahashi Y, Zhu J, Puvion-Dutilleul F, Guegan S, Janin A & De Thé H (2006) Characterization of endogenous human promyelocytic leukemia isoforms. *Cancer Res* 66: 6192–6198

Corpet A, Kleijwegt C, Roubille S, Juillard F, Jacquet K, Texier P & Lomonte P (2020) PML nuclear bodies and chromatin dynamics: catch me if you can! *Nucleic Acids Res* 48: 11890–11912

Covello KL (2006) HIF-2 regulates Oct-4: effects of hypoxia on stem cell function, embryonic development, and tumor growth. *Genes Dev* 20: 557–570

Creighton CJ, Morgan M, Gunaratne PH, Wheeler DA, Gibbs RA, Robertson G, Chu A, Beroukhim R, Cibulskis K, Signoretti S, *et al* (2013) Comprehensive molecular characterization of clear cell renal cell carcinoma. *Nature* 499: 43–49

Cuvillier O (2017) The therapeutic potential of HIF-2 antagonism in renal cell carcinoma. *Transl Androl Urol* 6: 131–133

Dames SA, Martinez-Yamout M, De Guzman RN, Dyson HJ & Wright PE (2002) Structural basis for Hif-1 /CBP recognition in the cellular hypoxic response. *Proc Natl Acad Sci* 99: 5271–5276

Van Damme E, Laukens K, Dang TH & Van Ostade X (2010) A manually curated network of the PML nuclear body interactome reveals an important role for PML-NBs in SUMOylation dynamics. *Int J Biol Sci* 6: 51–67

Das S, Lin Y-H, Vernon RM, Forman-Kay JD & Chan HS (2020) Comparative roles of charge, π , and hydrophobic interactions in sequence-dependent phase separation of intrinsically disordered proteins. *Proc Natl Acad Sci* 117: 28795–28805

Datta N, Chakraborty S, Basu M & Ghosh MK (2020) Tumor Suppressors Having Oncogenic Functions: The Double Agents. *Cells* 10: 46

Davis CF, Ricketts CJ, Wang M, Yang L, Cherniack AD, Shen H, Buhay C, Kang H, Kim SC, Fahey CC, *et al* (2014) The Somatic Genomic Landscape of Chromophobe Renal Cell Carcinoma. *Cancer Cell* 26: 319–330

Degtyarev M, Reichelt M & Lin K (2014) Novel Quantitative Autophagy Analysis by Organelle Flow Cytometry after Cell Sonication. *PLoS One* 9: e87707

Delbarre E, Ivanauskiene K, Spirkoski J, Shah A, Vekterud K, Moskaug JØ, Bøe SO, Wong LH, Küntziger T & Collas P (2017) PML protein organizes heterochromatin domains where it regulates histone H3.3 deposition by ATRX/DAXX. *Genome Res* 27: 913–921

Dellaire G & Bazett-Jones DP (2004) PML nuclear bodies: dynamic sensors of DNA damage and cellular stress. *BioEssays* 26: 963–977

Dellaire G, Ching RW, Ahmed K, Jalali F, Tse KCK, Bristow RG & Bazett-Jones DP (2006) Promyelocytic leukemia nuclear bodies behave as DNA damage sensors whose response to DNA double-strand breaks is regulated by NBS1 and the kinases ATM, Chk2, and ATR. *J Cell Biol* 175: 55–66

Dengler VL, Galbraith MD & Espinosa JM (2014) Transcriptional regulation by hypoxia inducible factors. *Crit Rev Biochem Mol Biol* 49: 1–15

Dhatwalia SK, Kumar M & Dhawan DK (2018) Role of EGCG in Containing the Progression of Lung Tumorigenesis – A Multistage Targeting Approach. *Nutr Cancer* 70: 334–349

Dimri GP, Lee X, Basile G, Acosta M, Scott G, Roskelley C, Medrano EE, Linskens M, Rubelj I & Pereira-Smith O (1995) A biomarker that identifies senescent human cells in culture and in aging skin in vivo. *Proc Natl Acad Sci* 92: 9363–9367

Doe MR, Ascano JM, Kaur M & Cole MD (2012) Myc Posttranscriptionally Induces HIF1 Protein and Target Gene Expression in Normal and Cancer Cells. *Cancer Res* 72: 949–957

Dörr JR, Yu Y, Milanovic M, Beuster G, Zasada C, Däbritz JHM, Lisec J, Lenze D, Gerhardt A, Schleicher K, *et al* (2013) Synthetic lethal metabolic targeting of cellular senescence in cancer therapy. *Nature* 501: 421–425

Du W, Zhang L, Brett-Morris A, Aguila B, Kerner J, Hoppel CL, Puchowicz M, Serra D, Herrero L, Rini BI, *et al* (2017) HIF drives lipid deposition and cancer in ccRCC via repression of fatty acid metabolism. *Nat Commun* 8: 1769

Elias R, Tcheuyap VT, Kaushik AK, Cantarel BL, Kapur P & Brugarolas J (2021) Article A renal cell carcinoma tumorgraft platform to advance precision medicine ll ll Article A renal cell carcinoma tumorgraft platform to advance precision

medicine.

Everett RD (2001) DNA viruses and viral proteins that interact with PML nuclear bodies. *Oncogene* 20: 7266–7273

Everett RD, Freemont P, Saitoh H, Dasso M, Orr A, Kathoria M & Parkinson J (1998) The Disruption of ND10 during Herpes Simplex Virus Infection Correlates with the Vmw110- and Proteasome-Dependent Loss of Several PML Isoforms. *J Virol* 72: 6581–6591

Ferbeyre G, de Stanchina E, Querido E, Baptiste N, Prives C & Lowe SW (2000) PML is induced by oncogenic ras and promotes premature senescence. *Genes Dev* 14: 2015–27

Fisher GH, Orsulic S, Holland E, Hively WP, Li Y, Lewis BC, Williams BO & Varmus HE (1999) Development of a flexible and specific gene delivery system for production of murine tumor models. *Oncogene* 18: 5253–5260

Fonin A V., Silonov SA, Shpironok OG, Antifeeva IA, Petukhov A V., Romanovich AE, Kuznetsova IM, Uversky VN & Turoverov KK (2021) The role of non-specific interactions in canonical and ALT-associated PML-bodies formation and dynamics. *Int J Mol Sci* 22: 1–18

Forristal CE, Wright KL, Hanley NA, Oreffo ROC & Houghton FD (2010) Hypoxia inducible factors regulate pluripotency and proliferation in human embryonic stem cells cultured at reduced oxygen tensions. *REPRODUCTION* 139: 85–97

Freund A, Laberge R-M, Demaria M & Campisi J (2012) Lamin B1 loss is a senescence-associated biomarker. *Mol Biol Cell* 23: 2066–2075

Frew IJ & Moch H (2015) A Clearer View of the Molecular Complexity of Clear Cell Renal Cell Carcinoma. *Annu Rev Pathol Mech Dis* 10: 263–289

Fu L, Wang G, Shevchuk MM, Nanus DM & Gudas LJ (2011) Generation of a Mouse Model of Von Hippel–Lindau Kidney Disease Leading to Renal Cancers by Expression of a Constitutively Active Mutant of HIF1α. *Cancer Res* 71: 6848–6856

Fu L, Wang G, Shevchuk MM, Nanus DM & Gudas LJ (2013) Activation of HIF2α in Kidney Proximal Tubule Cells Causes Abnormal Glycogen Deposition but not Tumorigenesis. *Cancer Res* 73: 2916–2925

Gao J, Aksoy BA, Dogrusoz U, Dresdner G, Gross B, Sumer SO, Sun Y, Jacobsen A,

Sinha R, Larsson E, *et al* (2013) Integrative Analysis of Complex Cancer Genomics and Clinical Profiles Using the cBioPortal. *Sci Signal* 6: 1–20

Gebhard RL, Clayman R V., Prigge WF, Figenshau R, Staley NA, Reesey C & Bear A (1987) Abnormal cholesterol metabolism in renal clear cell carcinoma. *J Lipid Res* 28: 1177–1184

Gentric G, Kieffer Y, Mieulet V, Goundiam O, Bonneau C, Nemati F, Hurbain I, Raposo G, Popova T, Stern M-H, *et al* (2019) PML-Regulated Mitochondrial Metabolism Enhances Chemosensitivity in Human Ovarian Cancers. *Cell Metab* 29: 156-173.e10

Giacomini I, Gianfanti F, Desbats MA, Orso G, Berretta M, Prayer-Galetti T, Ragazzi E & Cocetta V (2021) Cholesterol Metabolic Reprogramming in Cancer and Its Pharmacological Modulation as Therapeutic Strategy. *Front Oncol* 11: 1–23

Gilkes DM & Semenza GL (2013) Role of hypoxia-inducible factors in breast cancer metastasis. *Futur Oncol* 9: 1623–1636

Gkretsi V & Stylianopoulos T (2018) Cell Adhesion and Matrix Stiffness: Coordinating Cancer Cell Invasion and Metastasis. *Front Oncol* 8

Goddard AD, Borrow J, Freemont PS & Solomon E (1991) Characterization of a Zinc Finger Gene Disrupted by the t(15;17) in Acute Promyelocytic Leukemia. *Science (80-)* 254: 1371–1374

Gordan JD, Bertout JA, Hu C-J, Diehl JA & Simon MC (2007) HIF-2α Promotes Hypoxic Cell Proliferation by Enhancing c-Myc Transcriptional Activity. *Cancer Cell* 11: 335–347

Gordan JD, Lal P, Dondeti VR, Letrero R, Parekh KN, Oquendo CE, Greenberg RA, Flaherty KT, Rathmell WK, Keith B, *et al* (2008) HIF-α Effects on c-Myc Distinguish Two Subtypes of Sporadic VHL-Deficient Clear Cell Renal Carcinoma. *Cancer Cell* 14: 435–446

Gosselin K, Deruy E, Martien S, Vercamer C, Bouali F, Dujardin T, Slomianny C, Houel-Renault L, Chelli F, De Launoit Y, *et al* (2009) Senescent Keratinocytes Die by Autophagic Programmed Cell Death. *Am J Pathol* 174: 423–435

Graham AM & Presnell JS (2017) Hypoxia Inducible Factor (HIF) transcription factor family expansion, diversification, divergence and selection in eukaryotes. *PLoS One* 12: 1–15

Gu Y-F, Cohn S, Christie A, McKenzie T, Wolff N, Do QN, Madhuranthakam AJ, Pedrosa I, Wang T, Dey A, *et al* (2017) Modeling Renal Cell Carcinoma in Mice: Bap1 and Pbrm1 Inactivation Drive Tumor Grade. *Cancer Discov* 7: 900–917

Gu YZ, Moran SM, Hogenesch JB, Wartman L & Bradfield CA (1998) Molecular characterization and chromosomal localization of a third alpha-class hypoxia inducible factor subunit, HIF3alpha. *Gene Expr* 7: 205–13

Gurrieri C, Capodieci P, Bernardi R, Scaglioni PP, Nafa K, Rush LJ, Verbel DA, Cordon-Cardo C & Pandolfi PP (2004) Loss of the tumor suppressor PML in human cancers of multiple histologic origins. *J Natl Cancer Inst* 96: 269–279

Haake SM, Weyandt JD & Rathmell WK (2016) Insights into the Genetic Basis of the Renal Cell Carcinomas from The Cancer Genome Atlas. *Mol Cancer Res* 14: 589–598

Hakimi AA, Reznik E, Lee C-H, Creighton CJ, Brannon AR, Luna A, Aksoy BA, Liu EM, Shen R, Lee W, *et al* (2016) An Integrated Metabolic Atlas of Clear Cell Renal Cell Carcinoma. *Cancer Cell* 29: 104–116

Hanahan D & Weinberg RA (2011) Hallmarks of Cancer: The Next Generation. *Cell* 144: 646–674

Harlander S, Schönenberger D, Toussaint NC, Prummer M, Catalano A, Brandt L, Moch H, Wild PJ & Frew IJ (2017) Combined mutation in Vhl, Trp53 and Rb1 causes clear cell renal cell carcinoma in mice. *Nat Med* 23: 869–877

Hatfield SM, Kjaergaard J, Lukashev D, Belikoff B, Schreiber TH, Sethumadhavan S, Abbott R, Philbrook P, Thayer M, Shujia D, *et al* (2014) Systemic oxygenation weakens the hypoxia and hypoxia inducible factor 1α-dependent and extracellular adenosine-mediated tumor protection. *J Mol Med* 92: 1283–1292

Hayashi Y, Yokota A, Harada H & Huang G (2019) Hypoxia/pseudohypoxia-mediated activation of hypoxia-inducible factor-1α in cancer. *Cancer Sci* 110: 1510–1517

Herman JG, Latif F, Weng Y, Lerman MI, Zbar B, Liu S, Samid D, Duan DS, Gnarra JR & Linehan WM (1994) Silencing of the VHL tumor-suppressor gene by DNA methylation in renal carcinoma. *Proc Natl Acad Sci* 91: 9700–9704

Hernandez-Segura A, de Jong T V., Melov S, Guryev V, Campisi J & Demaria M (2017) Unmasking Transcriptional Heterogeneity in Senescent Cells. *Curr Biol* 27: 2652-2660.e4

Herranz N & Gil J (2018) Mechanisms and functions of cellular senescence. *J Clin Invest* 128: 1238–1246

Ho P-C, Bihuniak JD, Macintyre AN, Staron M, Liu X, Amezquita R, Tsui Y-C, Cui G, Micevic G, Perales JC, *et al* (2015) Phosphoenolpyruvate Is a Metabolic Checkpoint of Anti-tumor T Cell Responses. *Cell* 162: 1217–1228

Hoefflin R, Harlander S, Schäfer S, Metzger P, Kuo F, Schönenberger D, Adlesic M, Peighambari A, Seidel P, Chen C, *et al* (2020) HIF-1α and HIF-2α differently regulate tumour development and inflammation of clear cell renal cell carcinoma in mice. *Nat Commun* 11: 4111

Hoischen C, Monajembashi S, Weisshart K & Hemmerich P (2018) Multimodal light microscopy approaches to reveal structural and functional properties of promyelocytic leukemia nuclear bodies. *Front Oncol* 8

Honzumi S, Takeuchi M, Kurihara M, Fujiyoshi M, Uchida M, Watanabe K, Suzuki T & Ishii I (2018) The effect of cholesterol overload on mouse kidney and kidney-derived cells. *Ren Fail* 40: 43–50

Hoskin D, Mader J, Furlong S, Conrad D & Blay J (2008) Inhibition of T cell and natural killer cell function by adenosine and its contribution to immune evasion by tumor cells (Review). *Int J Oncol* 32: 527–535

Hou W & Ji Z (2018) Generation of autochthonous mouse models of clear cell renal cell carcinoma: mouse models of renal cell carcinoma. *Exp Mol Med* 50: 1–10

Hsu JK, Lin T & Tsai RYL (2012) Nucleostemin prevents telomere damage by promoting PML-IV recruitment to SUMOylated TRF1. *J Cell Biol* 197: 613–624

Hu C, Wang L, Chodosh LA, Keith B & Simon MC (2003) Differential Roles of Hypoxia-Inducible Factor 1 ␣ (HIF-1 ␣) and HIF-2 ␣ in Hypoxic Gene Regulation. 23: 9361–9374

Huang D, Li T, Li X, Zhang L, Sun L, He X, Zhong X, Jia D, Song L, Semenza GL, *et al* (2014) HIF-1-Mediated Suppression of Acyl-CoA Dehydrogenases and Fatty Acid Oxidation Is Critical for Cancer Progression. *Cell Rep* 8: 1930–1942

Huang LE, Gu J, Schau M & Bunn HF (1998) Regulation of hypoxia-inducible factor 1 is mediated by an O2-dependent degradation domain via the ubiquitin-proteasome pathway. *Proc Natl Acad Sci* 95: 7987–7992

Hyun Park W, Hee Cho Y, Won Jung C, Oh Park J, Kim K, Hyuck Im Y, Lee MH, Ki

Kang W & Park K (2003) Arsenic trioxide inhibits the growth of A498 renal cell carcinoma cells via cell cycle arrest or apoptosis. *Biochem Biophys Res Commun* 300: 230–5

Iommarini L, Porcelli AM, Gasparre G & Kurelac I (2017) Non-Canonical Mechanisms Regulating Hypoxia-Inducible Factor 1 Alpha in Cancer. *Front Oncol* 7: 1–9

Ito K, Bernardi R, Morotti A, Matsuoka S, Saglio G, Ikeda Y, Rosenblatt J, Avigan DE, Teruya-Feldstein J & Pandolfi PP (2008) PML targeting eradicates quiescent leukaemia-initiating cells. *Nature* 453: 1072–1078

Ito K, Carracedo A, Weiss D, Arai F, Ala U, Avigan DE, Schafer ZT, Evans RM, Suda T, Lee C-H, *et al* (2012) A PML–PPAR-δ pathway for fatty acid oxidation regulates hematopoietic stem cell maintenance. *Nat Med* 18: 1350–1358

Ivanschitz L, Takahashi Y, Jollivet F, Ayrault O, Bras M Le & De Thé H (2015) PML IV/ARF interaction enhances p53 SUMO-1 conjugation, activation, and senescence. *Proc Natl Acad Sci U S A* 112: 14278–14283

Jaakkola P, Mole DR, Tian Y-M, Wilson MI, Gielbert J, Gaskell SJ, Kriegsheim A v., Hebestreit HF, Mukherji M, Schofield CJ, *et al* (2001) Targeting of HIF-alpha to the von Hippel-Lindau Ubiquitylation Complex by O2-Regulated Prolyl Hydroxylation. *Science (80-)* 292: 468–472

Jensen K, Shiels C & Freemont PS (2001) PML protein isoforms and the RBCC/TRIM motif. *Oncogene* 20: 7223–7233

Jiang B-H, Rue E, Wang GL, Roe R & Semenza GL (1996) Dimerization, DNA Binding, and Transactivation Properties of Hypoxia-inducible Factor 1. *J Biol Chem* 271: 17771–17778

Jin F, Brockmeier U, Otterbach F & Metzen E (2012) New Insight into the SDF-1/CXCR4 Axis in a Breast Carcinoma Model: Hypoxia-Induced Endothelial SDF-1 and Tumor Cell CXCR4 Are Required for Tumor Cell Intravasation. *Mol Cancer Res* 10: 1021–1031

Joshi S, Tolkunov D, Aviv H, Hakimi AA, Yao M, Hsieh JJ, Ganesan S, Chan CS & White E (2015) The Genomic Landscape of Renal Oncocytoma Identifies a Metabolic Barrier to Tumorigenesis. *Cell Rep* 13: 1895–1908

Kaku H, Ito S, Ebara S, Ouchida M, Nasu Y, Tsushima T, Kumon H & Shimizu K (2004) Positive correlation between allelic loss at chromosome 14q24-31 and poor

prognosis of patients with renal cell carcinoma. *Urology* 64: 176–181

Keith B & Simon MC (2007) Hypoxia-Inducible Factors, Stem Cells, and Cancer. *Cell* 129: 465–472

Kießlich A, Von Mikecz A & Hemmerich P (2002) Cell cycle-dependent association of PML bodies with sites of active transcription in nuclei of mammalian cells. *J Struct Biol* 140: 167–179

Kim JJ, Lee SB, Jang J, Yi S-Y, Kim S-H, Han S-A, Lee J-M, Tong S-Y, Vincelette ND, Gao B, *et al* (2015) WSB1 promotes tumor metastasis by inducing pVHL degradation. *Genes Dev* 29: 2244–2257

Kim MK, Yang S, Lee K-H, Um J-H, Liu M, Kang H, Park SJ & Chung JH (2011) Promyelocytic leukemia inhibits adipogenesis, and loss of promyelocytic leukemia results in fat accumulation in mice. *Am J Physiol Metab* 301: E1130–E1142

Kirkland JL & Tchkonia T (2020) Senolytic drugs: from discovery to translation. *J Intern Med* 288: 518–536

Koh MY, Lemos R, Liu X & Powis G (2011) The Hypoxia-Associated Factor Switches Cells from HIF-1α- to HIF-2α-Dependent Signaling Promoting Stem Cell Characteristics, Aggressive Tumor Growth and Invasion. *Cancer Res* 71: 4015–4027

Koh MY, Nguyen V, Lemos R, Darnay BG, Kiriakova G, Abdelmelek M, Ho TH, Karam J, Monzon FA, Jonasch E, *et al* (2015) Hypoxia-Induced SUMOylation of E3 Ligase HAF Determines Specific Activation of HIF2 in Clear-Cell Renal Cell Carcinoma. *Cancer Res* 75: 316–329

Koh MY & Powis G (2009) HAF: The new player in oxygen-independent HIF-1α degradation. *Cell Cycle* 8: 1359–1366

Koshiji M, Kageyama Y, Pete EA, Horikawa I, Barrett JC & Huang LE (2004) HIF-1α induces cell cycle arrest by functionally counteracting Myc. *EMBO J* 23: 1949–1956

Kotas T, Analysis E, Buildings S, Society A, Engineers A, Analysis E & Buildings S (2017) Biosensors and Biodetection Prickril B & Rasooly A (eds) New York, NY: Springer New York

KOTOWSKI U, HEIDUSCHKA G, BRUNNER M, EROVIC BM, MARTINEK H & THURNHER D (2012) Arsenic trioxide enhances the cytotoxic effect of cisplatin

in head and neck squamous cell carcinoma cell lines. *Oncol Lett* 3: 1326–1330

Kuleshov M V., Jones MR, Rouillard AD, Fernandez NF, Duan Q, Wang Z, Koplev S, Jenkins SL, Jagodnik KM, Lachmann A, *et al* (2016) Enrichr: a comprehensive gene set enrichment analysis web server 2016 update. *Nucleic Acids Res* 44: W90–W97

Kurihara M, Kato K, Sanbo C, Shigenobu S, Ohkawa Y, Fuchigami T & Miyanari Y (2020) Genomic Profiling by ALaP-Seq Reveals Transcriptional Regulation by PML Bodies through DNMT3A Exclusion. *Mol Cell* 78: 493-505.e8

Kuwayama K, Matsuzaki K, Mizobuchi Y, Mure H, Kitazato KT, Kageji T, Nakao M & Nagahiro S (2009) Promyelocytic leukemia protein induces apoptosis due to caspase-8 activation via the repression of NFκB activation in glioblastoma. *Neuro Oncol* 11: 132–141

Kwitkowski VE, Prowell TM, Ibrahim A, Farrell AT, Justice R, Mitchell SS, Sridhara R & Pazdur R (2010) FDA Approval Summary: Temsirolimus as Treatment for Advanced Renal Cell Carcinoma. *Oncologist* 15: 428–435

Kwon SM, Hong SM, Lee Y-K, Min S & Yoon G (2019) Metabolic features and regulation in cell senescence. *BMB Rep* 52: 5–12

Labbaye C, Valtieri M, Grignani F, Puglisi R, Luchetti L, Masella B, Alcalay M, Testa U & Peschle C (1999) Expression and role of PML gene in normal adult hematopoiesis: functional interaction between PML and Rb proteins in erythropoiesis. *Oncogene* 18: 3529–3540

Lallemand-Breitenbach V, Jeanne M, Benhenda S, Nasr R, Lei M, Peres L, Zhou J, Zhu J, Raught B & de Thé H (2008) Arsenic degrades PML or PML–RARα through a SUMO-triggered RNF4/ubiquitin-mediated pathway. *Nat Cell Biol* 10: 547–555

Lallemand-Breitenbach V & de The H (2010) PML Nuclear Bodies. *Cold Spring Harb Perspect Biol* 2: a000661–a000661

Lallemand-Breitenbach V, Zhu J, Puvion F, Koken M, Honoré N, Doubeikovsky A, Duprez E, Pandolfi PP, Puvion E, Freemont P, *et al* (2001) Role of Promyelocytic Leukemia (Pml) Sumolation in Nuclear Body Formation, 11s Proteasome Recruitment, and as2O3-Induced Pml or Pml/Retinoic Acid Receptor α Degradation. *J Exp Med* 193: 1361–1372

Lando D (2002) FIH-1 is an asparaginyl hydroxylase enzyme that regulates the

transcriptional activity of hypoxia-inducible factor. *Genes Dev* 16: 1466–1471

Lång A, Lång E & Bøe SO (2019) PML Bodies in Mitosis. *Cells* 8: 893

Laughner E, Taghavi P, Chiles K, Mahon PC & Semenza GL (2001) HER2 (neu) Signaling Increases the Rate of Hypoxia-Inducible Factor 1α (HIF-1α) Synthesis: Novel Mechanism for HIF-1-Mediated Vascular Endothelial Growth Factor Expression. *Mol Cell Biol* 21: 3995–4004

Lee J-J, Park IH, Rhee WJ, Kim HS & Shin J-S (2019) HMGB1 modulates the balance between senescence and apoptosis in response to genotoxic stress. *FASEB J* 33: 10942–10953

Lendahl U, Lee KL, Yang H & Poellinger L (2009) Generating specificity and diversity in the transcriptional response to hypoxia. *Nat Rev Genet* 10: 821–832

Leroy X, Zini L, Leteurtre E, Zerimech F, Porchet N, Aubert J-P, Gosselin B & Copin M-C (2002) Morphologic Subtyping of Papillary Renal Cell Carcinoma: Correlation with Prognosis and Differential Expression of MUC1 between the Two Subtypes. *Mod Pathol* 15: 1126–1130

Li C, Peng Q, Wan X, Sun H & Tang J (2017) C-terminal motifs in PML isoforms critically regulate PML-NB formation. *J Cell Sci* 130: 3496–3506

Li J, Guo L, Chai L & Ai Z (2019) Comprehensive Analysis of Driver Genes in Personal Genomes of Clear Cell Renal Cell Carcinoma. *Technol Cancer Res Treat* 18: 153303381983096

Li W, Ferguson BJ, Khaled WT, Tevendale M, Stingl J, Poli V, Rich T, Salomoni P & Watson CJ (2009) PML depletion disrupts normal mammary gland development and skews the composition of the mammary luminal cell progenitor pool. *Proc Natl Acad Sci* 106: 4725–4730

Li Y, Sun X-X, Qian DZ & Dai M-S (2020) Molecular Crosstalk Between MYC and HIF in Cancer. *Front Cell Dev Biol* 8: 1–11

Lin YC, Lu LT, Chen HY, Duan X, Lin X, Feng XH, Tang MJ & Chen RH (2014) SCP phosphatases suppress renal cell carcinoma by stabilizing PML and inhibiting mTOR/HIF signaling. *Cancer Res* 74: 6935–6946

Liu SB, Shen ZF, Guo YJ, Cao LX & Xu Y (2017) PML silencing inhibits cell proliferation and induces DNA damage in cultured ovarian cancer cells. *Biomed Reports* 7: 29–35

Lo-Coco F, Avvisati G, Vignetti M, Thiede C, Orlando SM, Iacobelli S, Ferrara F, Fazi P, Cicconi L, Di Bona E, *et al* (2013) Retinoic Acid and Arsenic Trioxide for Acute Promyelocytic Leukemia. *N Engl J Med* 369: 111–121

Lo-Coco F, Cicconi L & Breccia M (2016) Current standard treatment of adult acute promyelocytic leukaemia. *Br J Haematol* 172: 841–854

Loe TK, Zhou Li JS, Zhang Y, Azeroglu B, Boddy MN & Denchi EL (2020) Telomere length heterogeneity in ALT cells is maintained by PML-dependent localization of the BTR complex to telomeres. *Genes Dev* 34: 650–662

Loenarz C, Coleman ML, Boleininger A, Schierwater B, Holland PWH, Ratcliffe PJ & Schofield CJ (2011) The hypoxia-inducible transcription factor pathway regulates oxygen sensing in the simplest animal, Trichoplax adhaerens. *EMBO Rep* 12: 63–70

Loh C-Y, Chai J, Tang T, Wong W, Sethi G, Shanmugam M, Chong P & Looi C (2019) The E-Cadherin and N-Cadherin Switch in Epithelial-to-Mesenchymal Transition: Signaling, Therapeutic Implications, and Challenges. *Cells* 8: 1118

Luciani JJ, Depetris D, Missirian C, Mignon-Ravix C, Metzler-Guillemain C, Megarbane A, Moncla A & Mattei M-G (2005) Subcellular distribution of HP1 proteins is altered in ICF syndrome. *Eur J Hum Genet* 13: 41–51

Magliulo D & Bernardi R (2018) HIF-α factors as potential therapeutic targets in leukemia. *Expert Opin Ther Targets* 22: 917–928

Mahon PC (2001) FIH-1: a novel protein that interacts with HIF-1alpha and VHL to mediate repression of HIF-1 transcriptional activity. *Genes Dev* 15: 2675–2686

Mandriota SJ, Turner KJ, Davies DR, Murray PG, Morgan N V., Sowter HM, Wykoff CC, Maher ER, Harris AL, Ratcliffe PJ, *et al* (2002) HIF activation identifies early lesions in VHL kidneys. *Cancer Cell* 1: 459–468

Maranchie JK, Vasselli JR, Riss J, Bonifacino JS, Linehan WM & Klausner RD (2002) The contribution of VHL substrate binding and HIF1-α to the phenotype of VHL loss in renal cell carcinoma. *Cancer Cell* 1: 247–255

Martín-Martín N, Piva M, Urosevic J, Aldaz P, Sutherland JD, Fernández-Ruiz S, Arreal L, Torrano V, Cortazar AR, Planet E, *et al* (2016) Stratification and therapeutic potential of PML in metastatic breast cancer. *Nat Commun* 7: 12595

Martin N, Benhamed M, Nacerddine K, Demarque MD, van Lohuizen M, Dejean A &

Bischof O (2012) Physical and functional interaction between PML and TBX2 in the establishment of cellular senescence. *EMBO J* 31: 95–109

Matt S & Hofmann TG (2018) Crosstalk between p53 modifiers at PML bodies. *Mol Cell Oncol* 5: e1074335

Maxwell PH, Wiesener MS, ChangGW, Clifford SC, Vaux EC, Cockman ME, Wykoff CC, Pugh CW & Maher ERRatcliffe PJ (1999) The tumour suppressorprotein VHL targetshypoxia-inducible factors foroxygen-dependent proteolysis. *Nature* 399: 271–275

May C, Page SEEL, Zhang X, Yan X, Zhou Z, Yang F, Wu Z & Sun H (2010) the PML-RAR a Oncoprotein by. *Science (80-)* 328: 240–243

Maynard MA, Qi H, Chung J, Lee EHL, Kondo Y, Hara S, Conaway RC, Conaway JW & Ohh M (2003) Multiple Splice Variants of the Human HIF-3α Locus Are Targets of the von Hippel-Lindau E3 Ubiquitin Ligase Complex. *J Biol Chem* 278: 11032–11040

Mazza M & Pelicci PG (2013) Is PML a Tumor Suppressor? *Front Oncol* 3: 1–9

McIntyre K & Hirsch MS (2018) Kidney: Renal Oncocytoma. *Atlas Genet Cytogenet Oncol Haematol* 22: 358–361

McKeown SR (2014) Defining normoxia, physoxia and hypoxia in tumours - Implications for treatment response. *Br J Radiol* 87: 1–12

McNally BA, Trgovcich J, Maul GG, Liu Y & Zheng P (2008) A Role for Cytoplasmic PML in Cellular Resistance to Viral Infection. *PLoS One* 3: e2277

Melnick A & Licht JD (1999) Deconstructing a Disease: RAR□, Its Fusion Partners, and Their Roles in the Pathogenesis of Acute Promyelocytic Leukemia. *Blood* 93: 3167–3215

van der Mijn JC, Fu L, Khani F, Zhang T, Molina AM, Barbieri CE, Chen Q, Gross SS, Gudas LJ & Nanus DM (2020) Combined Metabolomics and Genome-Wide Transcriptomics Analyses Show Multiple HIF1α-Induced Changes in Lipid Metabolism in Early Stage Clear Cell Renal Cell Carcinoma. *Transl Oncol* 13: 177–185

Missiroli S, Bonora M, Patergnani S & Giorgi C (2017) Novel function of the tumor suppressor PML at ER-mitochondria sites in the control of autophagy. *Oncotarget* 8: 81723–81724

Mitsumori K, Kittleson JM, Itoh N, Delahunt B, Heathcott RW, Stewart JH, McCredie MRE & Reeve AE (2002) Chromosome 14q LOH in localized clear cell renal cell carcinoma. *J Pathol* 198: 110–114

Moch H & Ohashi R (2021) Chromophobe renal cell carcinoma: current and controversial issues. *Pathology* 53: 101–108

Mole DR, Blancher C, Copley RR, Pollard PJ, Gleadle JM, Ragousis J & Ratcliffe PJ (2009) Genome-wide association of hypoxia-inducible factor (HIF)-1α and HIF-2α DNA binding with expression profiling of hypoxia-inducible transcripts. *J Biol Chem* 284: 16767–16775

Moreira M, Pobel C, Epaillard N, Simonaggio A, Oudard S & Vano Y-A (2020) https://cdrjournal.com/article/view/3531. *Cancer Drug Resist* 3: 454–471

Mounira L Chelbi-Alix & The H de (1999) Herpes virus induced proteasome-dependent degradation of the nuclear bodies-associated PML and Sp100 proteins. *Oncogene* 5: 935–941

Nagao A, Kobayashi M, Koyasu S, Chow CCT & Harada H (2019) HIF-1-Dependent Reprogramming of Glucose Metabolic Pathway of Cancer Cells and Its Therapeutic Significance. *Int J Mol Sci* 20: 238

Neely BA, Wilkins CE, Marlow LA, Malyarenko D, Kim Y, Ignatchenko A, Sasinowska H, Sasinowski M, Nyalwidhe JO, Kislinger T, *et al* (2016) Proteotranscriptomic Analysis Reveals Stage Specific Changes in the Molecular Landscape of Clear-Cell Renal Cell Carcinoma. *PLoS One* 11: e0154074

Neerukonda SN (2021) Interplay between rna viruses and promyelocytic leukemia nuclear bodies. *Vet Sci* 8

Nickerson ML, Jaeger E, Shi Y, Durocher JA, Mahurkar S, Zaridze D, Matveev V, Janout V, Kollarova H, Bencko V, *et al* (2008) Improved Identification of von Hippel-Lindau Gene Alterations in Clear Cell Renal Tumors. *Clin Cancer Res* 14: 4726–4734

Nisole S, Maroui MA, Mascle XH, Aubry M & Chelbi-Alix MK (2013) Differential roles of PML isoforms. *Front Oncol* 3 MAY: 1–17

Niu G, Briggs J, Deng J, Ma Y, Lee H, Kortylewski M, Kujawski M, Kay H, Cress WD, Jove R, *et al* (2008) Signal Transducer and Activator of Transcription 3 Is Required for Hypoxia-Inducible Factor-1α RNA Expression in Both Tumor Cells

and Tumor-Associated Myeloid Cells. *Mol Cancer Res* 6: 1099–1105

O'Rourke JF, Tian Y-M, Ratcliffe PJ & Pugh CW (1999) Oxygen-regulated and Transactivating Domains in Endothelial PAS Protein 1: Comparison with Hypoxia-inducible Factor-1α. *J Biol Chem* 274: 2060–2071

Ohsaki Y, Kawai T, Yoshikawa Y, Cheng J, Jokitalo E & Fujimoto T (2016) PML isoform II plays a critical role in nuclear lipid droplet formation. *J Cell Biol* 212: 29–38

Pandolfi PP, Alcalay M, Fagioli M, Zangrilli D, Mencarelli A, Diverio D, Biondi A, Lo Coco F, Rambaldi A, Grignani F, *et al* (1992) Genomic variability and alternative splicing generate multiple PML/RARα transcripts that encode aberrant PML proteins and PML/RARα isoforms in acute promyelocytic leukaemia. *EMBO J* 11: 1397–1407

Park WH, Seol JG, Kim ES, Hyun JM, Jung CW, Lee CC, Kim BK & Lee YY (2000) Arsenic trioxide-mediated growth inhibition in MC/CAR myeloma cells via cell cycle arrest in association with induction of cyclin-dependent kinase inhibitor, p21, and apoptosis. *Cancer Res* 60: 3065–71

Peña-Llopis S, Christie A, Xie X-J & Brugarolas J (2013) Cooperation and Antagonism among Cancer Genes: The Renal Cancer Paradigm. *Cancer Res* 73: 4173–4179

Perlman R, Schiemann WP, Brooks MW, Lodish HF & Weinberg RA (2001) TGF-β-induced apoptosis is mediated by the adapter protein Daxx that facilitates JNK activation. *Nat Cell Biol* 3: 708–714

Polański R, Noon AP, Blaydes J, Phillips A, Rubbi CP, Parsons K, Vlatković N & Boyd MT (2014) Senescence induction in renal carcinoma cells by Nutlin-3: a potential therapeutic strategy based on MDM2 antagonism. *Cancer Lett* 353: 211–219

Ponente M, Campanini L, Cuttano R, Piunti A, Delledonne GA, Coltella N, Valsecchi R, Villa A, Cavallaro U, Pattini L, *et al* (2017) PML promotes metastasis of triple-negative breast cancer through transcriptional regulation of HIF1A target genes. *JCI Insight* 2

Prats C, Gómez-Cabello A & Hansen A V. (2011) Intracellular compartmentalization of skeletal muscle glycogen metabolism and insulin signalling. *Exp Physiol* 96: 385–390

Psaila B & Lyden D (2009) The metastatic niche: adapting the foreign soil. *Nat Rev*

Cancer 9: 285–293

Purdue MP, Johansson M, Zelenika D, Toro JR, Scelo G, Moore LE, Prokhortchouk E, Wu X, Kiemeney LA, Gaborieau V, *et al* (2011) Genome-wide association study of renal cell carcinoma identifies two susceptibility loci on 2p21 and 11q13.3. *Nat Genet* 43: 60–65

Qi X, Li Q, Che X, Wang Q & Wu G (2021) The Uniqueness of Clear Cell Renal Cell Carcinoma: Summary of the Process and Abnormality of Glucose Metabolism and Lipid Metabolism in ccRCC. *Front Oncol* 11: 1–14

Qiu B, Ackerman D, Sanchez DJ, Li B, Ochocki JD, Grazioli A, Bobrovnikova-Marjon E, Diehl JA, Keith B & Simon MC (2015) HIF2α-Dependent Lipid Storage Promotes Endoplasmic Reticulum Homeostasis in Clear-Cell Renal Cell Carcinoma. *Cancer Discov* 5: 652–667

Rankin EB, Tomaszewski JE & Haase VH (2006) Renal Cyst Development in Mice with Conditional Inactivation of the von Hippel-Lindau Tumor Suppressor. *Cancer Res* 66: 2576–2583

Raval RR, Lau KW, Tran MGB, Sowter HM, Mandriota SJ, Li J, Pugh CW, Maxwell PH, Harris AL, Ratcliffe PJ, *et al* (2005) Contrasting Properties of Hypoxia-Inducible Factor 1 (HIF-1) and HIF-2 in von Hippel-Lindau-Associated Renal Cell Carcinoma. 25: 5675–5686

Regad T, Bellodi C, Nicotera P & Salomoni P (2009) The tumor suppressor Pml regulates cell fate in the developing neocortex. *Nat Neurosci* 12: 132–140

Regad T & Chelbi-Alix MK (2001) Role and fate of PML nuclear bodies in response to interferon and viral infections. *Oncogene* 20: 7274–7286

Rey S & Semenza GL (2010) Hypoxia-inducible factor-1-dependent mechanisms of vascularization and vascular remodelling. *Cardiovasc Res* 86: 236–242

Riscal R, Bull CJ, Mesaros C, Finan JM, Carens M, Ho ES, Xu JP, Godfrey J, Brennan P, Johansson M, *et al* (2021) Cholesterol Auxotrophy as a Targetable Vulnerability in Clear Cell Renal Cell Carcinoma. *Cancer Discov* 11: 3106–3125

Rodier F, Muñoz DP, Teachenor R, Chu V, Le O, Bhaumik D, Coppé J-P, Campeau E, Beauséjour CM, Kim S-H, *et al* (2011) DNA-SCARS: distinct nuclear structures that sustain damage-induced senescence growth arrest and inflammatory cytokine secretion. *J Cell Sci* 124: 68–81

Rogers JL, Bayeh L, Scheuermann TH, Longgood J, Key J, Naidoo J, Melito L, Shokri C, Frantz DE, Bruick RK, *et al* (2013) Development of Inhibitors of the PAS-B Domain of the HIF-2α Transcription Factor J. Med. Chem. 2014, 57, 9139−9151.pdf. *J Med Chem* 56: 1739–1747

Rohwer N, Welzel M, Daskalow K, Pfander D, Wiedenmann B, Detjen K & Cramer T (2008) Hypoxia-Inducible Factor 1 Mediates Anoikis Resistance via Suppression of 5 Integrin. *Cancer Res* 68: 10113–10120

Sachini N, Arampatzi P, Klonizakis A, Nikolaou C, Makatounakis T, Lam EWF, Kretsovali A & Papamatheakis J (2019) Promyelocytic leukemia protein (PML) controls breast cancer cell proliferation by modulating Forkhead transcription factors. *Mol Oncol* 13: 1369–1387

Sahin U, Ferhi O, Jeanne M, Benhenda S, Berthier C, Jollivet F, Niwa-Kawakita M, Faklaris O, Setterblad N, de Thé H, *et al* (2014) Oxidative stress–induced assembly of PML nuclear bodies controls sumoylation of partner proteins. *J Cell Biol* 204: 931–945

Saito K, Arai E, Maekawa K, Ishikawa M, Fujimoto H, Taguchi R, Matsumoto K, Kanai Y & Saito Y (2016) Lipidomic Signatures and Associated Transcriptomic Profiles of Clear Cell Renal Cell Carcinoma. *Sci Rep* 6: 28932

Samanta D, Gilkes DM, Chaturvedi P, Xiang L & Semenza GL (2014) Hypoxia-inducible factors are required for chemotherapy resistance of breast cancer stem cells. *Proc Natl Acad Sci* 111: E5429–E5438

Samanta D, Park Y, Andrabi SA, Shelton LM, Gilkes DM & Semenza GL (2016) PHGDH Expression Is Required for Mitochondrial Redox Homeostasis, Breast Cancer Stem Cell Maintenance, and Lung Metastasis. *Cancer Res* 76: 4430–4442

Sang N, Stiehl DP, Bohensky J, Leshchinsky I, Srinivas V & Caro J (2003) MAPK Signaling Up-regulates the Activity of Hypoxia-inducible Factors by Its Effects on p300. *J Biol Chem* 278: 14013–14019

Sato Y, Yoshizato T, Shiraishi Y, Maekawa S, Okuno Y, Kamura T, Shimamura T, Sato-Otsubo A, Nagae G, Suzuki H, *et al* (2013) Integrated molecular analysis of clear-cell renal cell carcinoma. *Nat Genet* 45: 860–867

Saxton RA & Sabatini DM (2017) mTOR Signaling in Growth, Metabolism, and Disease. *Cell* 168: 960–976

Scheuermann TH, Li Q, Ma H-W, Key J, Zhang L, Chen R, Garcia JA, Naidoo J, Longgood J, Frantz DE, *et al* (2013) Allosteric inhibition of hypoxia inducible factor-2 with small molecules. *Nat Chem Biol* 9: 271–276

Schito L & Semenza GL (2016) Hypoxia-Inducible Factors: Master Regulators of Cancer Progression. *Trends in Cancer* 2: 758–770

Schokrpur S, Hu J, Moughon DL, Liu P, Lin LC, Hermann K, Mangul S, Guan W, Pellegrini M, Xu H, *et al* (2016) CRISPR-Mediated VHL Knockout Generates an Improved Model for Metastatic Renal Cell Carcinoma. *Nat Publ Gr*: 1–13

Sciacovelli M & Frezza C (2016) Oncometabolites: Unconventional triggers of oncogenic signalling cascades. *Free Radic Biol Med* 100: 175–181

Sekiya S, Shimizu T, Yamato M & Okano T (2013) Hormone Supplying Renal Cell Sheet In Vivo Produced by Tissue Engineering Technology. *Biores Open Access* 2: 12–19

Semenza GL (2013) HIF-1 mediates metabolic responses to intratumoral hypoxia and oncogenic mutations. *J Clin Invest* 123: 3664–3671

Serzan MT & Atkins MB (2021) Current and emerging therapies for first line treatment of metastatic clear cell renal cell carcinoma. *J Cancer Metastasis Treat* 7

Shao W, Fanelli M, Ferrara FF, Riccioni R, Rosenauer A, Davison K, Lamph WW, Waxman S, Pelicci PG, Lo Coco F, *et al* (1998) Arsenic trioxide as an inducer of apoptosis and loss of PML/RARα protein in acute promyelocytic leukemia cells. *J Natl Cancer Inst* 90: 124–133

Shen C, Beroukhim R, Schumacher SE, Zhou J, Chang M, Signoretti S & Kaelin WG (2011) Genetic and Functional Studies Implicate HIF1 α as a 14q Kidney Cancer Suppressor Gene. *Cancer Discov* 1: 222–235

Shen C & Kaelin WG (2013) The VHL/HIF axis in clear cell renal carcinoma. *Semin Cancer Biol* 23: 18–25

Shenoy N (2020) HIF1α is not a target of 14q deletion in clear cell renal cancer. *Sci Rep* 10: 17642

Shenoy N & Pagliaro L (2018) Re: Targeting Renal Cell Carcinoma with a HIF-2 Antagonist. *Eur Urol* 73: 304–305

Smythies JA, Sun M, Masson N, Salama R, Simpson PD, Murray E, Neumann V, Cockman ME, Choudhry H, Ratcliffe PJ, *et al* (2019) Inherent <scp>DNA</scp> -

binding specificities of the <scp>HIF</scp> -1α and <scp>HIF</scp> -2α transcription factors in chromatin. *EMBO Rep* 20: 1–17

SORBELLINI M, KATTAN MW, SNYDER ME, REUTER V, MOTZER R, GOETZL M, McKIERNAN J & RUSSO P (2005) A POSTOPERATIVE PROGNOSTIC NOMOGRAM PREDICTING RECURRENCE FOR PATIENTS WITH CONVENTIONAL CLEAR CELL RENAL CELL CARCINOMA. *J Urol* 173: 48–51

Soussi T & Wiman KG (2015) TP53: an oncogene in disguise. *Cell Death Differ* 22: 1239–1249

Spencer JA, Ferraro F, Roussakis E, Klein A, Wu J, Runnels JM, Zaher W, Mortensen LJ, Alt C, Turcotte R, *et al* (2014) Direct measurement of local oxygen concentration in the bone marrow of live animals. *Nature* 508: 269–273

Subastri A, Arun V, Sharma P, Preedia babu E, Suyavaran A, Nithyananthan S, Alshammari GM, Aristatile B, Dharuman V & Thirunavukkarasu C (2018) Synthesis and characterisation of arsenic nanoparticles and its interaction with DNA and cytotoxic potential on breast cancer cells. *Chem Biol Interact* 295: 73–83

Sung W-W, Ko P-Y, Chen W-J, Wang S-C & Chen S-L (2021) Trends in the kidney cancer mortality-to-incidence ratios according to health care expenditures of 56 countries. *Sci Rep* 11: 1479

Swiatek M, Jancewicz I, Kluebsoongnoen J, Zub R, Maassen A, Kubala S, Udomkit A, Siedlecki JA, Sarnowski TJ & Sarnowska E (2020) Various forms of <scp>HIF</scp> -1α protein characterize the clear cell renal cell carcinoma cell lines. *IUBMB Life* 72: 1220–1232

Takahashi Y, Lallemand-Breitenbach V, Zhu J & de Thé H (2004) PML nuclear bodies and apoptosis. *Oncogene* 23: 2819–2824

Al Tameemi W, Dale TP, Al-Jumaily RMK & Forsyth NR (2019) Hypoxia-Modified Cancer Cell Metabolism. *Front Cell Dev Biol* 7: 1–15

Taylor CT & McElwain JC (2010) Ancient atmospheres and the evolution of oxygen sensing via the hypoxia-inducible factor in metazoans. *Physiology* 25: 272–279

de Thé H, Le Bras M & Lallemand-Breitenbach V (2012) Acute promyelocytic leukemia, arsenic, and PML bodies. *J Cell Biol* 198: 11–21

de Thé H, Lavau C, Marchio A, Chomienne C, Degos L & Dejean A (1991) The PML-

RARα fusion mRNA generated by the t(15;17) translocation in acute promyelocytic leukemia encodes a functionally altered RAR. *Cell* 66: 675–684

Tian H, McKnight SL & Russell DW (1997) Endothelial PAS domain protein 1 (EPAS1), a transcription factor selectively expressed in endothelial cells. *Genes Dev* 11: 72–82

Turajlic S, Xu H, Litchfield K, Rowan A, Chambers T, Lopez JI, Nicol D, O'Brien T, Larkin J, Horswell S, *et al* (2018) Tracking Cancer Evolution Reveals Constrained Routes to Metastases: TRACERx Renal. *Cell* 173: 581-594.e12

Ulbricht T, Alzrigat M, Horch A, Reuter N, von Mikecz A, Steimle V, Schmitt E, Krämer OH, Stamminger T & Hemmerich P (2012) PML promotes MHC class II gene expression by stabilizing the class II transactivator. *J Cell Biol* 199: 49–63

Vadde R, Vemula S, Jinka R, Merchant N, Bramhachari PV & Nagaraju GP (2017) Role of hypoxia-inducible factors (HIF) in the maintenance of stemness and malignancy of colorectal cancer. *Crit Rev Oncol Hematol* 113: 22–27

Vancurova M, Hanzlikova H, Knoblochova L, Kosla J, Majera D, Mistrik M, Burdova K, Hodny Z & Bartek J (2019) PML nuclear bodies are recruited to persistent DNA damage lesions in an RNF168-53BP1 dependent manner and contribute to DNA repair. *DNA Repair (Amst)* 78: 114–127

Verhaak R (2016) FDA Approves Drug Combo for Kidney Cancer. *Cancer Discov* 6: 687–688

Verlander JW (1998) Normal Renal Function and Alterations of Renal Function in States of Nephrotoxicity Normal Ultrastructure of the Kidney and Lower Urinary Tract*. *Toxicol Pathol* 26: 1–17

Vernier M, Bourdeau V, Gaumont-Leclerc MF, Moiseeva O, Bégin V, Saad F, Mes-Masson AM & Ferbeyre G (2011) Regulation of E2Fs and senescence by PML nuclear bodies. *Genes Dev* 25: 41–50

Vertegaal ACO, Ogg SC, Jaffray E, Rodriguez MS, Hay RT, Andersen JS, Mann M & Lamond AI (2004) A Proteomic Study of SUMO-2 Target Proteins. *J Biol Chem* 279: 33791–33798

Wang GL, Jiang BH, Rue EA & Semenza GL (1995) Hypoxia-inducible factor 1 is a basic-helix-loop-helix-PAS heterodimer regulated by cellular O2 tension. *Proc Natl Acad Sci* 92: 5510–5514

Wang GL & Semenza GL (1993) General involvement of hypoxia-inducible factor 1 in transcriptional response to hypoxia. *Proc Natl Acad Sci* 90: 4304–4308

Wang J, Shiels C, Sasieni P, Wu PJ, Islam SA, Freemont PS & Sheer D (2004) Promyelocytic leukemia nuclear bodies associate with transcriptionally active genomic regions. *J Cell Biol* 164: 515–526

Wang M, Wang L, Qian M, Tang X, Liu Z, Lai Y, Ao Y, Huang Y, Meng Y, Shi L, *et al* (2020) PML2-mediated thread-like nuclear bodies mark late senescence in Hutchinson–Gilford progeria syndrome. *Aging Cell* 19: 1–14

Wang Y-T, Chen J, Chang C-W, Jen J, Huang T-Y, Chen C-M, Shen R, Liang S-Y, Cheng I-C, Yang S-C, *et al* (2017) Ubiquitination of tumor suppressor PML regulates prometastatic and immunosuppressive tumor microenvironment. *J Clin Invest* 127: 2982–2997

Wang ZG, Delva L, Gaboli M, Rivi R, Giorgio M, Cordon-Cardo C, Grosveld F & Pandolfi PP (1998) Role of PML in cell growth and the retinoic acid pathway. *Science (80-)* 279: 1547–1551

Waypa GB, Smith KA & Schumacker PT (2016) O 2 sensing, mitochondria and ROS signaling: The fog is lifting. *Mol Aspects Med* 47–48: 76–89

Wettersten HI, Hakimi AA, Morin D, Bianchi C, Johnstone ME, Donohoe DR, Trott JF, Aboud OA, Stirdivant S, Neri B, *et al* (2015) Grade-Dependent Metabolic Reprogramming in Kidney Cancer Revealed by Combined Proteomics and Metabolomics Analysis. *Cancer Res* 75: 2541–2552

Wiederschain D, Susan W, Chen L, Loo A, Yang G, Huang A, Chen Y, Caponigro G, Yao Y, Lengauer C, *et al* (2009) Single-vector inducible lentiviral RNAi system for oncology target validation. *Cell Cycle* 8: 498–504

Wu H-C, Lin Y-C, Liu C-H, Chung H-C, Wang Y-T, Lin Y-W, Ma H-I, Tu P-H, Lawler SE & Chen R-H (2014) USP11 regulates PML stability to control Notch-induced malignancy in brain tumours. *Nat Commun* 5: 3214

Xie H, Song J, Godfrey J, Riscal R, Skuli N, Nissim I & Simon MC (2021) Glycogen metabolism is dispensable for tumour progression in clear cell renal cell carcinoma. *Nat Metab* 3: 327–336

Xu JX, Maher VE, Zhang L, Tang S, Sridhara R, Ibrahim A, Kim G & Pazdur R (2017) FDA Approval Summary: Nivolumab in Advanced Renal Cell Carcinoma After

Anti-Angiogenic Therapy and Exploratory Predictive Biomarker Analysis. *Oncologist* 22: 311–317

Xu Q, Briggs J, Park S, Niu G, Kortylewski M, Zhang S, Gritsko T, Turkson J, Kay H, Semenza GL, *et al* (2005) Targeting Stat3 blocks both HIF-1 and VEGF expression induced by multiple oncogenic growth signaling pathways. *Oncogene* 24: 5552–5560

Yang Q, Liao L, Deng X, Chen R, Gray NS, Yates JR & Lee JD (2013) BMK1 is involved in the regulation of p53 through disrupting the PML-MDM2 interaction. *Oncogene* 32: 3156–3164

Yang X, Khosravi-Far R, Chang HY & Baltimore D (1997) Daxx, a Novel Fas-Binding Protein That Activates JNK and Apoptosis. *Cell* 89: 1067–1076

Ye J, Fan J, Venneti S, Wan Y-W, Pawel BR, Zhang J, Finley LWS, Lu C, Lindsten T, Cross JR, *et al* (2014) Serine Catabolism Regulates Mitochondrial Redox Control during Hypoxia. *Cancer Discov* 4: 1406–1417

Yeung PL, Denissova NG, Nasello C, Hakhverdyan Z, Chen JD & Brenneman MA (2011) Promyelocytic leukemia nuclear bodies support a late step in DNA double-strand break repair by homologous recombination. *J Cell Biochem* 113: n/a-n/a

Yim WW-Y & Mizushima N (2020) Lysosome biology in autophagy. *Cell Discov* 6: 6

Yu J, Lan J, Wang C, Wu Q, Zhu Y, Lai X, Sun J, Jin C & Huang H (2010) PML3 interacts with TRF1 and is essential for ALT-associated PML bodies assembly in U2OS cells. *Cancer Lett* 291: 177–186

Yuan W-C, Lee Y-R, Huang S-F, Lin Y-M, Chen T-Y, Chung H-C, Tsai C-H, Chen H-Y, Chiang C-T, Lai C-K, *et al* (2011) A Cullin3-KLHL20 Ubiquitin Ligase-Dependent Pathway Targets PML to Potentiate HIF-1 Signaling and Prostate Cancer Progression. *Cancer Cell* 20: 214–228

Zhang H, Dai Z, Wu W, Wang Z, Zhang N, Zhang L, Zeng W-J, Liu Z & Cheng Q (2021a) Regulatory mechanisms of immune checkpoints PD-L1 and CTLA-4 in cancer. *J Exp Clin Cancer Res* 40: 184

Zhang H, Gao P, Fukuda R, Kumar G, Krishnamachary B, Zeller KI, Dang C V. & Semenza GL (2007) HIF-1 Inhibits Mitochondrial Biogenesis and Cellular Respiration in VHL-Deficient Renal Cell Carcinoma by Repression of C-MYC Activity. *Cancer Cell* 11: 407–420

Zhang H, Wong CCL, Wei H, Gilkes DM, Korangath P, Chaturvedi P, Schito L, Chen J, Krishnamachary B, Winnard PT, *et al* (2012) HIF-1-dependent expression of angiopoietin-like 4 and L1CAM mediates vascular metastasis of hypoxic breast cancer cells to the lungs. *Oncogene* 31: 1757–1770

Zhang JM, Genois MM, Ouyang J, Lan L & Zou L (2021b) Alternative lengthening of telomeres is a self-perpetuating process in ALT-associated PML bodies. *Mol Cell* 81: 1027-1042.e4

Zhong H, Chiles K, Feldser D, Laughner E, Hanrahan C, Georgescu MM, Simons JW & Semenza GL (2000) Modulation of hypoxia-inducible factor 1α expression by the epidermal growth factor/phosphatidylinositol 3-kinase/PTEN/AKT/FRAP pathway in human prostate cancer cells: Implications for tumor angiogenesis and therapeutics. *Cancer Res* 60: 1541–1545

Zhou W, Cheng L, Shi Y, Ke SQ, Huang Z, Fang X, Chu C, Xie Q, Bian X, Rich JN, *et al* (2015) Arsenic trioxide disrupts glioma stem cells via promoting PML degradation to inhibit tumor growth. *Oncotarget* 6: 37300–37315